The Energy Dependence of the Underlying Event in Hadronic Collisions

Rick Field
Department of Physics, University of Florida
Gainesville, Florida, 32611, USA

and

Craig Group and David Wilson
Department of Physics, University of Virginia
Charlottesville, Virginia, 22904, USA

November 12, 2012 (Version 4)

Abstract

We study charged particles production (p_T > 0.5 GeV/c, $|\eta| < \eta_{cut}$) with η_{cut} = 0.8 and 1.0 in proton-antiproton collisions at 300 GeV, 900 GeV, and 1.96 TeV. The 300 GeV and 900 GeV data are a result of the "Tevatron Energy Scan" which was performed just before the Tevatron was shut down. We use the direction of the leading charged particle in each event, PTmax, to define three regions of η-ϕ space; "toward", "away", and "transverse". The "transverse" region is very sensitive to the "underlying event". The data are corrected to the particle level and are compared with the PYTHIA 6.2 Tune A and Tune DW, and the PYTHIA 6.4 Tune Z1 at the particle level (*i.e.* generator level). The goal is to study the energy dependence of the underlying event by examining the behavior of the "transverse" region as a function of PTmax at three energies.

I. Introduction

The total antiproton-proton cross section is the sum of the elastic and inelastic components, $\sigma_{tot} = \sigma_{EL} + \sigma_{IN}$. Three distinct processes contribute to the inelastic cross section; single diffraction, double-diffraction, and everything else which is referred to as "non-diffractive". For elastic scattering neither of the beam particles breaks apart (*i.e.* color singlet exchange). For single and double diffraction one or both of the beam particles are excited into a high mass color singlet state (*i.e.* N* states) which then decays. Single and double diffraction also corresponds to color singlet exchange between the beam hadrons. When color is exchanged the outgoing remnants are no longer color singlets and one has a separation of color resulting in a multitude of quark-antiquark pairs being pulled out of the vacuum. The "non-diffractive" component, σ_{ND}, involves color exchange and the separation of color. However, the "non-diffractive" collisions have both a "soft" and "hard" component. Most of the time the color exchange between partons in the beam hadrons occurs through a soft interaction (*i.e.* no high transverse momentum) and the two beam hadrons "ooze" through each other producing lots of soft particles with a uniform distribution in rapidity and many particles flying down the beam pipe. Occasionally, there is a hard scattering among the constituent partons producing outgoing particles and "jets" with high transverse momentum.

Min-bias (MB) is a generic term which refers to events that are selected with a "loose" trigger that accepts a large fraction of the overall inelastic cross section. All triggers produce some bias and the term "min-bias" is meaningless until one specifies the precise trigger used to collect the data. The CDF MB trigger requires at least one charged particle in the forward region $3.2 < \eta < 5.9$ and simultaneously at least one charged particle in the backward region $-5.9 < \eta < -3.2$. The underlying event (UE) consists of the beam-beam remnants (BBR) and the multiple parton interactions (MPI) that accompany a hard scattering. The UE is an unavoidable background to hard-scattering collider events. MB and UE are not the same object! The majority of MB collisions are "soft" while the UE is studied in events in which a hard-scattering has occurred. One uses the structure of the hard hadron-hadron collision to experimentally study the UE. As shown in Fig. 1, on an event-by-event bases, a "leading object" is used to define three regions of η-ϕ space. The pseudo-rapidity $\eta = -\log(\tan(\theta_{cm}/2))$, where θ_{cm} is the center-of-mass polar scattering angle and ϕ is the azimuthal angle of outgoing charged particles. In particular, the "transverse" region is roughly perpendicular to the plane of the hard 2-to-2 parton-parton scattering and is therefore very sensitive to the UE. The "leading object" can be the leading charged particle jet or calorimeter jet. It can also be the leading charged particle, PTmax, or a Z-boson.

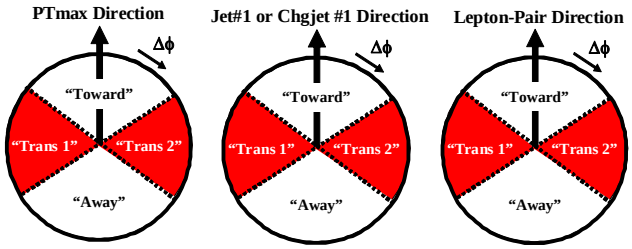

Fig. 1: Illustration of correlations in azimuthal angle $\Delta\phi$ relative to the direction of a "leading object" in the event. The relative angle $\Delta\phi = \phi - \phi_L$, where ϕ_L is the azimuthal angle of the "leading object" and ϕ is the azimuthal angle of a charged particle. The "toward" region is defined by $|\Delta\phi| < 60^o$ and $|\eta| < \eta_{cut}$, while the "away" region is $|\Delta\phi| > 120^o$ and $|\eta| < \eta_{cut}$. The two "transverse" regions $60^o < -\Delta\phi < 120^o$, $|\eta| < \eta_{cut}$ and $60^o < \Delta\phi < 120^o$, $|\eta| < \eta_{cut}$ are referred to as "transverse 1" and "transverse 2". The overall transverse region corresponds to combining the transverse-1 and transverse-2 regions.

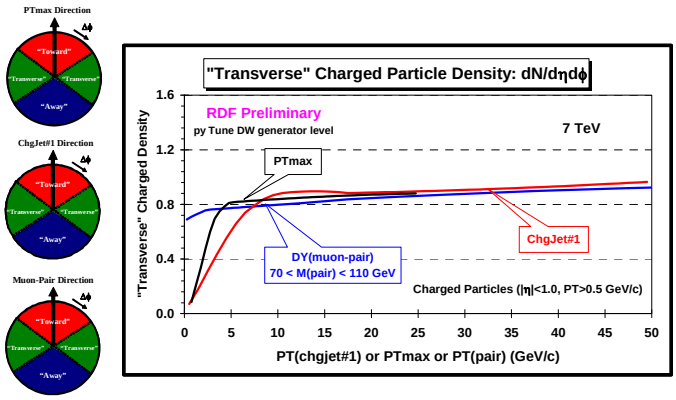

Fig. 2: Shows the charged particle density in the "transverse" region for charged particles ($p_T > 0.5$ GeV/c, $|\eta| < 1$) at 7 TeV as defined by the leading charged particle, PTmax, the leading charged particle jet, chgjet#1, and the muon-pair in Z-boson production as predicted from PYTHIA 6.2 Tune DW at the particle level. For Z-boson production the muon-pair are excluded from the charged particle density. Charged particle jets are constructed using the Anti-KT algorithm with d = 0.5.

In Run 1 at CDF we looked only at charged particles and used the leading charged particle jet to define the "transverse" region [1]. Later in Run 2 we studied the UE using the leading calorimeter jet and Z-bosons [2]. Figure 2 shows the charged particle density in the "transverse"

region for charged particles at 7 TeV as defined by PTmax, PT(chgjet#1), and PT(muon-pair) as predicted from PYTHIA Tune DW. QCD Monte-Carlo generators such as PYTHIA [3] have parameters which may be adjusted to control the behavior of their event modeling. A specified set of these parameters that has been adjusted to better fit some aspects of the data is referred to as a tune [4,5]. The CDF PYTHIA 6.2 tune A was determined by fitting the CDF Run 1 UE data [1] and the PYTHIA 6.2 Tune DW does a very nice job in describing both the CDF Run 1 and Run 2 UE data [2]. However, Tune DW does not reproduce perfectly all the features of the LHC data and after seeing the data one can construct improved LHC UE tunes [6]. The first CMS LHC tune was the PYTHIA 6.4 Tune Z1 [7]. Early LHC UE data used the PTmax approach to study the UE.

Table 1. Observables examined in this analysis as they are defined at the particle level and the detector level. Charged tracks are considered "good" if they pass the selection criterion given in Table 3. These observables are constructed in the "toward", "away", and "transverse" regions as defined by the leading charged particle, PTmax, as shown in Fig. 1. Events are required to have at least one charged particle with $p_T > 0.5$ GeV/c and $|\eta| < \eta_{cut}$ and PTmax is not included in the "toward" observables. For the average p_T and the PTmax we require that there is at least one charge particle present, while the charged particle and PTsum densities are taken to be zero if there are no charged particles present.

Observable	Particle Level	Detector level
$dN/d\eta d\phi$	Number of charged particles per unit η-ϕ ($p_T > 0.5$ GeV/c, $\|\eta\| < \eta_{cut}$)	Number of "good" charged tracks per unit η-ϕ ($p_T > 0.5$ GeV/c, $\|\eta\| < \eta_{cut}$)
$dPT/d\eta d\phi$	Scalar p_T sum of charged particles per unit η-ϕ ($p_T > 0.5$ GeV/c, $\|\eta\| < \eta_{cut}$)	Scalar p_T sum of "good" charged tracks per unit η-ϕ ($p_T > 0.5$ GeV/c, $\|\eta\| < \eta_{cut}$)
$\langle p_T \rangle$	Average p_T of charged particles ($p_T > 0.5$ GeV/c, $\|\eta\| < \eta_{cut}$) Require at least 1 charged particle	Average p_T of "good" charged tracks ($p_T > 0.5$ GeV/c, $\|\eta\| < \eta_{cut}$) Require at least 1 "good" track
PTmax	Maximum p_T charged particle ($p_T > 0.5$ GeV/c, $\|\eta\| < \eta_{cut}$) Require at least 1 charged particle	Maximum p_T "good" charged tracks ($p_T > 0.5$ GeV/c, $\|\eta\| < \eta_{cut}$) Require at least 1 "good" track

The data for this analysis are collected with the CDF MB trigger and we study charged particles ($p_T > 0.5$ GeV/c, $|\eta| < \eta_{cut}$) that are produced in association with the leading charged particle, PTmax. As shown in Table 1, the observables are constructed in the "toward", "away", and "transverse" regions as defined by the leading charged particle, PTmax, as illustrated in Fig. 1. Events are required to have at least one charged particle with $p_T > 0.5$ GeV/c and $|\eta| < \eta_{cut}$ and PTmax is not included in the "toward" observables. For the average p_T and the PTmax we require that there is at least one charge particle present, while the charged particle and PTsum density is taken to be zero if there are no charged particles present. At present this note contains results for the "transverse" charged particle density, the "transverse" charged PTsum density, and the "transverse" charged particle average p_T for $p_T > 0.5$ GeV/c and $|\eta| < \eta_{cut}$. Later this note will be updated to include the other observables. We have done the analysis with two different values for η_{cut}. We use $\eta_{cut} = 1.0$ to compare with our previous CDF UE studies. However, we also include $\eta_{cut} = 0.8$ in order to directly compare with the LHC UE results.

In Section II we discuss the data and vertex selection and the track cuts. In Section III we correct the data to the particle level and construct the systematic errors. The techniques employed here are identical to those used in our previous CDF UE analyses and are documented

in several CDF notes [9-11]. The results and comparisons with the PYTHIA tunes are shown in Section IV. Section V is reserved for summary and conclusions.

II. Data Selection and Track Cuts

(1) Data and Vertex Selection

Table 2 shows the data used in this analysis. We use all the 300 GeV and 900 GeV MB data. At 1.96 TeV we are currently including the MB data through period 10. At each energy we consider two sets of data. One set (V01) requires zero or one quality 12 vertex within $|z| < 60$ cm and the other set (V1) requires events to have one and only one quality 12 vertex within $|z| <$ 60 cm.

Table 2. Number of MB events at 1.96 TeV (period 0-10), 900 GeV, and 300 GeV with 0 or 1 quality 12 vertex (V01) and with one and only one quality 12 vertex (V1).

Event Selection	1.96 TeV	900 GeV	300 GeV
"Good" Events	47,860,199	54,061,290	12,000,290
V01: 0 or 1 Q12 ZVtx, $\|z\| < 60$ cm	35,718,812	47,183,876	10,662,585
V1: 1 Q12 ZVtx, $\|z\| < 60$ cm	26,684,272	29,921,921	5,251,686

Table 3. Track selection criterion, where d_0 is the transverse impact parameter. For events with one quality 12 vertex we require $|z - z_{Q12}| < \Delta Z_{cut}$, where $z - z_{Q12}$ is the longitudinal distance between the measured track and the primary quality 12 vertex. For events with no quality 12 vertex we require $|z - z_{max}| < 2\Delta Z_{cut}$, where $z - z_{max}$ is the longitudinal distance between the measured track and the leading track (*i.e.* PTmax).

Track Selection (loose)
COT measured tracks
$\|d_0\| < 1.0$ cm (*beam corrected*)
$\Delta Z_{cut} = 3$ cm
NumAXseg(COT) $\geq$ 2 NumAXseg(COT) $\geq$ 2
NumAXhits(COT) $\geq$ 10 NumAXhits(COT) $\geq$ 10
χ^2(track fit)/DoF < 10
0.5 GeV/c < p_T < 150 GeV/c
$\|\eta\| < 1$

Track Selection (tight)
COT measured tracks
$\|d_0\| < 0.5$ cm (*beam corrected*)
$\Delta Z_{cut} = 2$ cm
NumAXseg(COT) $\geq$ 2 NumAXseg(COT) $\geq$ 2
NumAXhits(COT) $\geq$ 10 NumAXhits(COT) $\geq$ 10
χ^2(track fit)/DoF < 10
0.5 GeV/c < p_T < 150 GeV/c
$\|\eta\| < 1$

(2) Track Cuts (Loose and Tight)

We consider only COT measured charged tracks in the region $0.5 < p_T < 150$ GeV/c and $|\eta| < \eta_{cut}$ for $\eta_{cut} = 0.8$ and 1.0 where efficiency is high. The upper limit of 150 GeV/c is chosen to prevent miss-measured tracks with very high p_T from contributing to the observables in Table 2 (at high p_T the track resolution deteriorates). As Table 3 shows, we employ both a "loose" and a "tight" track criterion. For both the "tight" and "loose" case the transverse impact parameter is

corrected for the beam position. Both the "loose" and "tight" data are corrected to the particle level (with different correction factors) and the differences are used as a systematic error. Table 4 shows the remaining number of events with at least one charged particle with $p_T > 0.5$ GeV/c and $|\eta| < 1.0$ at each energy for the three datasets: TC1_V01, LC1_V01, and TC1_V1.

Table 4. Number of events with at least one charged particle with $p_T > 0.5$ GeV/c and $|\eta| < 1.0$.

Data Set	1.96 TeV	900 GeV	300 GeV
TC1_V01: (0 or 1 ZVtx, tight track cuts)	30,262,961	37,075,521	7,233,840
LC1_V01: (0 or 1 ZVtx, loose track cuts)	30,986,931	38,306,127	7,484,571
TC1_V1: (1 ZVtx, tight track cuts)	25,371,145	28,524,566	4,886,354

III. Correcting the Data to the Particle Level

(1) Pile-Up Corrections at 1.96 TeV

Although we require zero or one quality 12 vertex, the observables in Table 1 can still be affected by pile-up (*i.e.* more that one proton-antiproton collision in the event). Tracks are required to point back to the primary vertex, but the track observables are affected by pile-up when two vertices overlap. Vertices within about 3 cm of each other merge together as one. Fig. 3 shows how pile-up affects the "transverse" charged particle density at 1.96 TeV. Large luminosity implies more pile-up. The average luminosity in this data set about 33×10^{30} $cm^{-2}s^{-1}$. Fig. 3 shows the dependence of the raw data on the instantaneous luminosity for the "transverse" charged particle density at 1.96 TeV as defined by the leading charged particle, PTmax, with $1.5 < PTmax < 2.0$ GeV/c. Each PTmax bin is plotted versus the instantaneous luminosity, iLumi, and fit to a straight line. This function is then used to correct the data for pile-up on an event-by-event bases resulting in the corrected (iLumiCOR) values shown in Fig. 3. As can be in Fig. 3 the pile-up corrections are less than 4%. The luminosities at 300 GeV and 900 GeV are so small that there is no need for pile-up corrections at these energies.

Figure 4 shows the pile-up corrected data on the "transverse" charged particle density at 1.96 TeV for the three datasets: TC1_V01, LC1_V01, TC1_V1. Fig. 4 also shows the raw data at 300 GeV and 900 GeV for the three data sets. For $PTmax < 4$ GeV/c there is a sizable difference between TC1_V01 and TC1_V1. Requiring at least one quality 12 vertex biases the data toward more active events. Most events with $PTmax > 4$ GeV/c, however, have at lease one quality 12 vertex and hence TC1_V01 and TC1_V1 become the same. TC1_V01 and LC1_V01 differ slightly at all PTmax values. The "loose" track cuts accept more tracks that the "tight" track cuts.

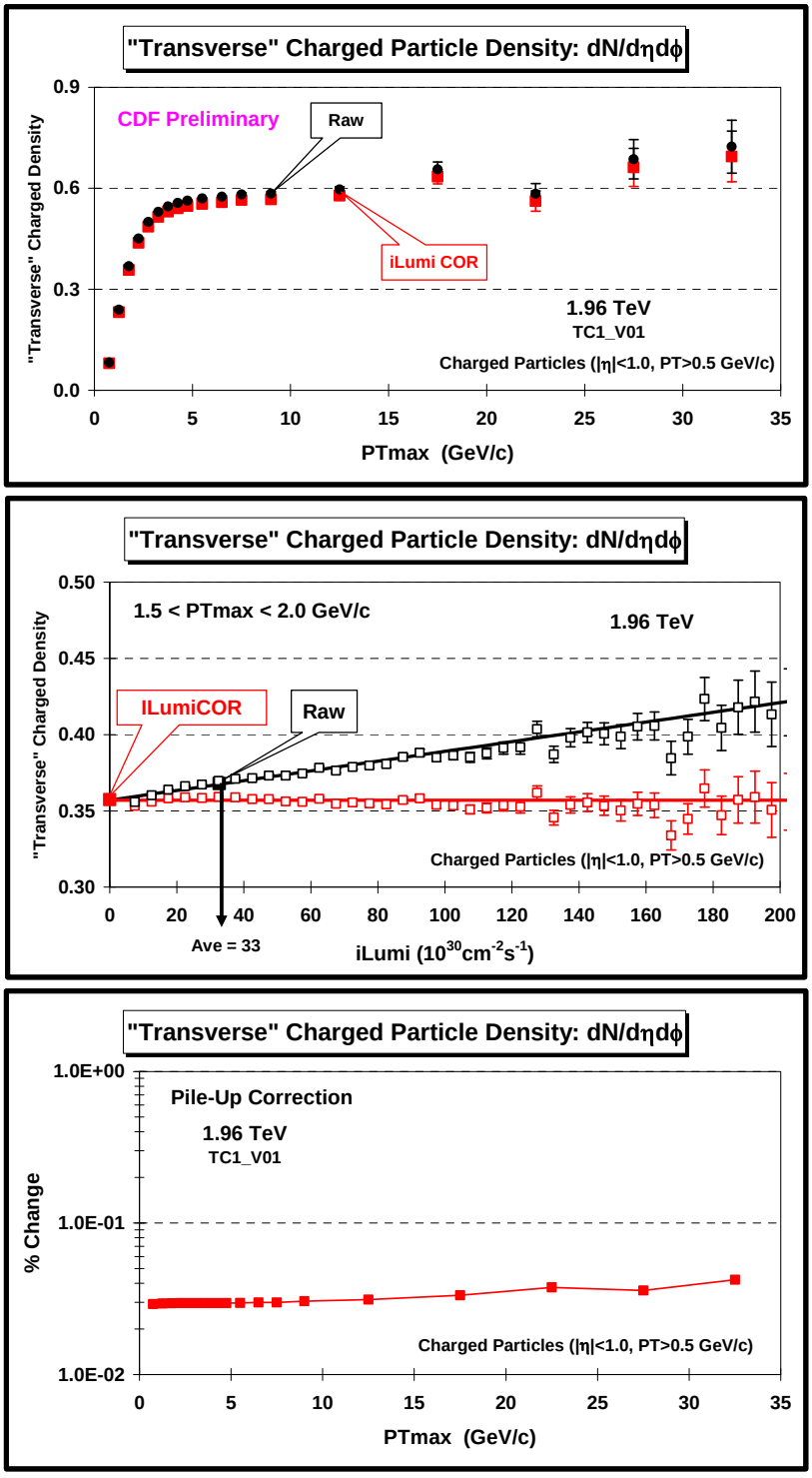

Fig. 3. (*top*) Shows the raw data (TC1_V01) and the pile-up corrected data (iLumiCOR) on the "transverse" charged particle density at 1.96 TeV as defined by the leading charged particle, PTmax, as a function of PTmax. (*middle*) Shows the dependence of the raw data (TC1_V01, black open squares) and the pile-up corrected data (iLumiCOR, red open squares) on the instantaneous luminosity for the "transverse" charged particle density at 1.96 TeV as defined by the leading charged particle, PTmax, with 1.5 < PTmax < 2.0 GeV/c. The overall raw data point (solid black square) is plotted at the average instantaneous luminosity value of 33 × 10^{30} $cm^{-2}s^{-1}$ and the pile-up corrected data point (solid red square) is plotted at zero instantaneous luminosity. (*bottom*) Shows the percent change due to the pile-up corrections versus PTmax.

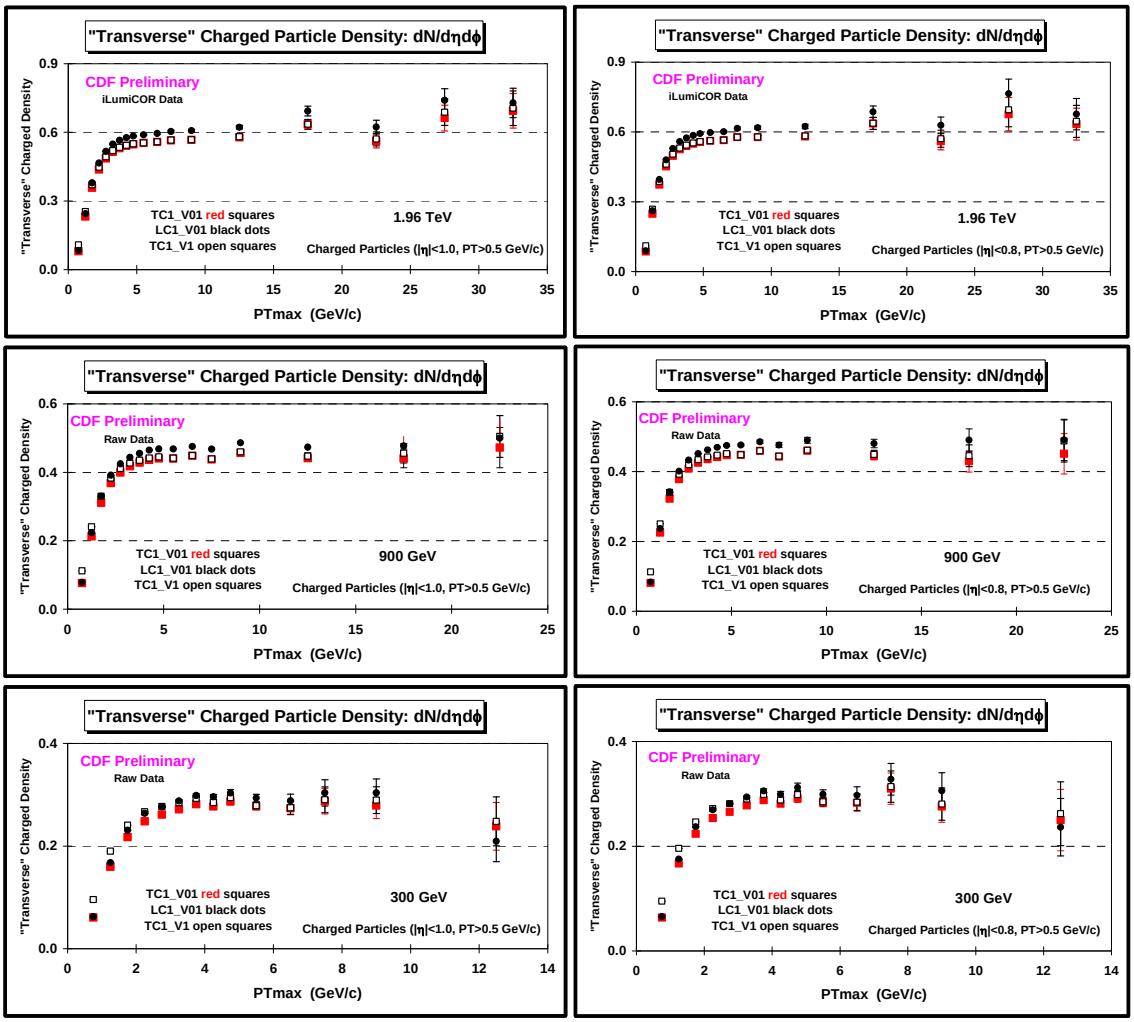

Fig. 4. (*top row*) Shows the pile-up corrected data (TC1_V01, LC1_V01, TC1_V1) on the "transverse" charged particle density at 1.96 TeV as defined by the leading charged particle, PTmax, as a function of PTmax. (*middle row*) Shows the raw data (TC1_V01, LC1_V01, TC1_V1) on the "transverse" charged particle density at 900 GeV as defined by the leading charged particle, PTmax, as a function of PTmax. (*bottom row*) Shows the raw data (TC1_V01, LC1_V01, TC1_V1) on the "transverse" charged particle density at 300 GeV as defined by the leading charged particle, PTmax, as a function of PTmax. The charged particles have $p_T > 0.5$ GeV and $|\eta| < 1.0$ (*left column*) and $|\eta| < 0.8$ (*right column*).

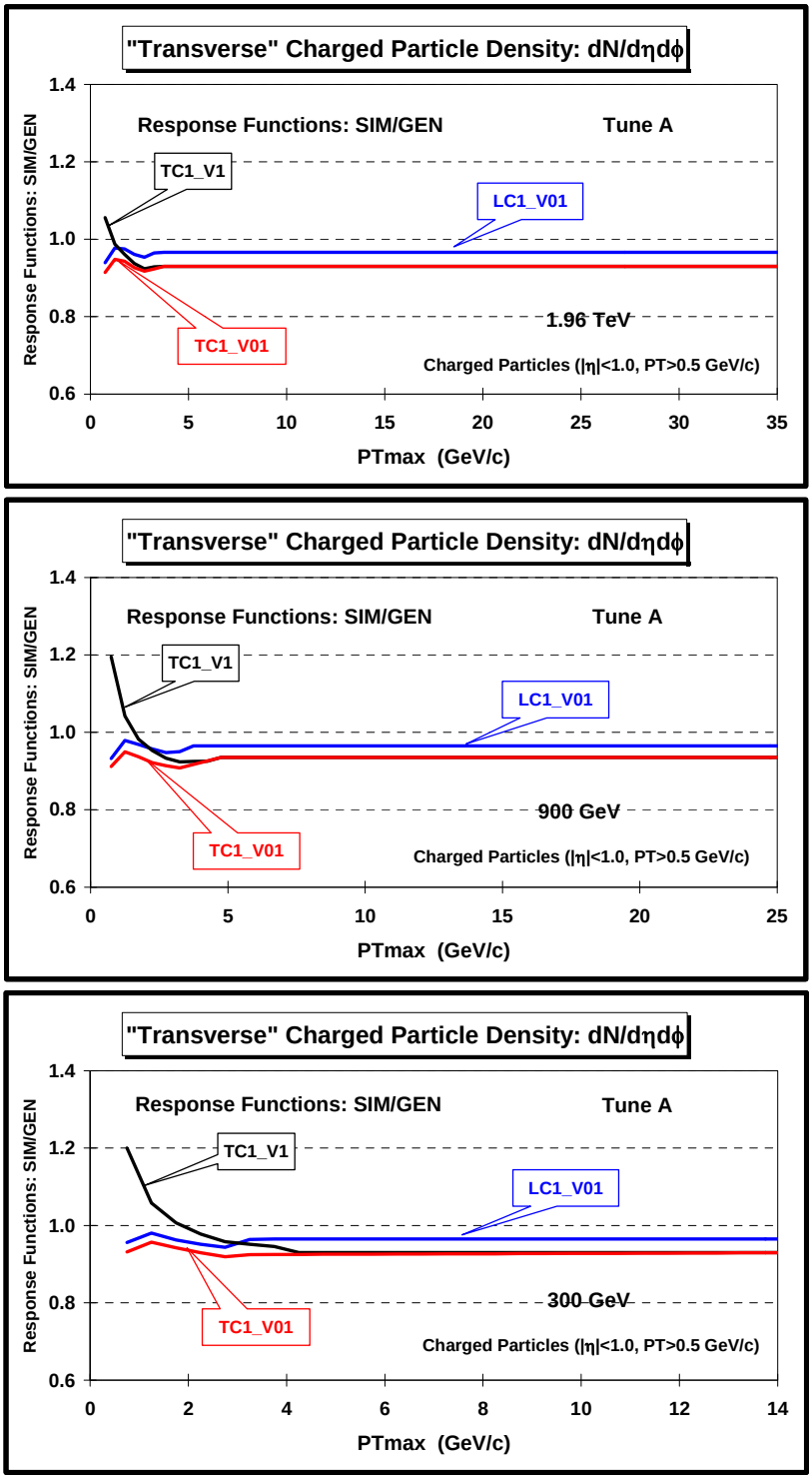

Fig. 5. Shows the ratio of the detector level to the particle level, SIM/GEN, for TC1_V01, LC1_V01, and TC1_V1 from PYTHIA Tune A (*i.e.* response factors) for the "transverse" charged particle density at 1.96 TeV (*top*), 900 GeV (*middle*), and 300 GeV (*bottom*) as defined by the leading charged particle, PTmax, as a function of PTmax, for charged particles have $p_T > 0.5$ GeV and $|\eta| < 1.0$.

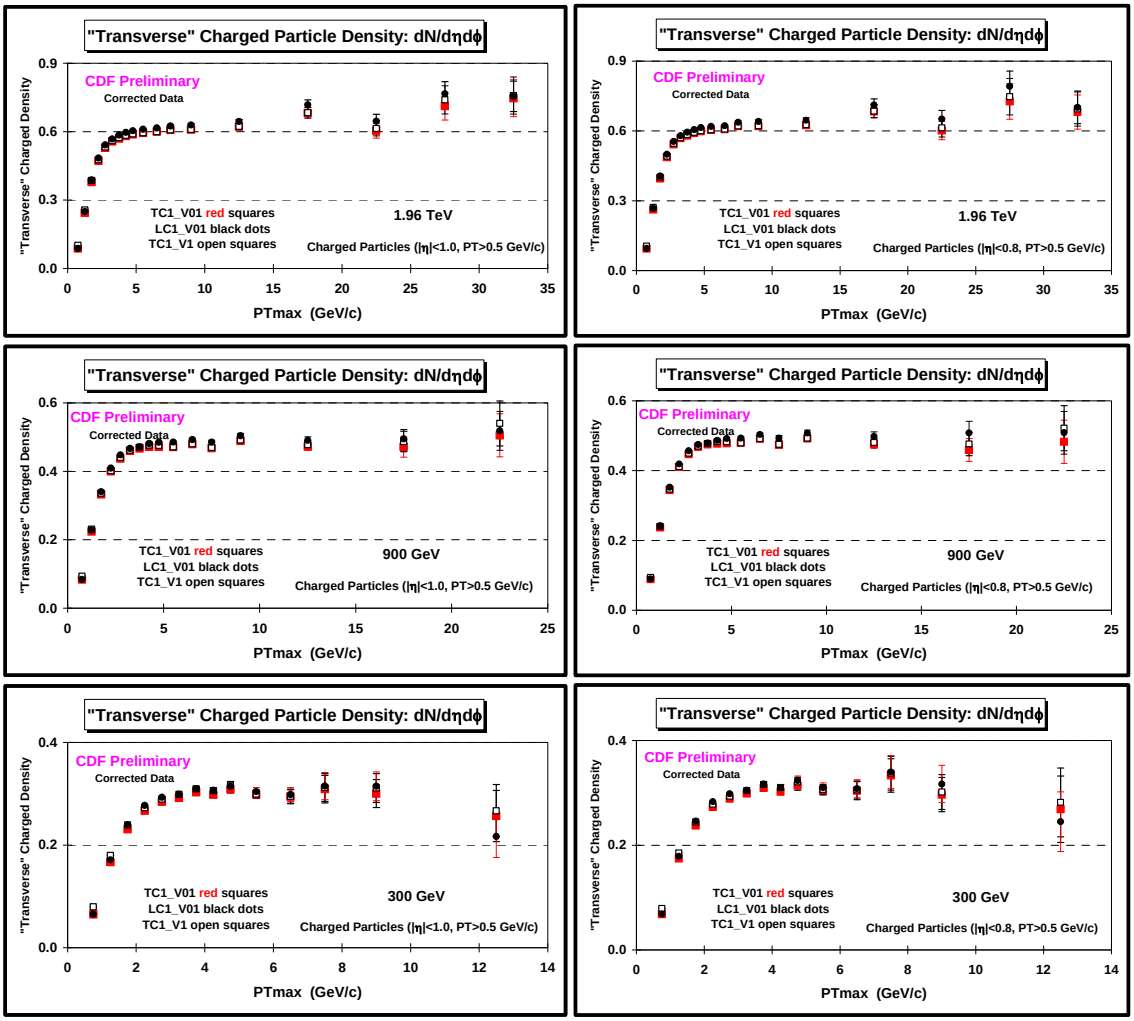

Fig. 6. Shows the corrected data (TC1_V01, LC1_V01, TC1_V1) on the "transverse" charged particle density at 1.96 TeV (*top row*), 900 GeV (*middle row*), and 300 GeV (*bottom row*) as defined by the leading charged particle, PTmax, as a function of PTmax. The charged particles have $p_T > 0.5$ GeV and $|\eta| < 1.0$ (*left column*) and $|\eta| < 0.8$ (*right column*).

(2) "Response" and "Correction" Factors

We use the "one-step" method to correct the data to the particle level [9-11]. PYTHIA Tune A is used to calculate the observables in Table 1 at the particle level in bins of the highest p_T charged particle PTmax (GEN) and at the detector level in bins the highest p_T track (uncorrected) (SIM). The detector level data in bins of the highest p_T track (uncorrected) are corrected by multiplying by the QCD Monte-Carlo "correction" factor, GEN/SIM, as described in Table 5. We refer to the ratio SIM/GEN as the "response" factor with the "correction" factor being the reciprocal. Smooth curves are drawn through the QCD Monte-Carlo predictions at both the generator level (GEN) and the detector level (SIM) to aid in comparing the theory with the data and also to construct the "correction" factors. Fig. 5 shows the ratio of the detector level to the particle level, SIM/GEN, for TC1_V01, LC1_V01, and TC1_V1 from PYTHIA Tune A (*i.e.* response factors) for the "transverse" charged particle density at 1.96 TeV, 900 GeV, and 300 GeV.

Table 5. PYTHIA Tune A is used to calculate the observables in Table 1 at the particle level in bins of the highest p_T charged particle PTmax (GEN) and at the detector level in bins of the highest p_T track (*uncorrected*). The detector level data in bins of the highest p_T track (*uncorrected*) are corrected by multiplying by QCD Monte-Carlo factor, GEN/SIM.

Particle Level Observable	Detector Level Observable	"Response" Factor	"Correction" Factor
GEN = Charged Particles PTmax Bin	SIM = Good Tracks Max Track Bin	SIM/GEN	GEN/SIM

(3) Systematic Uncertainties

The three datasets are each corrected to the particle level using their corresponding "correction factors" as shown in Fig. 6. If PYTHIA Tune A fit the data perfectly and if CDFSIM was perfect then the corrected data from the three methods, TC1_V01, LC1_V01, and TC1_V1 would all be identical. As shown in Table 6, the differences between the three methods are used as systematic errors. Fig. 7 shows the fractional statistical and systematic errors on the "transverse" charged particle density the three energies. The overall total error (Tot-Error) results from adding statistical error in quadrature with the three systematic errors. At low PTmax the overall error is dominated by Sys-Err2, while at large PTmax the overall error is predominately statistical.

Table 6. The errors on the corrected observables in Table 1 include both the statistical error and the systematic uncertainty (added in quadrature). The overall systematic uncertainty includes the uncertainties shown below. Sys-Err3 is included to take into account the accuracy of constructing the smooth theory curves.

Uncertainty	Origin
Sys-Err1	Bin by bin difference between the corrected data for LC1_V01 and TC1_V01.
Sys-Err2	Bin by bin difference between the corrected data for TC1_V1 and TC1_V01.
Sys-Err3	2%

Figures 8 shows the corrected data at 1.96 TeV, 900 GeV, and 300 GeV on the "transverse" charged particle density as defined by the leading charged particle, PTmax, as a function of PTmax. The data are corrected to the particle level with errors that include both the statistical error and the systematic uncertainty. Figure 9 compares directly the corrected data on the "transverse" charged particle density for $\eta_{cut} = 0.8$ and 1.0. The results for these two η cuts are almost identical.

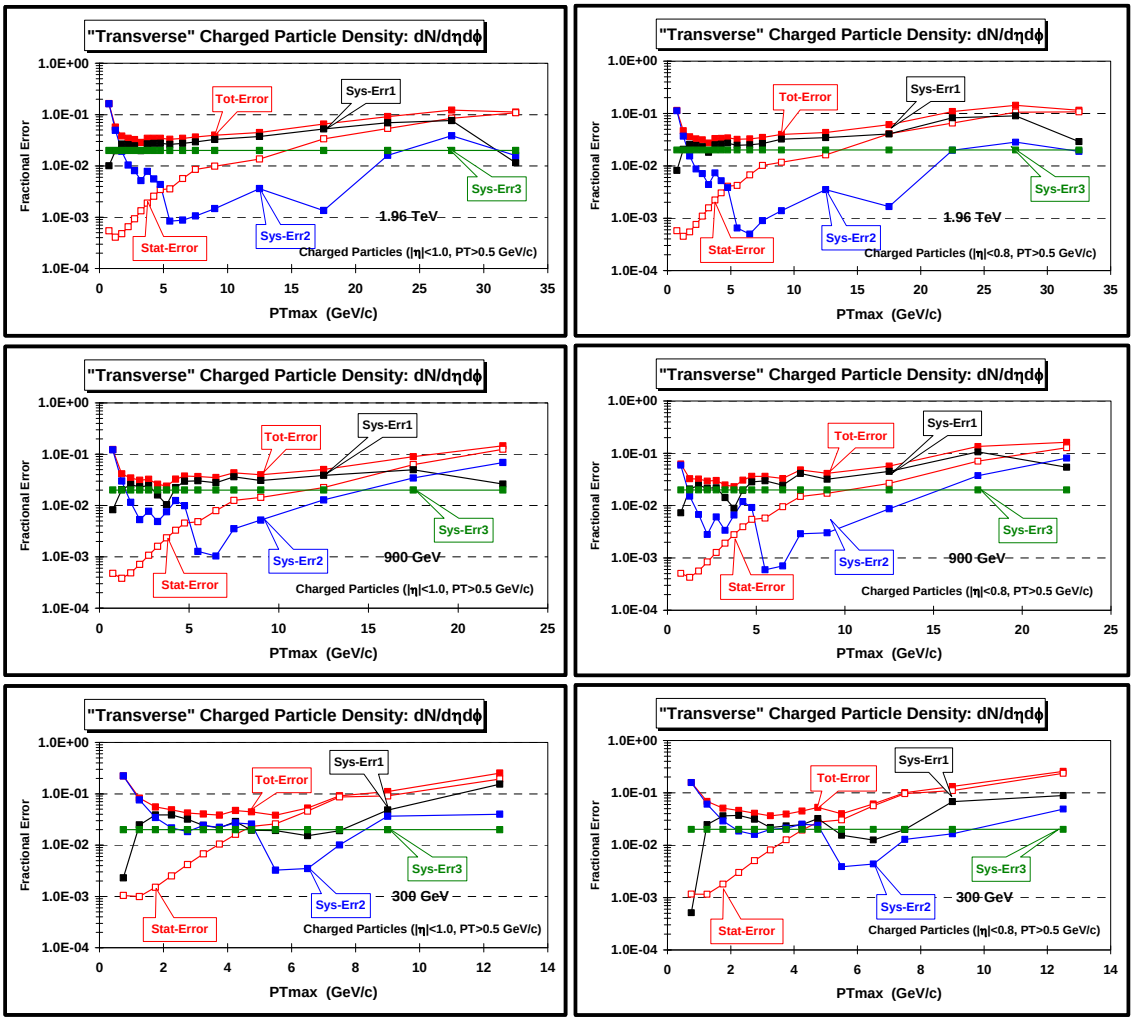

Fig. 7. Shows the fractional statistical and systematic errors on the "transverse" charged particle density at 1.96 TeV (*top row*), 900 GeV (*middle row*), and 300 GeV (*bottom row*) as defined by the leading charged particle, PTmax, as a function of PTmax. Stat-Error is the statistical error, Sys-Err1 = |LC1_V01 – TC1_V01|/TC1_V01, Sys-Err2 = |TC1_V01 – TC1_V1|/TC1_V01, and Sys-Err3 = 2%. The overall total error (Tot-Error) results from adding statistical error in quadrature with the three systematic errors. The charged particles have $p_T > 0.5$ GeV and $|\eta| < 1.0$ (*left column*) and $|\eta| < 0.8$ (*right column*).

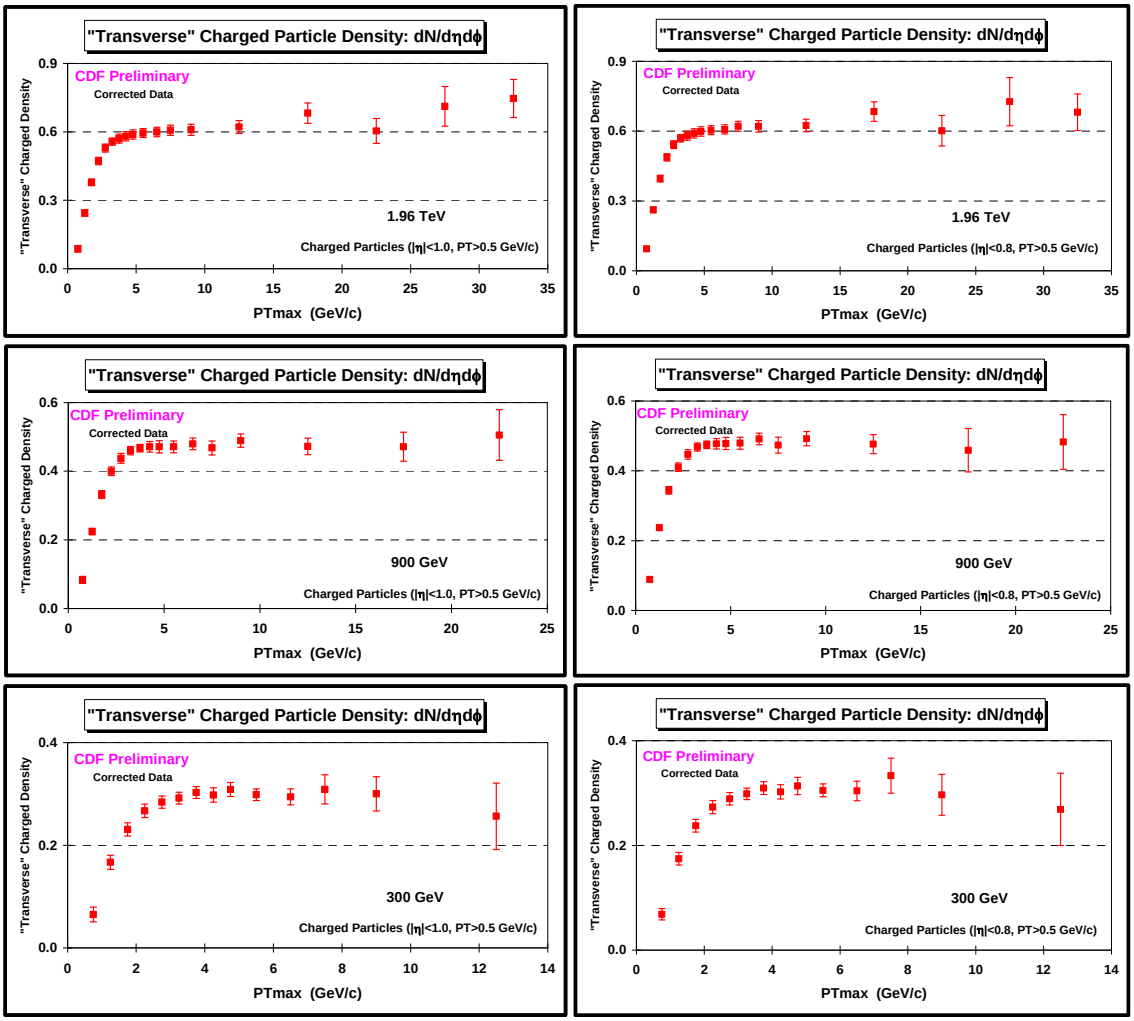

Fig. 8. Data at 1.96 TeV (*top row*), 900 GeV (*middle row*), and 300 GeV (*bottom row*) on the "transverse" charged particle density as defined by the leading charged particle, PTmax, as a function of PTmax. The data are corrected to the particle level with errors that include both the statistical error and the systematic uncertainty. The charged particles have $p_T > 0.5$ GeV and $|\eta| < 1.0$ (*left column*) and $|\eta| < 0.8$ (*right column*).

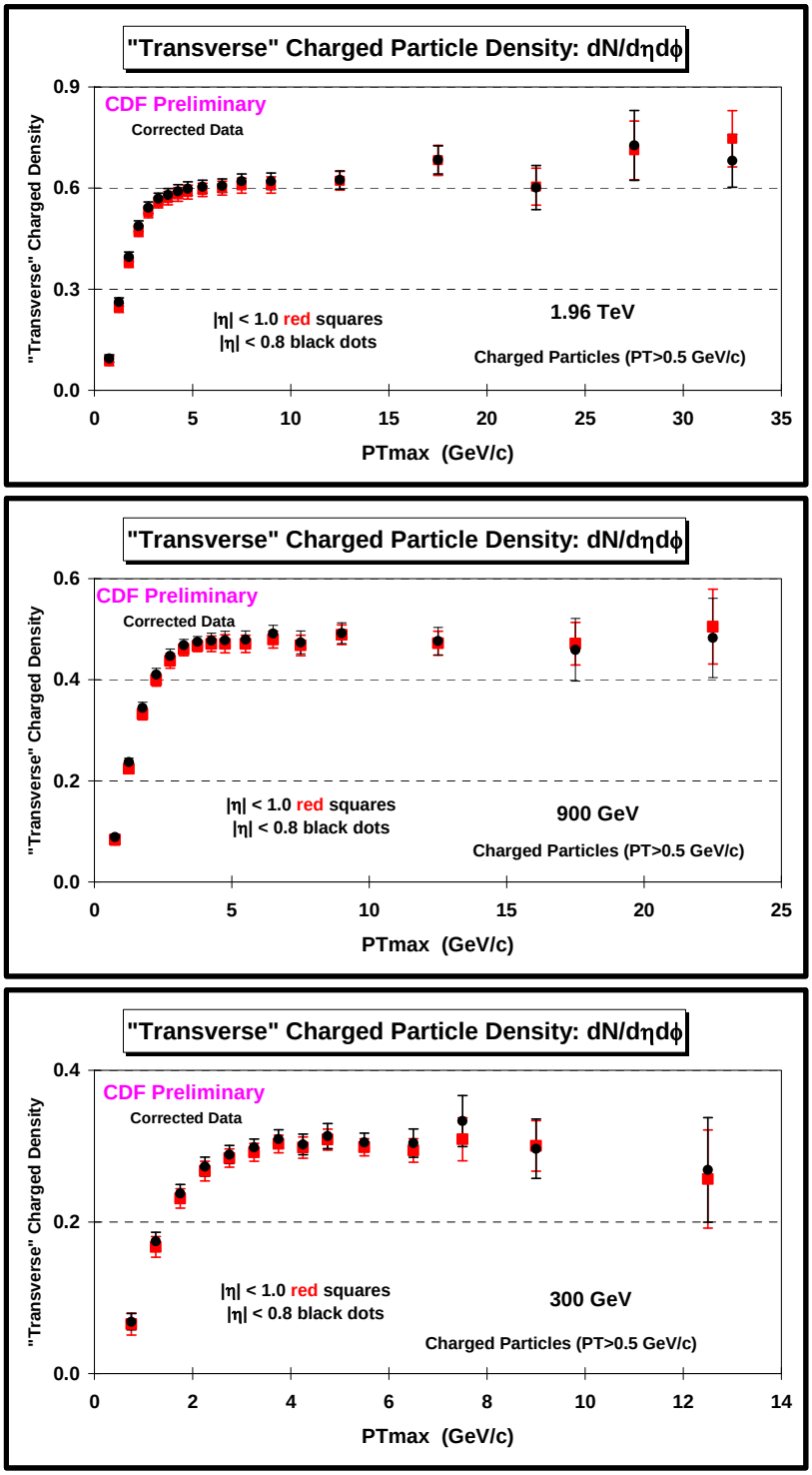

Fig. 9. Data at 1.96 TeV (*top*), 900 GeV (*middle*), and 300 GeV (*bottom*) on the "transverse" charged particle density as defined by the leading charged particle, PTmax, as a function of PTmax. The data are corrected to the particle level with errors that include both the statistical error and the systematic uncertainty. The charged particles have $p_T > 0.5$ GeV and $|\eta| < 1.0$ (*red squares*) and $|\eta| < 0.8$ (*black dots*).

(4) "Transverse" Charged PTsum Density and Average P_T

The "transverse" charged PTsum density is the scalar p_T sum of the charged particles in the "transverse" region divided by the area of the "transverse" region in η-ϕ space. Figure 10 shows the pile-up corrected data on the "transverse" charged PTsum density at 1.96 TeV for the three datasets: TC1_V01, LC1_V01, TC1_V1 together with the raw data at 300 GeV and 900 GeV for the three data sets. The pile-up corrections are very similar for the "transverse" charged particle and PTsum densities. The results after correcting these three datasets to the particle level using their corresponding "correction factors" are shown in Fig. 11. Fig. 12 shows the fractional statistical and systematic errors on the "transverse" charged PTsum density at the three energies which are constructed using the same method that was used for the "transverse" charged particle density (see Table 6). The systematic errors on the PTsum density are similar to those found on the charged particle density in Fig. 7. Figure 13 shows the resulting corrected data at 1.96 TeV, 900 GeV, and 300 GeV on the "transverse" charged PTsum density with errors that include both the statistical error and the systematic uncertainty. Figure 14 compares directly the corrected data on the "transverse" charged PTsum density for $\eta_{cut} = 0.8$ and 1.0. Again, the results for these two η cuts are almost identical.

The "transverse" charged particle average p_T is constructed on an event-by-event bases and then averaged over all the events, For the "transverse" average p_T we require that there is at least one charge particle present in the "transverse" region, while the "transverse" charged particle and PTsum densities are taken to be zero if there are no charged particles present. Fig. 15 shows the raw data on the "transverse" charged particle average p_T at 1.96 TeV, 900 GeV, and 300 GeV for the three datasets: TC1_V01, LC1_V01, TC1_V1. Pile-up has a negligible affect on the "transverse" average p_T. Also, unlike the "transverse" particle and PTsum densities the datasets TC1_V01 and TC1_V1 are nearly equal even at small PTmax. The results after correcting the three datasets to the particle level using their corresponding "correction factors" are shown in Fig. 16. Fig. 17 shows the fractional statistical and systematic errors on the "transverse" charged particle average p_T at the three energies which are constructed using the same method that was used for the "transverse" charged particle density (see Table 6). Sys-Err1 and Sys-Err2 are considerably smaller for the average p_T than for the charged particle and PTsum densities. Figure 18 shows the resulting corrected data at 1.96 TeV, 900 GeV, and 300 GeV on the "transverse" charged particle average p_T with errors that include both the statistical error and the systematic uncertainty. Figure 19 compares directly the corrected data on the "transverse" charged particle average p_T for $\eta_{cut} = 0.8$ and 1.0. The results for these two η cuts are nearly identical.

Fig. 20 shows the fractional total errors for the three "transverse" observables at the three energies and Fig. 21 compares the corrected data at the three energies. Fig. 22 shows the data at 1.96 TeV, 900 GeV, and 300 GeV on the "transverse" charged particle and PTsum densities as defined by the leading charged particle, PTmax, for $5.0 < PTmax < 6.0$ GeV/c plotted versus the center-of-mass energy (on a log scale). The "transverse" PTsum density increases slightly faster with center-of-mass energy than does the particle density. Fig. 22 also shows the data at 1.96 TeV, 900 GeV, and 300 GeV on the "transverse" charged particle average p_T, for $5.0 < PTmax < 6.0$ GeV/c plotted versus the center-of-mass energy (on a log scale). The "transverse" charged particle and PTsum densities increase rapidly with energy, while the "transverse" charged particle average p_T increase is small.

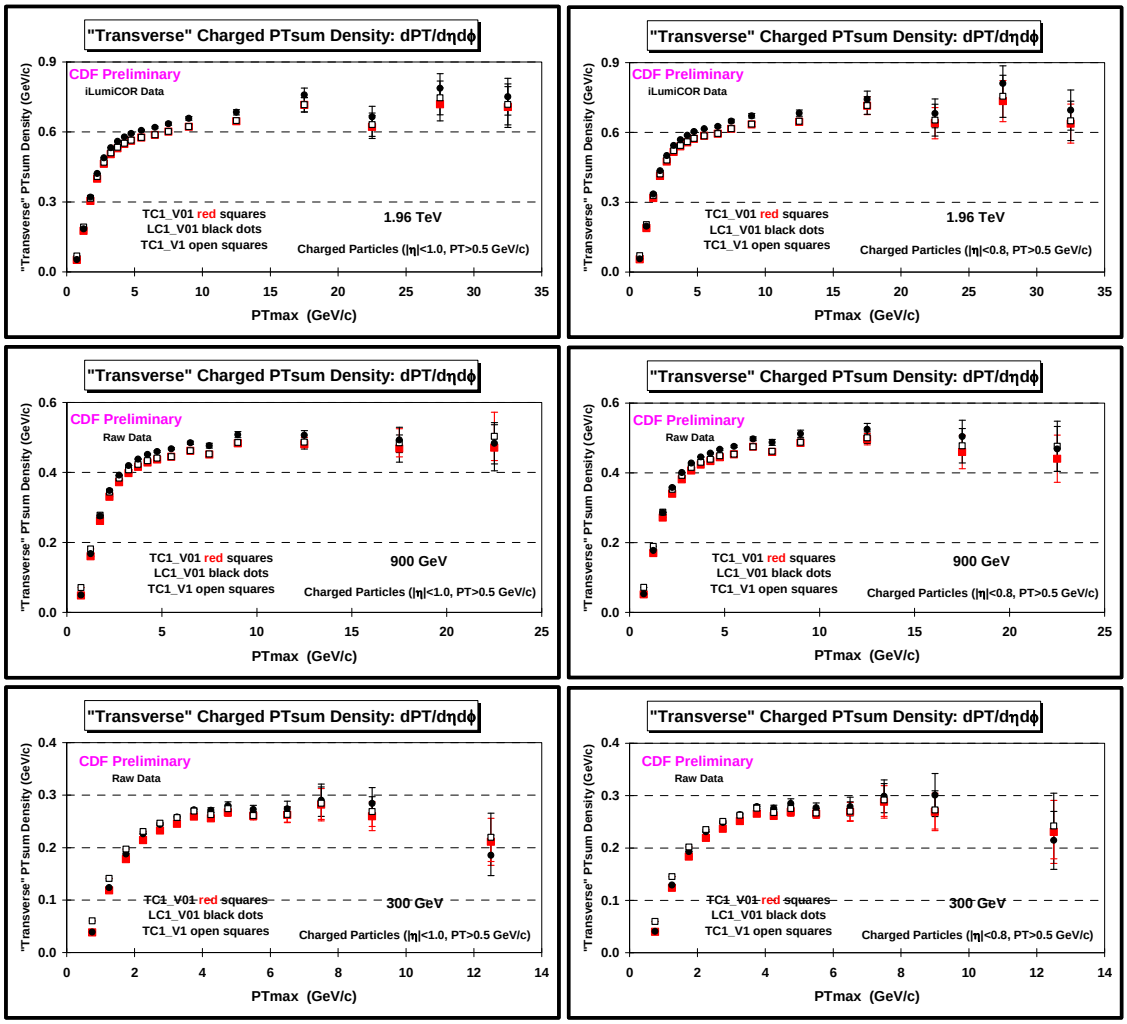

Fig. 10. (*top row*) Shows the pile-up corrected data (TC1_V01, LC1_V01, TC1_V1) on the "transverse" charged PTsum density at 1.96 TeV as defined by the leading charged particle, PTmax, as a function of PTmax. (*middle row*) Shows the raw data (TC1_V01, LC1_V01, TC1_V1) on the "transverse" charged PTsum density at 900 GeV as defined by the leading charged particle, PTmax, as a function of PTmax. (*bottom row*) Shows the raw data (TC1_V01, LC1_V01, TC1_V1) on the "transverse" charged PTsum density at 300 GeV as defined by the leading charged particle, PTmax, as a function of PTmax. The charged particles have $p_T > 0.5$ GeV and $|\eta| < 1.0$ (*left column*) and $|\eta| < 0.8$ (*right column*).

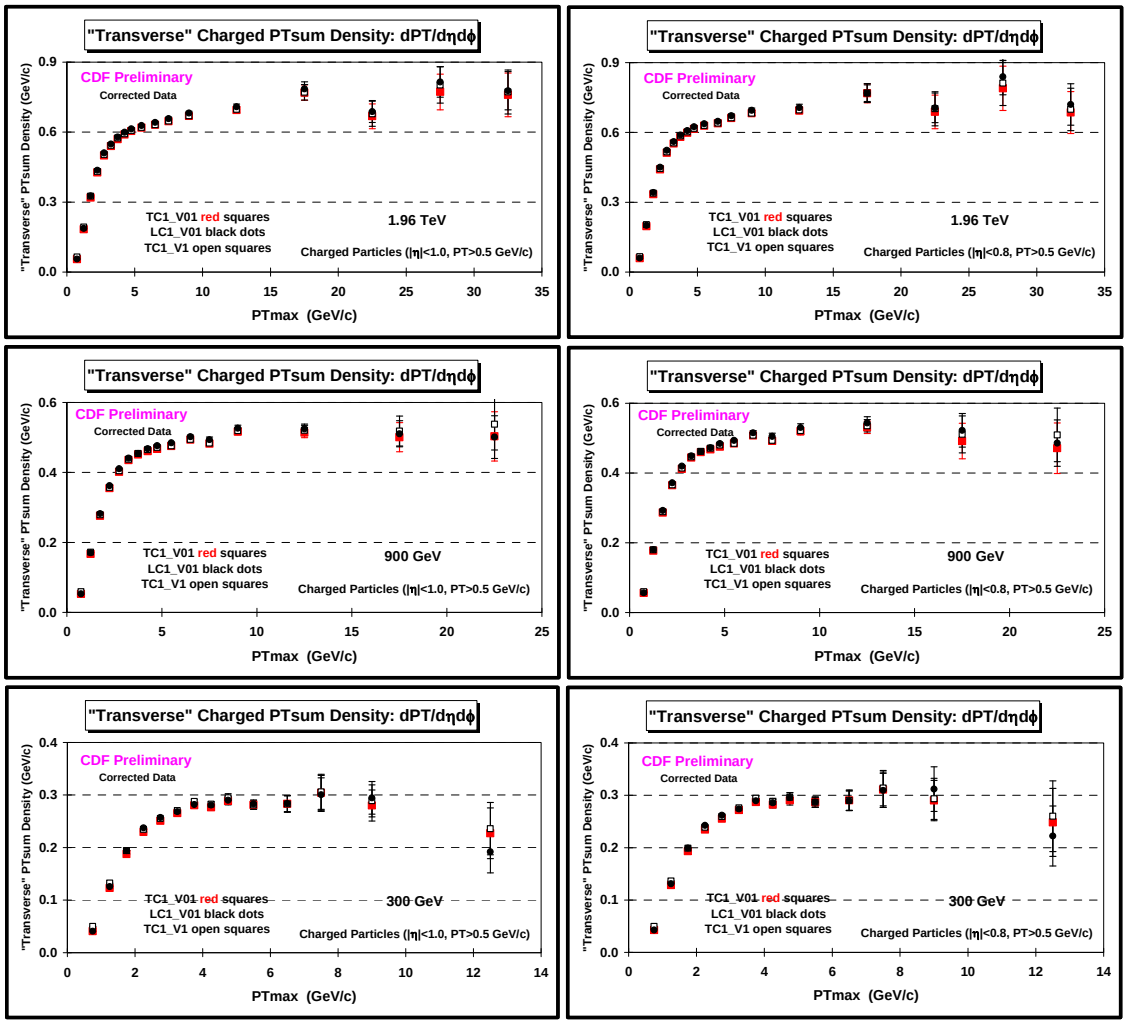

Fig. 11. Shows the corrected data (TC1_V01, LC1_V01, TC1_V1) on the "transverse" charged PTsum density at 1.96 TeV (*top row*), 900 GeV (*middle row*), and 300 GeV (*bottom row*) as defined by the leading charged particle, PTmax, as a function of PTmax. The charged particles have $p_T > 0.5$ GeV and $|\eta| < 1.0$ (*left column*) and $|\eta| < 0.8$ (*right column*).

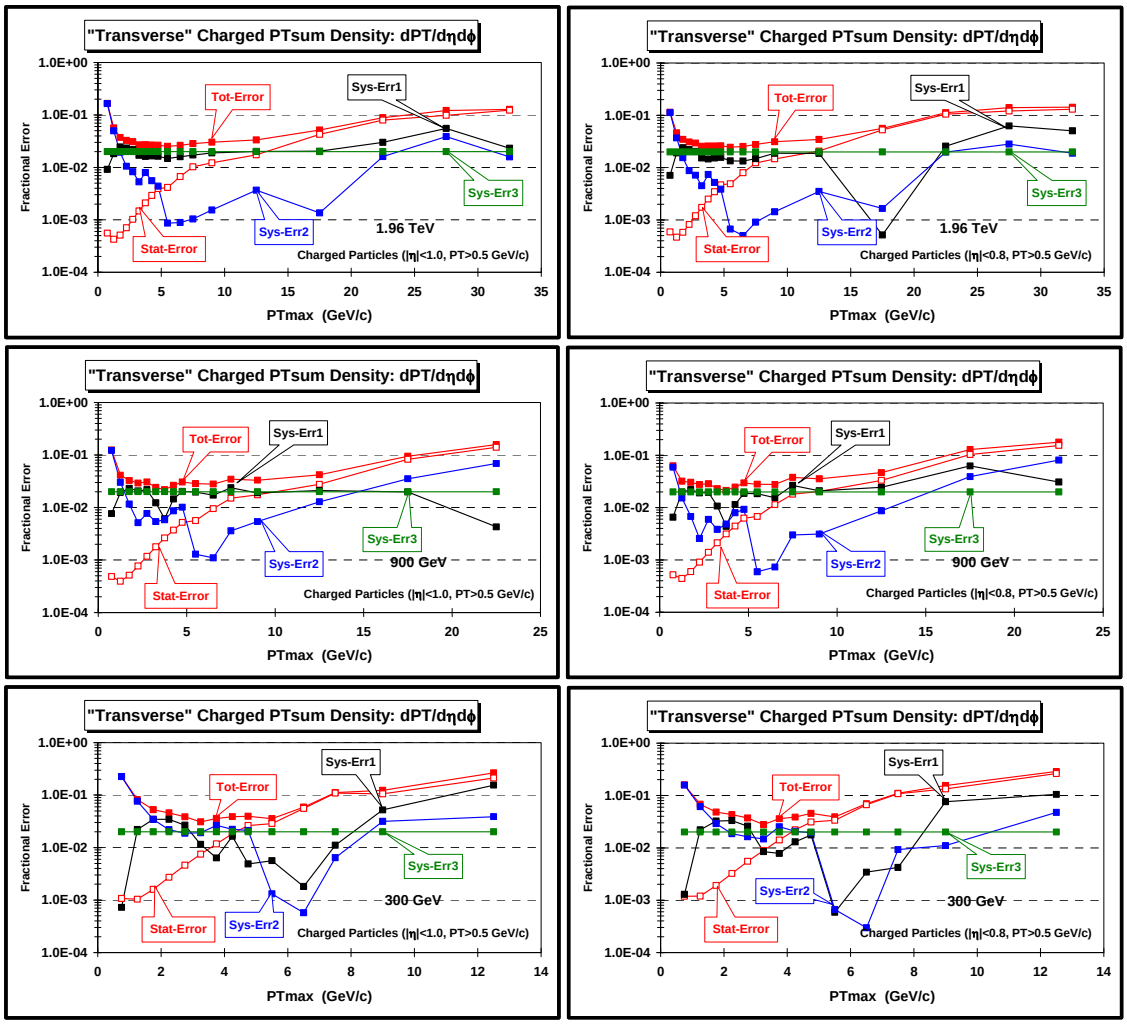

Fig. 12. Shows the fractional statistical and systematic errors on the "transverse" charged PTsum density at 1.96 TeV (*top row*), 900 GeV (*middle row*), and 300 GeV (*bottom row*) as defined by the leading charged particle, PTmax, as a function of PTmax. Stat-Error is the statistical error, Sys-Err1 = |LC1_V01 – TC1_V01|/TC1_V01, Sys-Err2 = |TC1_V01 – TC1_V1|/TC1_V01, and Sys-Err3 = 2%. The overall total error (Tot-Error) results from adding statistical error in quadrature with the three systematic errors. The charged particles have $p_T > 0.5$ GeV and $|\eta| < 1.0$ (*left column*) and $|\eta| < 0.8$ (*right column*).

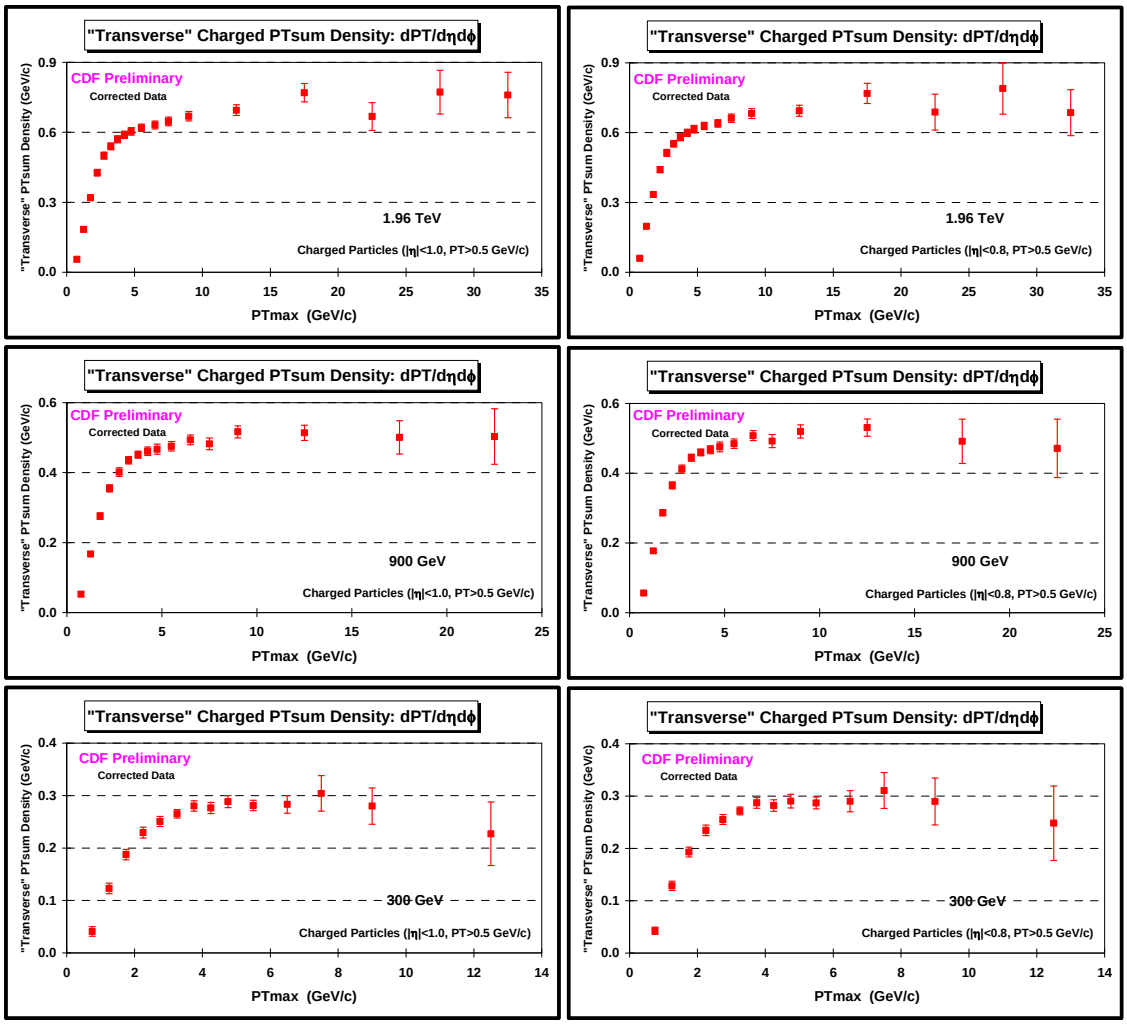

Fig. 13. Data at 1.96 TeV (*top row*), 900 GeV (*middle row*), and 300 GeV (*bottom row*) on the "transverse" charged PTsum density as defined by the leading charged particle, PTmax, as a function of PTmax. The data are corrected to the particle level with errors that include both the statistical error and the systematic uncertainty. The charged particles have $p_T > 0.5$ GeV and $|\eta| < 1.0$ (*left column*) and $|\eta| < 0.8$ (*right column*).

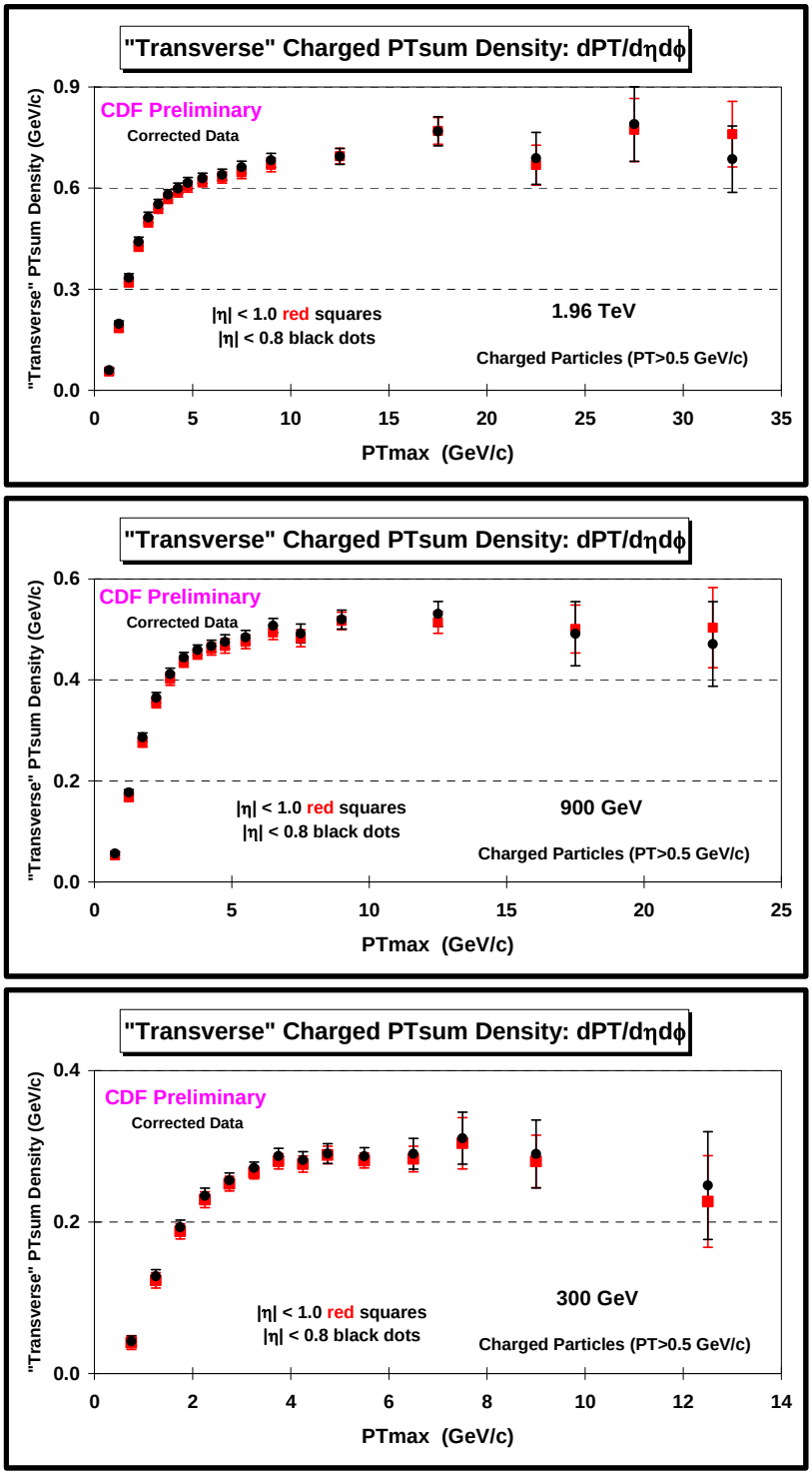

Fig. 14. Data at 1.96 TeV (*top*), 900 GeV (*middle*), and 300 GeV (*bottom*) on the "transverse" charged PTsum density as defined by the leading charged particle, PTmax, as a function of PTmax. The data are corrected to the particle level with errors that include both the statistical error and the systematic uncertainty. The charged particles have $p_T > 0.5$ GeV and $|\eta| < 1.0$ (*red squares*) and $|\eta| < 0.8$ (*black dots*).

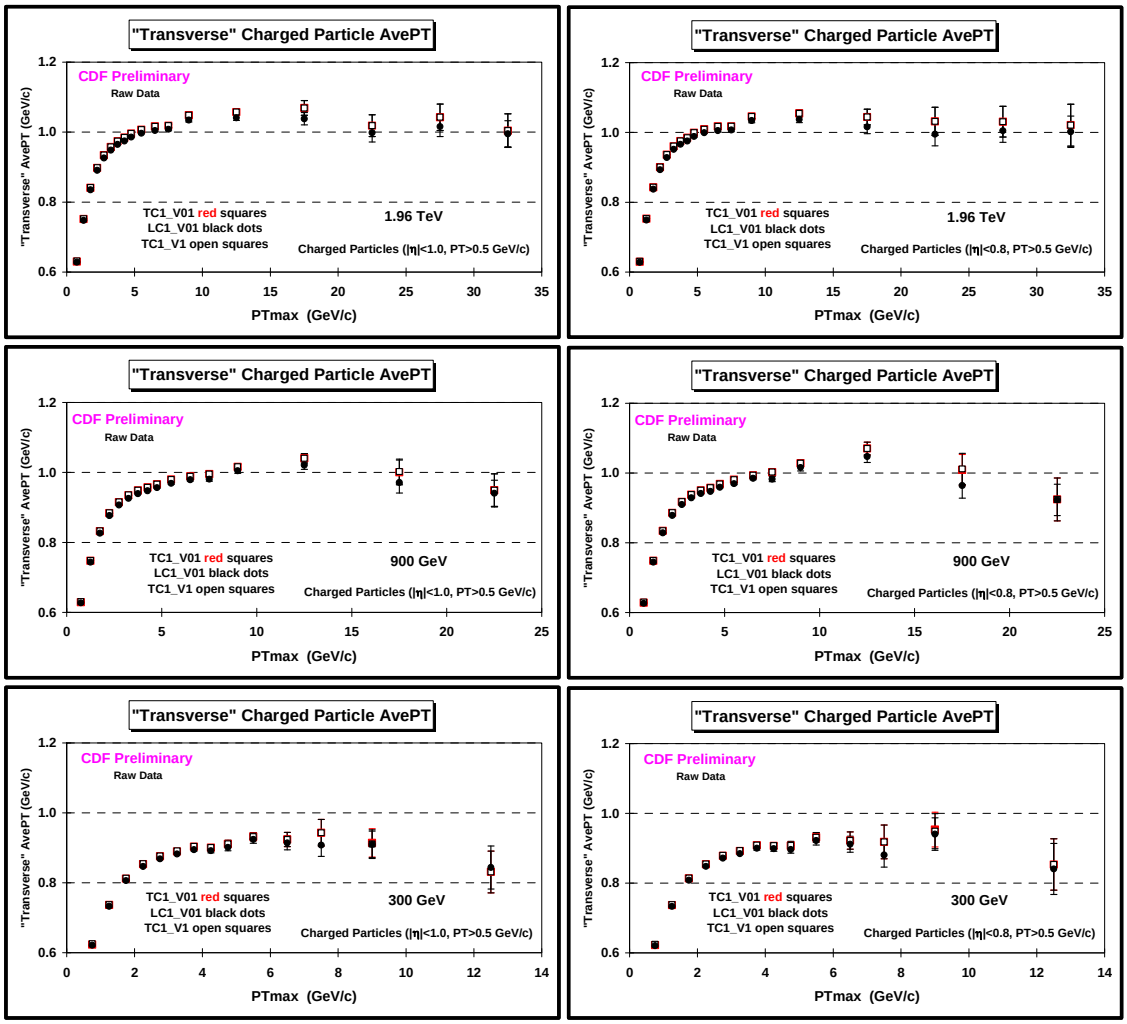

Fig. 15. Shows the raw uncorrected data (TC1_V01, LC1_V01, TC1_V1) on the "transverse" charged particle average p_T at 1.96 TeV (*top row*), 900 GeV (*middle row*), and 300 GeV (*bottom row*) as defined by the leading charged particle, PTmax, as a function of PTmax. The charged particles have $p_T > 0.5$ GeV and $|\eta| < 1.0$ (*left column*) and $|\eta| < 0.8$ (*right column*).

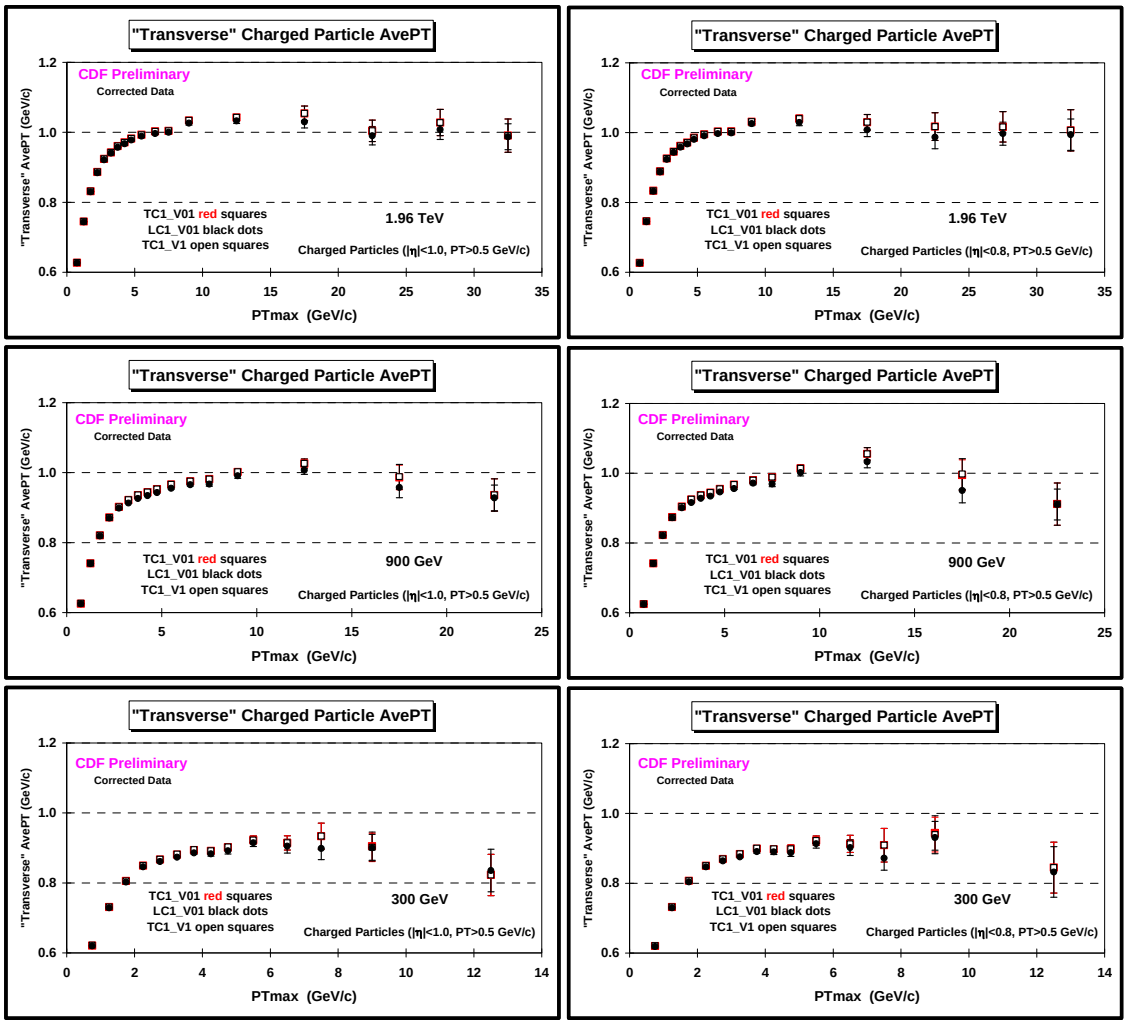

Fig. 16. Shows the corrected data (TC1_V01, LC1_V01, TC1_V1) on the "transverse" charged particle average p_T at 1.96 TeV (*top row*), 900 GeV (*middle row*), and 300 GeV (*bottom row*) as defined by the leading charged particle, PTmax, as a function of PTmax. The charged particles have $p_T > 0.5$ GeV and $|\eta| < 1.0$ (*left column*) and $|\eta| < 0.8$ (*right column*).

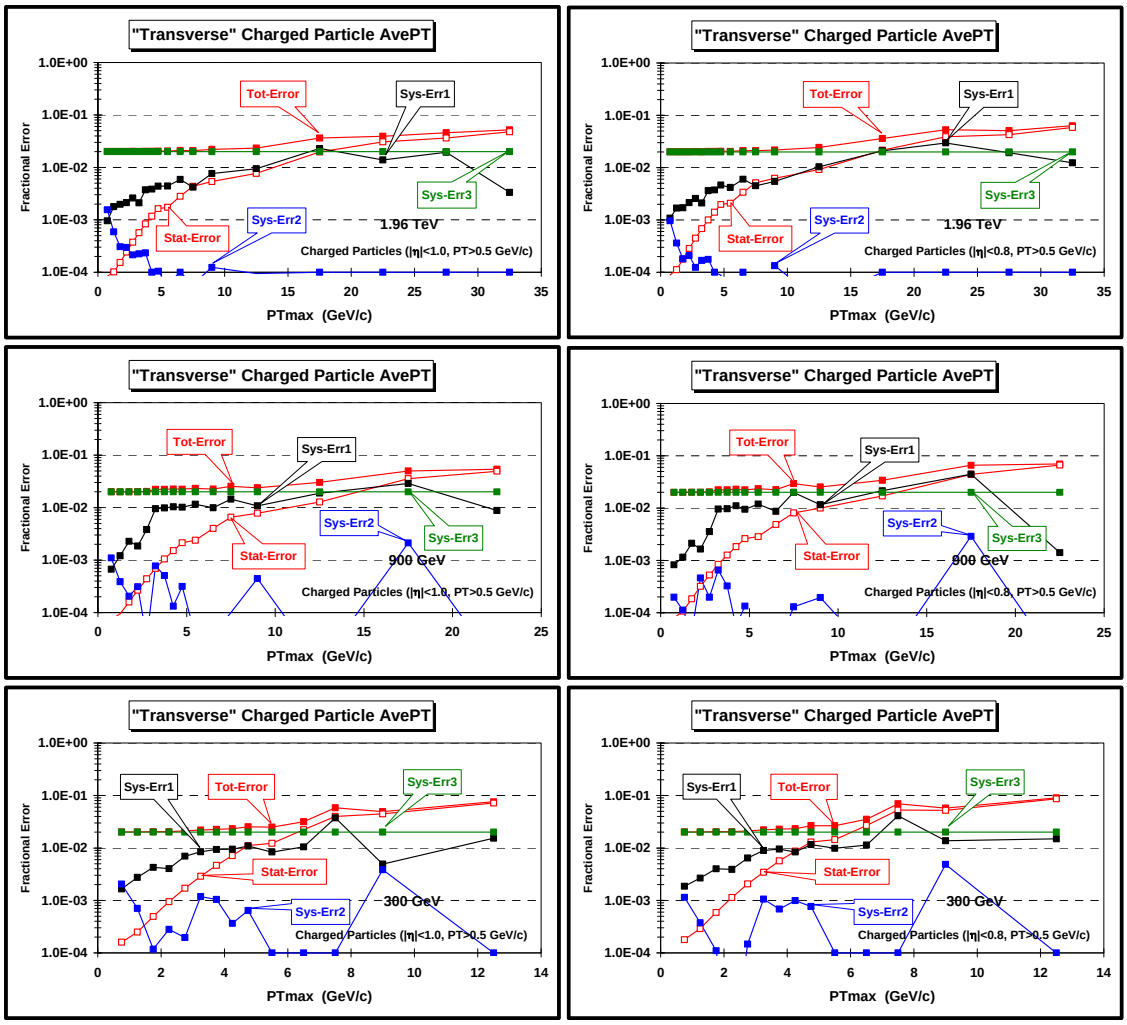

Fig. 17. Shows the fractional statistical and systematic errors on the "transverse" charged particle average p_T at 1.96 TeV (*top row*), 900 GeV (*middle row*), and 300 GeV (*bottom row*) as defined by the leading charged particle, PTmax, as a function of PTmax. Stat-Error is the statistical error, Sys-Err1 = |LC1_V01 – TC1_V01|/TC1_V01, Sys-Err2 = |TC1_V01 – TC1_V1|/TC1_V01, and Sys-Err3 = 2%. The overall total error (Tot-Error) results from adding statistical error in quadrature with the three systematic errors. The charged particles have $p_T > 0.5$ GeV and $|\eta| < 1.0$ (*left column*) and $|\eta| < 0.8$ (*right column*).

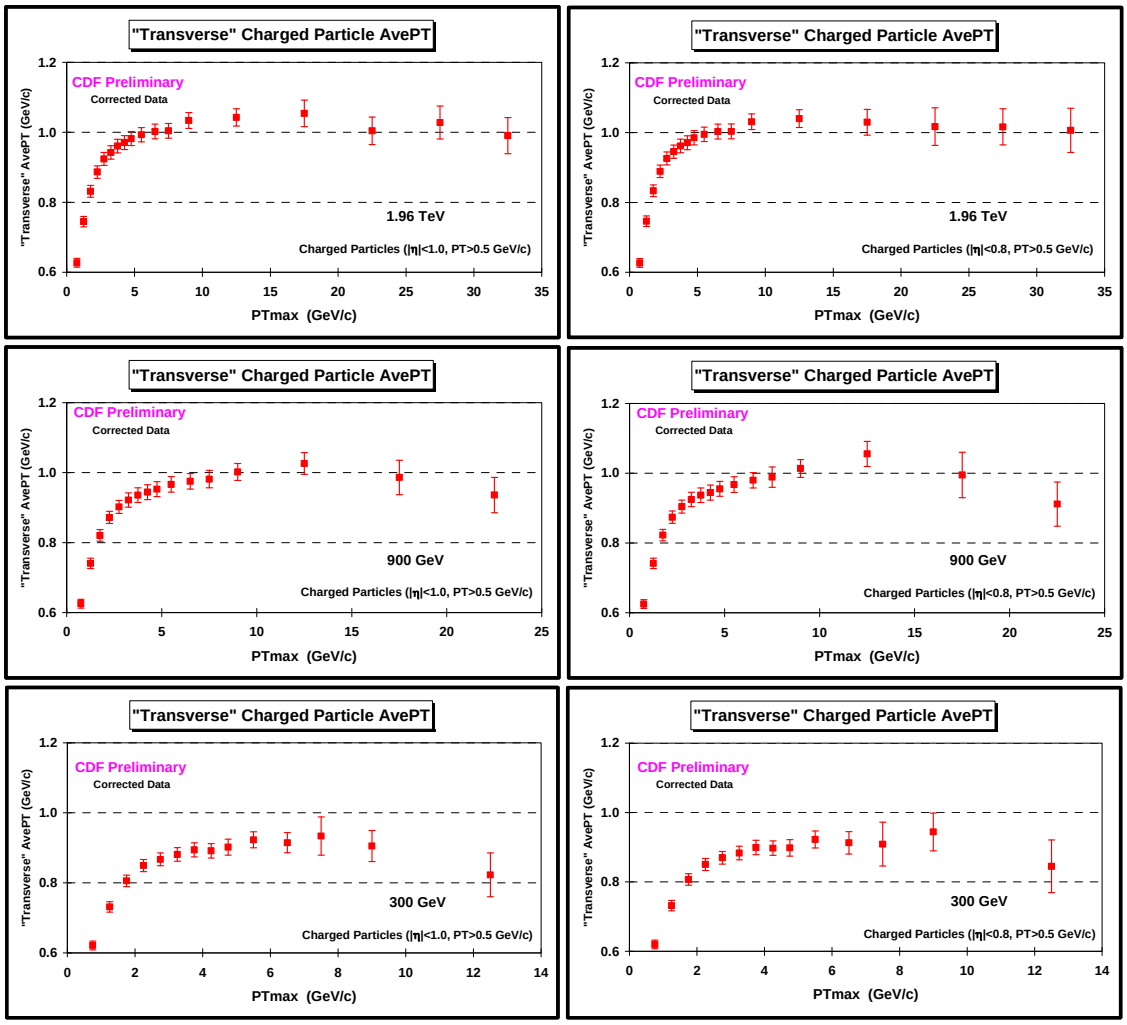

Fig. 18. Data at 1.96 TeV (*top row*), 900 GeV (*middle row*), and 300 GeV (*bottom row*) on the "transverse" charged particle average p_T as defined by the leading charged particle, PTmax, as a function of PTmax. The data are corrected to the particle level with errors that include both the statistical error and the systematic uncertainty. The charged particles have $p_T > 0.5$ GeV and $|\eta| < 1.0$ (*left column*) and $|\eta| < 0.8$ (*right column*).

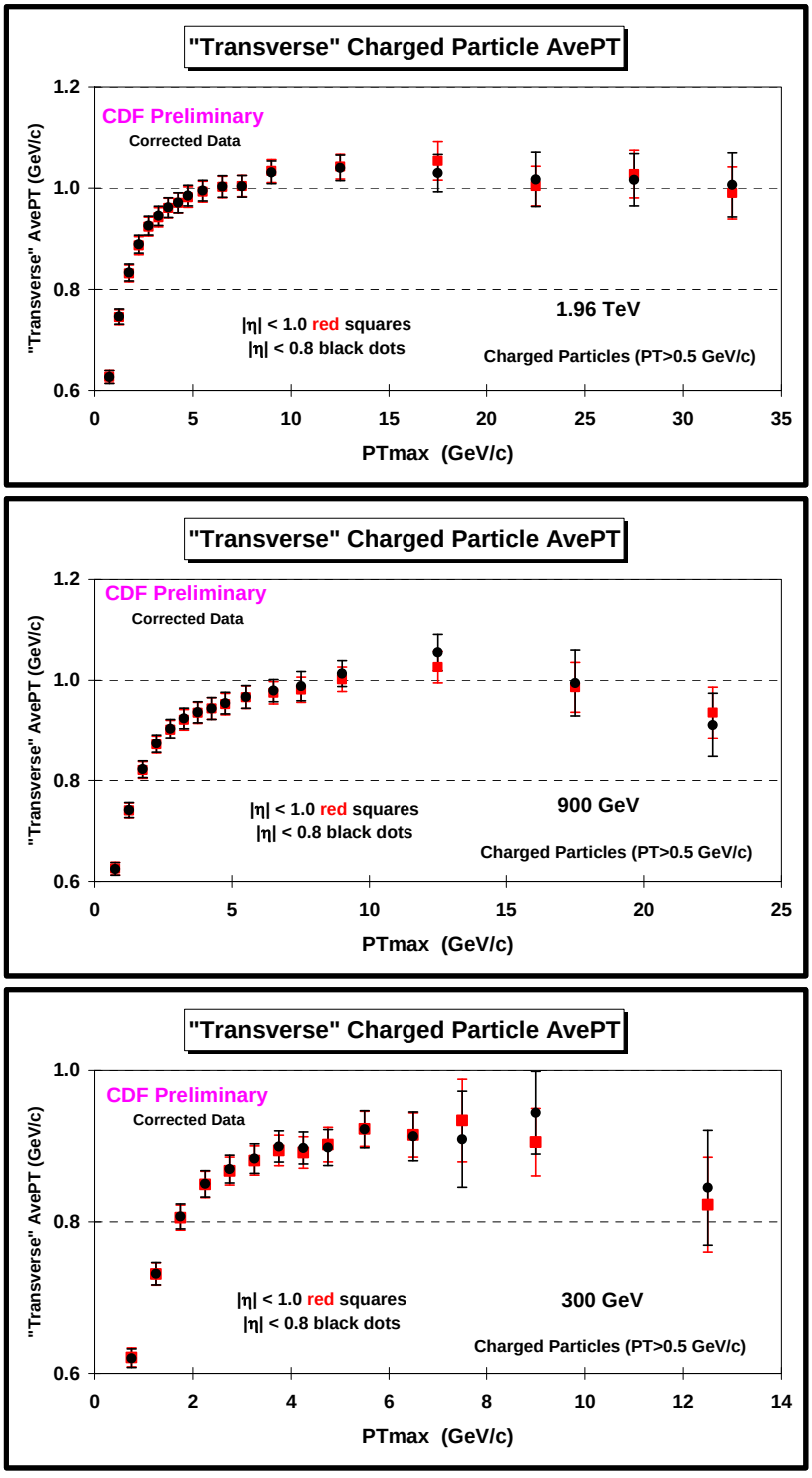

Fig. 19. Data at 1.96 TeV (*top*), 900 GeV (*middle*), and 300 GeV (*bottom*) on the "transverse" charged particle average p_T as defined by the leading charged particle, PTmax, as a function of PTmax. The data are corrected to the particle level with errors that include both the statistical error and the systematic uncertainty. The charged particles have $p_T > 0.5$ GeV and $|\eta| < 1.0$ (*red squares*) and $|\eta| < 0.8$ (*black dots*).

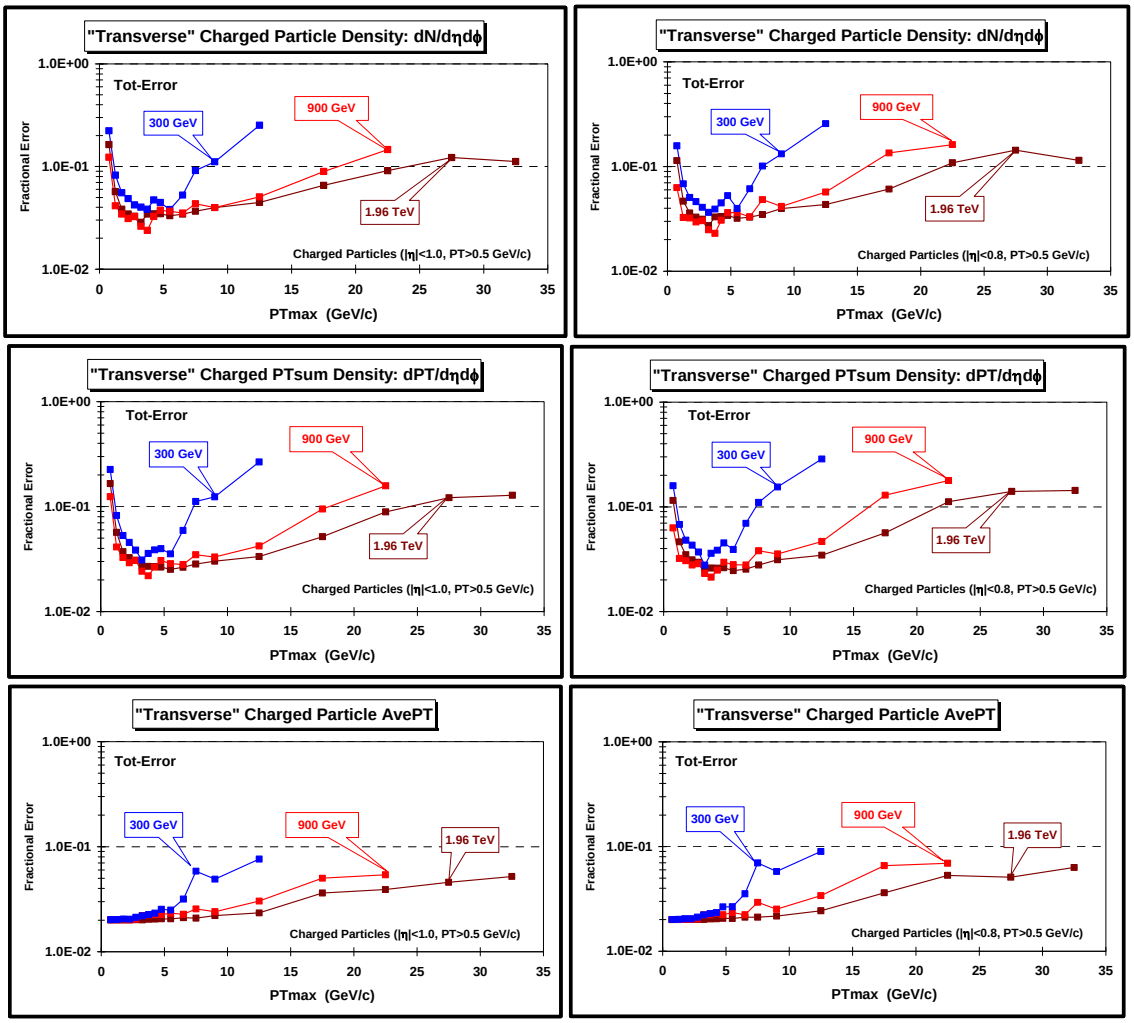

Fig. 20. Percentage total fractional errors for the data at 1.96 TeV, 900 GeV, and 300 GeV on the "transverse" charged particle density (*top row*), the "transverse" charged PTsum density (*bottom row*), and the "transverse" charged particle average p_T (*bottom row*) as defined by the leading charged particle, PTmax, as a function of PTmax. The charged particles have $p_T > 0.5$ GeV and $|\eta| < 1.0$ (*left column*) and $|\eta| < 0.8$ (*right column*).

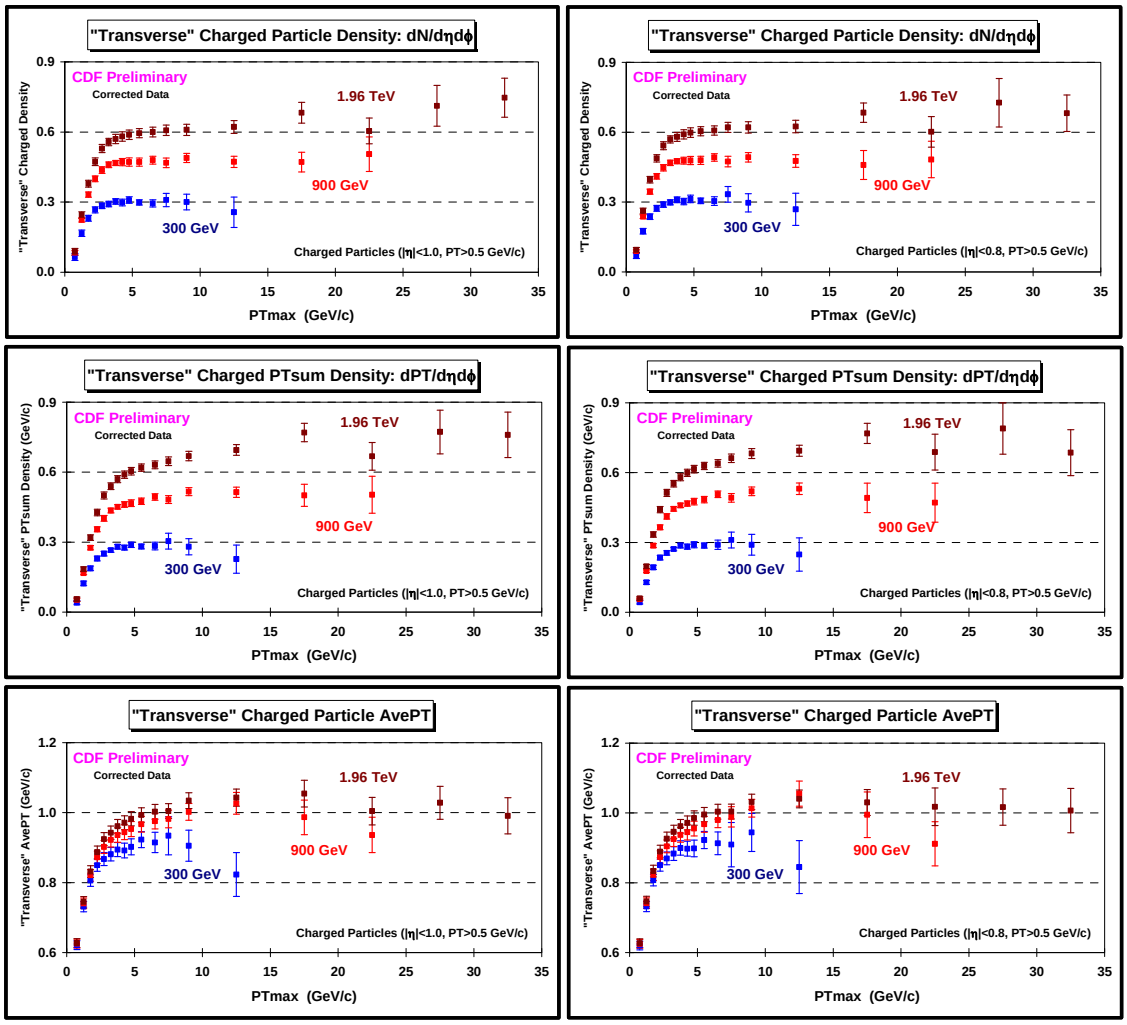

Fig. 21. Data at 1.96 TeV, 900 GeV, and 300 GeV on the "transverse" charged particle density (*top row*), the "transverse" charged PTsum density (*middle row*), and the "transverse" charged particle average p_T (*bottom row*) as defined by the leading charged particle, PTmax, as a function of PTmax. The data are corrected to the particle level with errors that include both the statistical error and the systematic uncertainty. The charged particles have $p_T > 0.5$ GeV and $|\eta| < 1.0$ (*left column*) and $|\eta| < 0.8$ (*right column*).

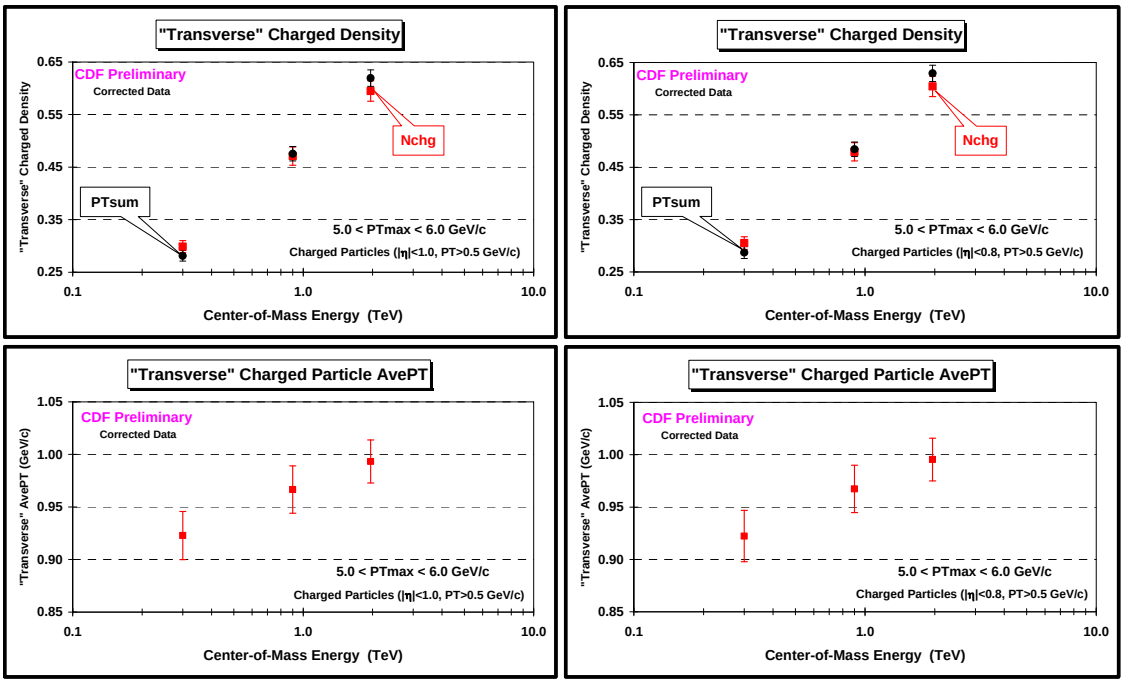

Fig. 22. (*top row*) Data at 1.96 TeV, 900 GeV, and 300 GeV on the "transverse" charged particle density and the "transverse" charged PTsum density as defined by the leading charged particle, PTmax, for 5.0 < PTmax < 6.0 GeV/c plotted versus the center-of-mass energy (on a log scale). (*bottom row*) Data at 1.96 TeV, 900 GeV, and 300 GeV on the "transverse" charged particle average p_T as defined by the leading charged particle, PTmax, for 5.0 < PTmax < 6.0 GeV/c plotted versus the center-of-mass energy (on a log scale). The charged particles have $p_T > 0.5$ GeV and $|\eta| < 1.0$ (*left column*) and $|\eta| < 0.8$ (*right column*).

Figure 23 compares directly the CDF results on the "transverse" charged particle and charged PTsum densities at 900 GeV for $\eta_{cut} = 0.8$ with the LHC results. The CDF, ATLAS, ALICE, and CMS results are all nearly the same, however, the CDF results are slightly higher in the "turn on" region (*i.e.* the approach to the "plateau"). Remember, the CDF results are for proton-antiproton collisions, while the LHC studies are for proton-proton collisions. Nevertheless, the QCD Monte-Carlo models predict that the "transverse" charged particle and charged PTsum densities are identical in proton-antiproton and proton-proton at the same center-of-mass energy.

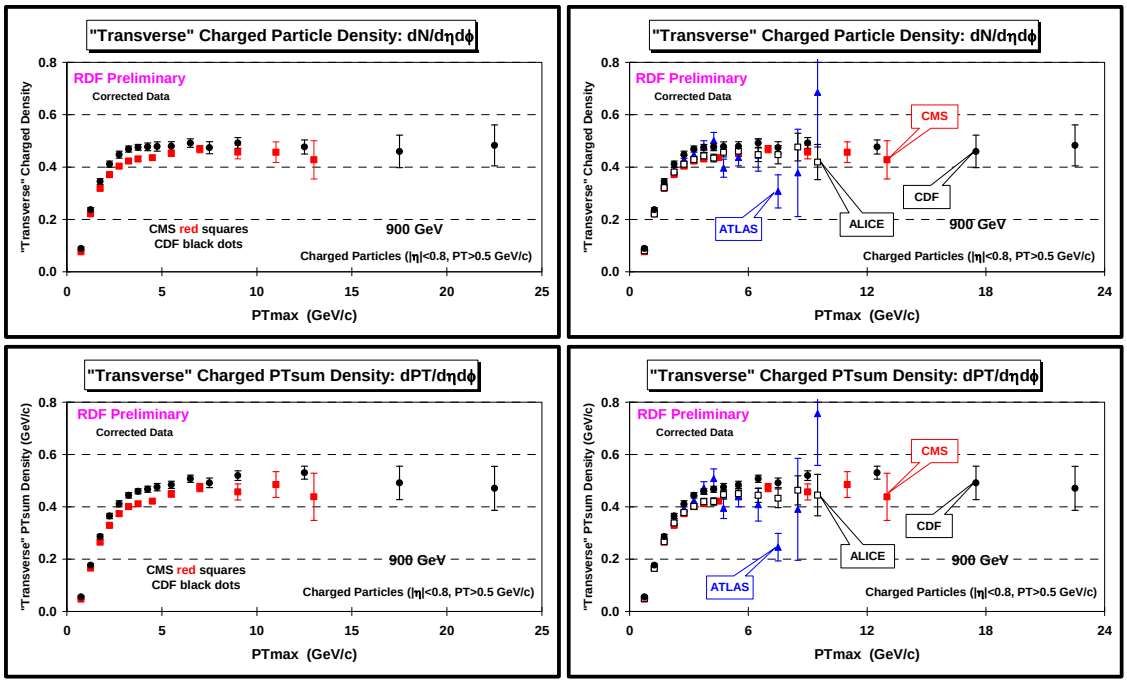

Fig. 23. CDF data (*black dots*) at 900 GeV on the "transverse" charged particle density (*top row*), and the "transverse" charged PTsum density (*bottom row*) as defined by the leading charged particle, PTmax, as a function of PTmax for charged particles with $p_T > 0.5$ GeV/c and $|\eta| < 0.8$. The data are corrected to the particle level with errors that include both the statistical error and the systematic uncertainty and are compared with the CMS data at 900 GeV (*left column*) and the CMS, ATLAS, and ALICE data at 900 GeV (*right column*).

(5) Center-of-Mass Energy Ratios

Figures 24, 25, and 26 show the bin-by-bin center-of-mass energy ratios for the "transverse" charged particle density, the "transverse" charged PTsum density, and the "transverse" charged particle average p_T, respectively. These ratios are determined by constructing the bin-by-bin ratio of the raw data for each of the three datasets TC1_V01, LC1_V01, and TC1_V1, and then correcting these ratios to the particle level using their corresponding "correction factors" (referred to as "corrected data ratio"). The systematic errors on the ratios are then determined from Table 6 and are added in quadrature with the statistical errors. Figures 27, 28, and 29 compare directly the corrected data ratios for $\eta_{cut} = 0.8$ and 1.0. Again, the results for these two η cuts are almost identical.

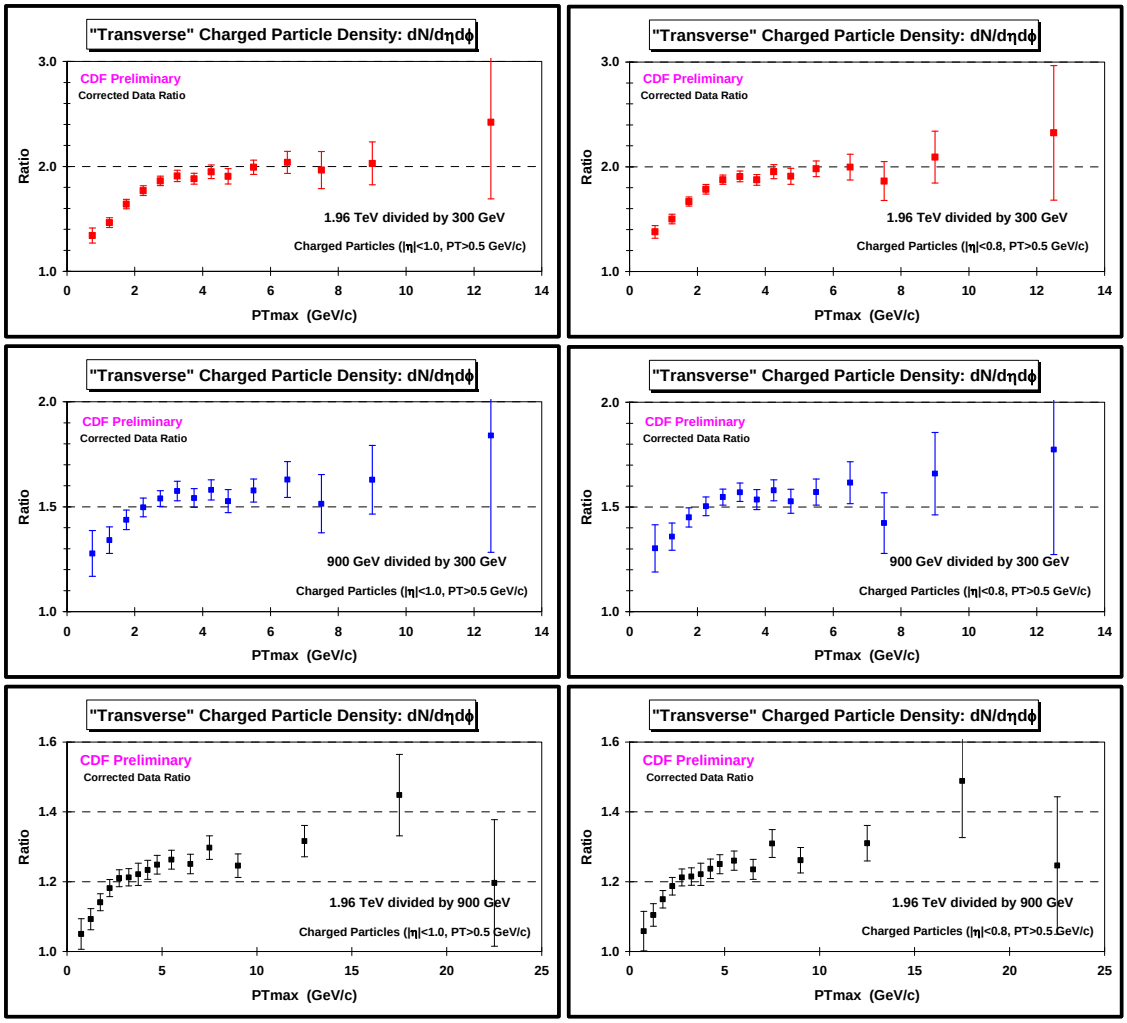

Fig. 24. (*top row*) Bin-by-bin ratio of the data at 1.96 TeV and 300 GeV on the "transverse" charged particle density as defined by the leading charged particle, PTmax, as a function of PTmax. (*middle row*) Bin-by-bin ratio of the data at 900 GeV and 300 GeV on the "transverse" charged particle density as defined by the leading charged particle, PTmax, as a function of PTmax. (*bottom row*) Bin-by-bin ratio of the data at 1.96 TeV and 900 GeV on the "transverse" charged particle density as defined by the leading charged particle, PTmax, as a function of PTmax. The charged particles have $p_T > 0.5$ GeV and $|\eta| < 1.0$ (*left column*) and $|\eta| < 0.8$ (*right column*).

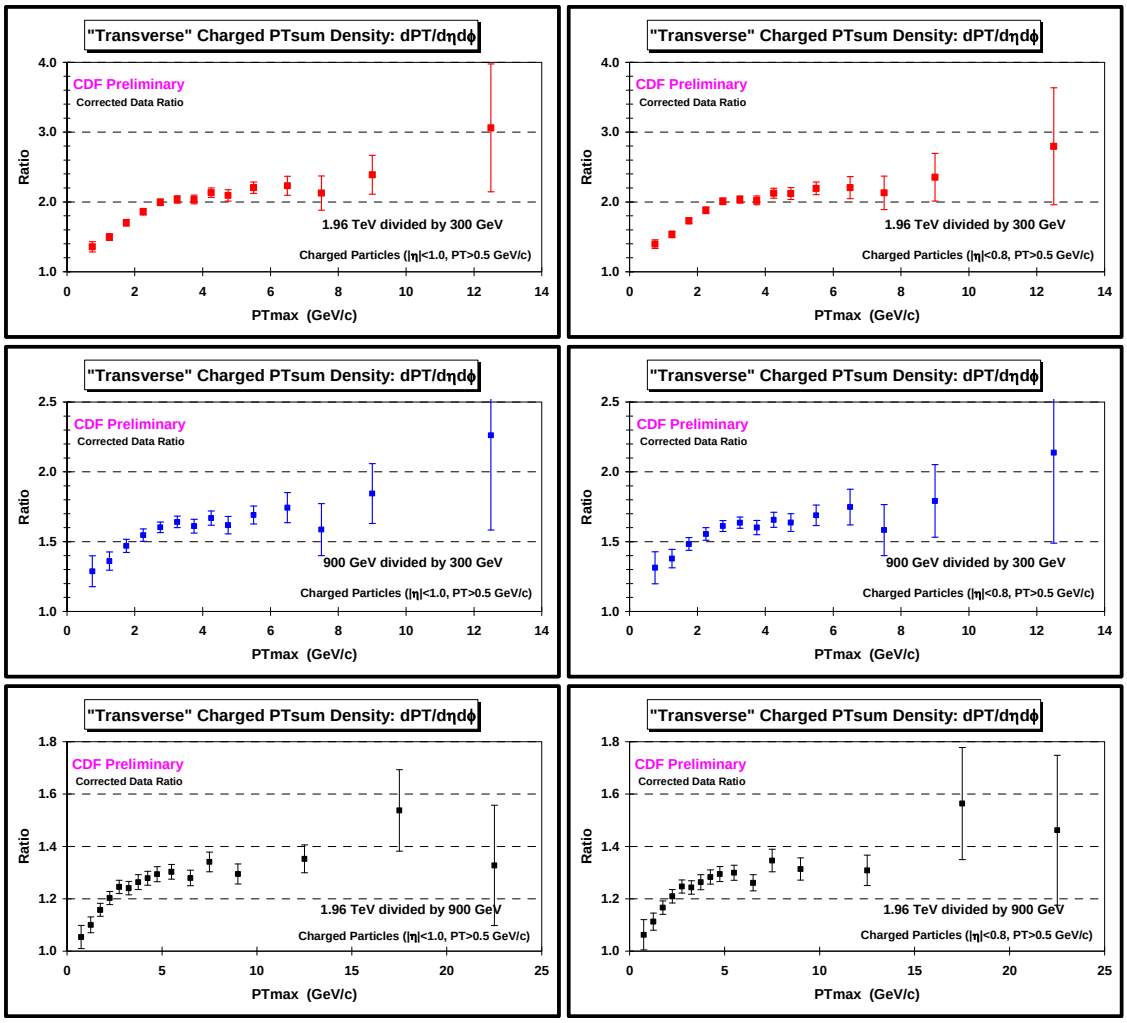

Fig. 25. (*top row*) Bin-by-bin ratio of the data at 1.96 TeV and 300 GeV on the "transverse" charged PTsum density as defined by the leading charged particle, PTmax, as a function of PTmax. (*middle row*) Bin-by-bin ratio of the data at 900 GeV and 300 GeV on the "transverse" charged PTsum density as defined by the leading charged particle, PTmax, as a function of PTmax. (*bottom row*) Bin-by-bin ratio of the data at 1.96 TeV and 900 GeV on the "transverse" charged PTsum density as defined by the leading charged particle, PTmax, as a function of PTmax. The charged particles have $p_T > 0.5$ GeV and $|\eta| < 1.0$ (*left column*) and $|\eta| < 0.8$ (*right column*).

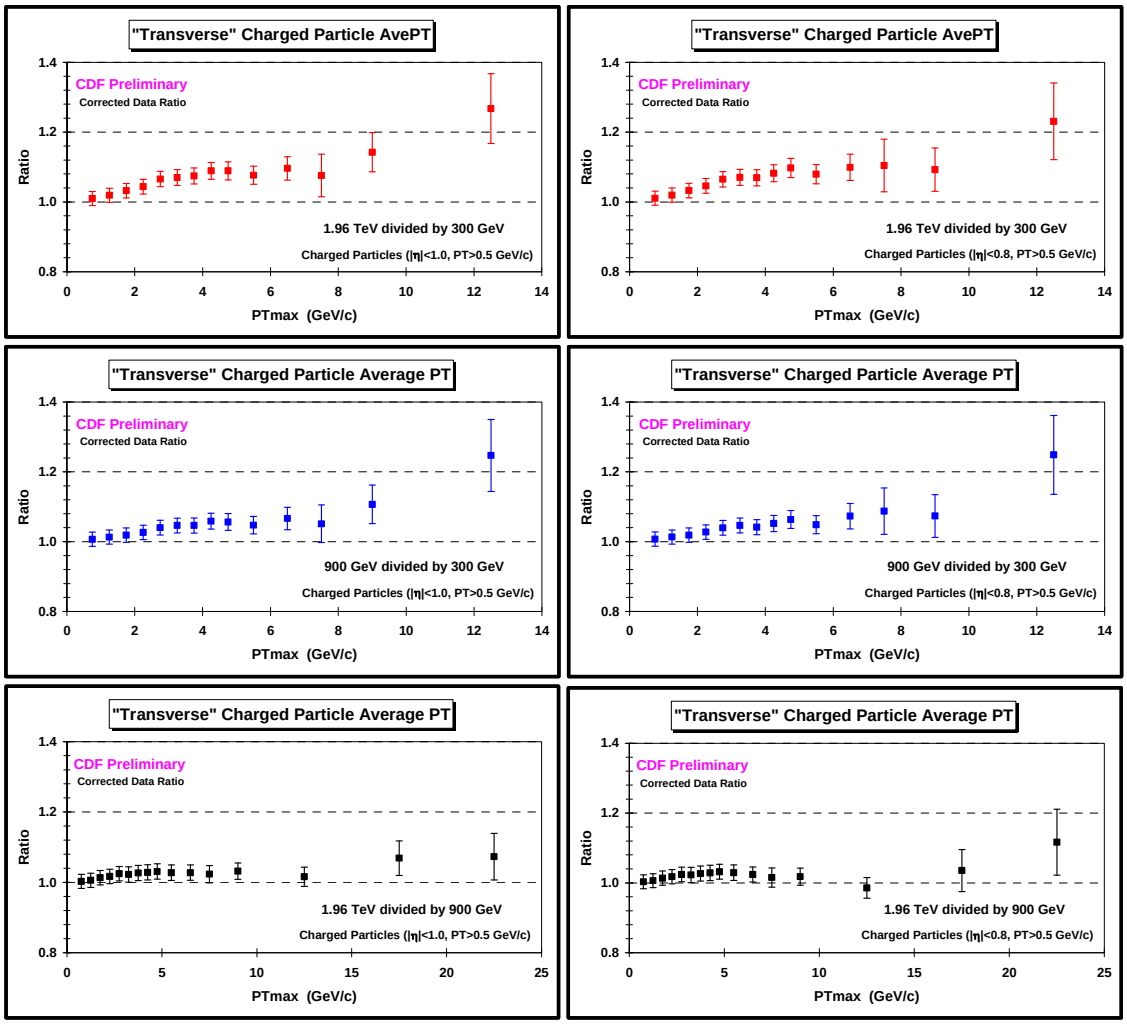

Fig. 26. (*top row*) Bin-by-bin ratio of the data at 1.96 TeV and 300 GeV on the "transverse" charged particle average p_T as defined by the leading charged particle, PTmax, as a function of PTmax. (*middle row*) Bin-by-bin ratio of the data at 900 GeV and 300 GeV on the "transverse" charged particle average p_T as defined by the leading charged particle, PTmax, as a function of PTmax. (*bottom row*) Bin-by-bin ratio of the data at 1.96 TeV and 900 GeV on the "transverse" charged particle average p_T as defined by the leading charged particle, PTmax, as a function of PTmax. The charged particles have $p_T > 0.5$ GeV and $|\eta| < 1.0$ (*left column*) and $|\eta| < 0.8$ (*right column*).

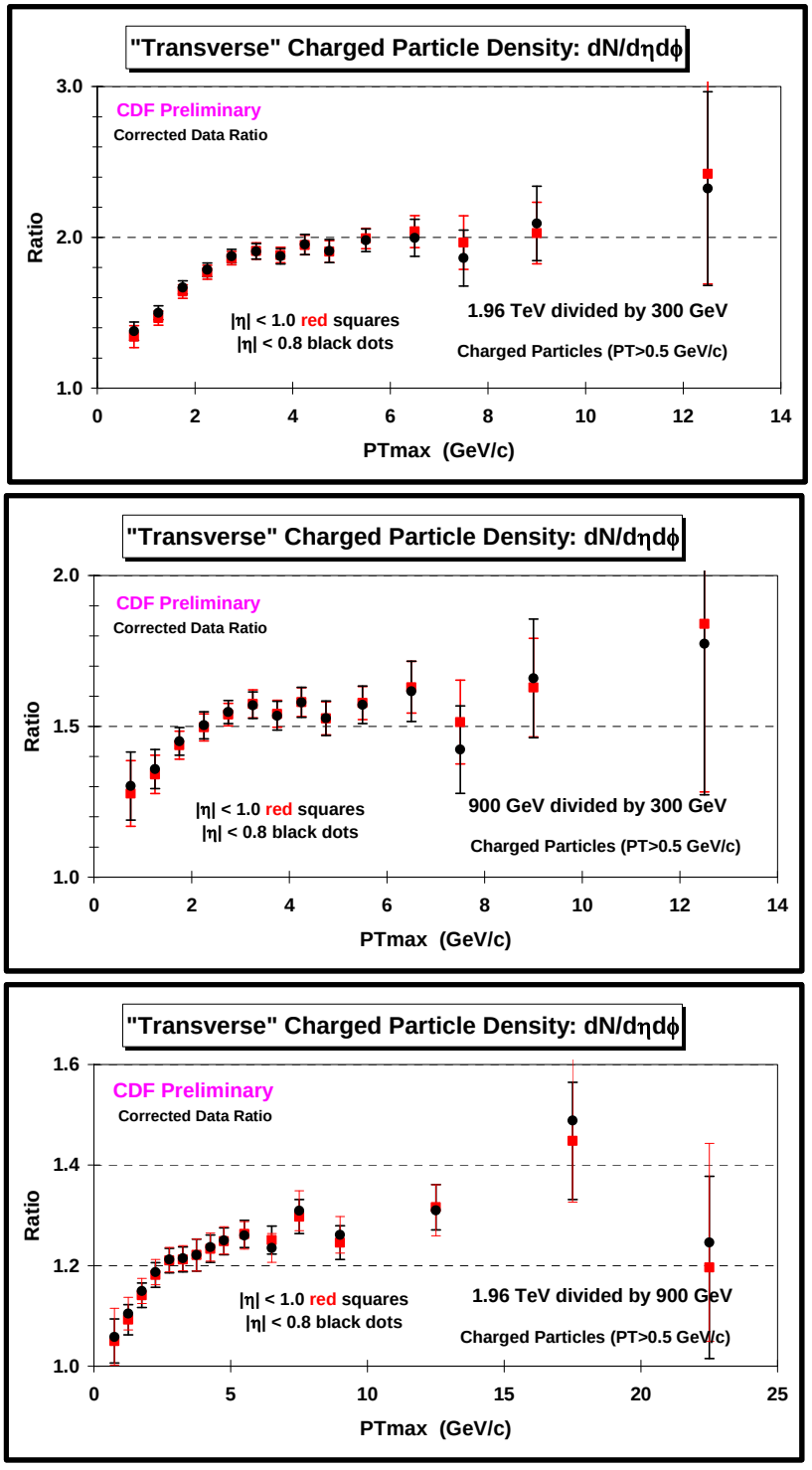

Fig. 27. (*top*) Bin-by-bin ratio of the data at 1.96 TeV and 300 GeV on the "transverse" charged particle density as defined by the leading charged particle, PTmax, as a function of PTmax. (*middle*) Bin-by-bin ratio of the data at 900 GeV and 300 GeV on the "transverse" charged particle density as defined by the leading charged particle, PTmax, as a function of PTmax. (*bottom*) Bin-by-bin ratio of the data at 1.96 TeV and 900 GeV on the "transverse" charged particle density as defined by the leading charged particle, PTmax, as a function of PTmax. The charged particles have $p_T > 0.5$ GeV and $|\eta| < 1.0$ (*red squares*) and $|\eta| < 0.8$ (*black dots*).

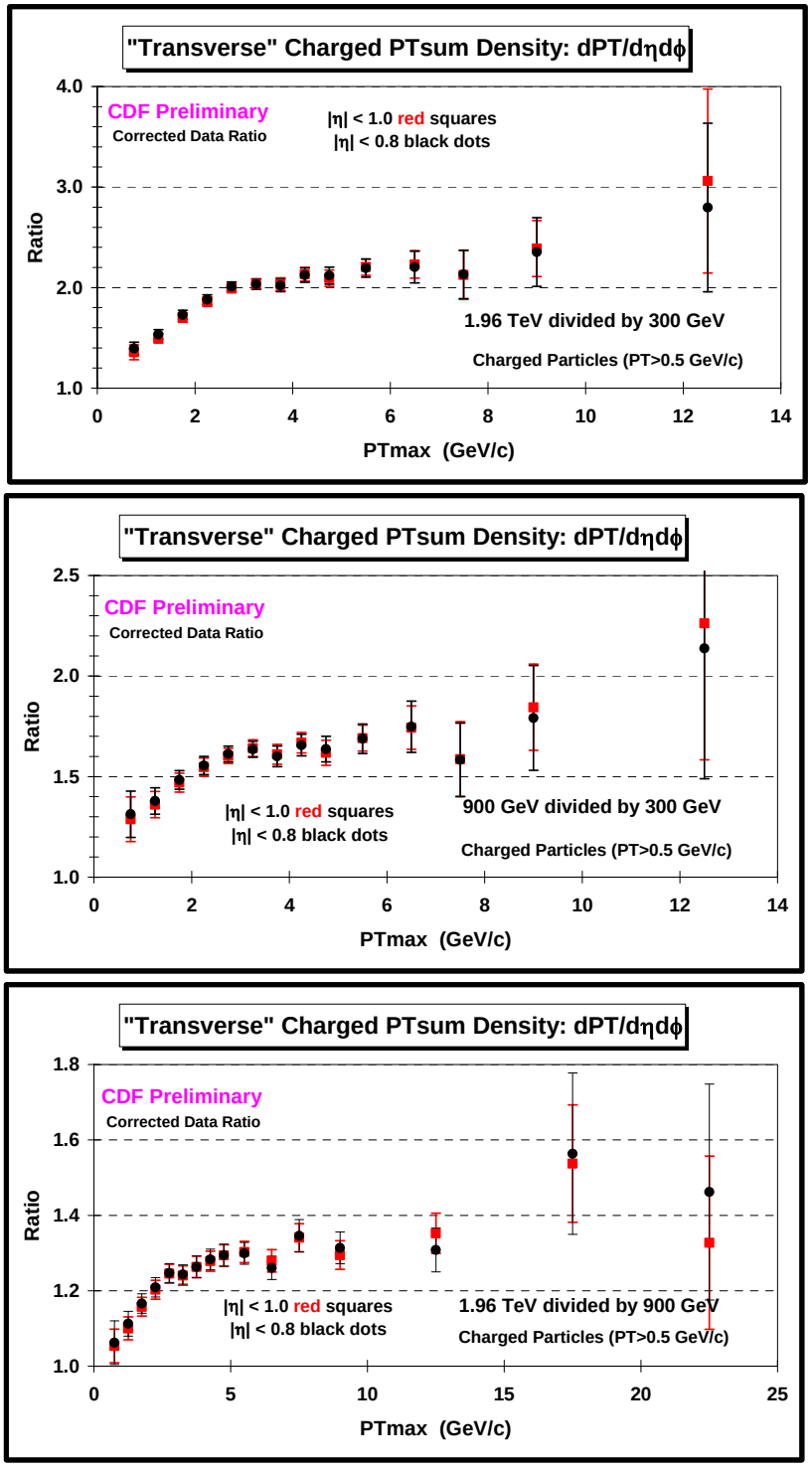

Fig. 28. (*top*) Bin-by-bin ratio of the data at 1.96 TeV and 300 GeV on the "transverse" charged PTsum density as defined by the leading charged particle, PTmax, as a function of PTmax. (*middle*) Bin-by-bin ratio of the data at 900 GeV and 300 GeV on the "transverse" charged PTsum density as defined by the leading charged particle, PTmax, as a function of PTmax. (*bottom*) Bin-by-bin ratio of the data at 1.96 TeV and 900 GeV on the "transverse" charged PTsum density as defined by the leading charged particle, PTmax, as a function of PTmax. The left column are the bin-by-bin ratio of the corrected data. The right column are the corrected bin-by-bin data ratios. The charged particles have $p_T > 0.5$ GeV and $|\eta| < 1.0$ (*red squares*) and $|\eta| < 0.8$ (*black dots*).

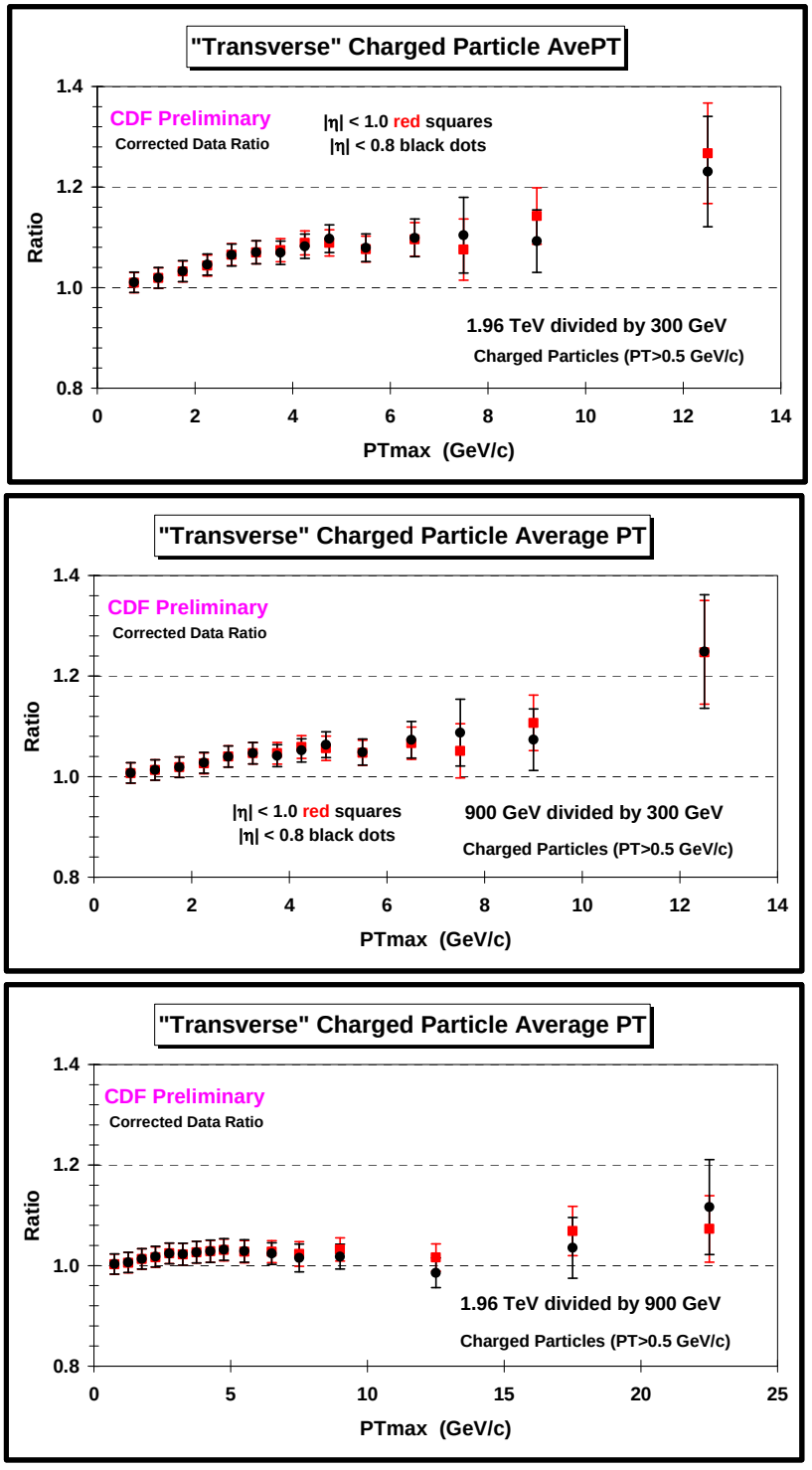

Fig. 29. (*top*) Bin-by-bin ratio of the data at 1.96 TeV and 300 GeV on the "transverse" charged particle average p_T as defined by the leading charged particle, PTmax, as a function of PTmax. (*middle*) Bin-by-bin ratio of the data at 900 GeV and 300 GeV on the "transverse" charged particle average p_T as defined by the leading charged particle, PTmax, as a function of PTmax. (*bottom*) Bin-by-bin ratio of the data at 1.96 TeV and 900 GeV on the "transverse" charged particle average p_T as defined by the leading charged particle, PTmax, as a function of PTmax. The left column are the bin-by-bin ratio of the corrected data. The right column are the corrected bin-by-bin data ratios. The charged particles have $p_T > 0.5$ GeV and $|\eta| < 1.0$ (*red squares*) and $|\eta| < 0.8$ (*black dots*).

(6) Charged Particle Pseudo-Rapidity Distributions

In order to compare with data from the LHC we construct the pseudo-rapidity distribution, dN/dη, for charged particles with $|\eta| < 0.8$ and $p_T > 0.5$ GeV/c or with $|\eta| < 0.8$ and $p_T > 1.0$ GeV/c for events with at least one charged particle with $|\eta| < 0.8$ and $p_T > 0.5$ GeV/c or $p_T > 1.0$ GeV/c, respectively. These plots were suggested by the MB&UE working group at the LHC Physics Center at CERN. The distributions correspond to the average number of charged particles per unit η and are normalized so that integral is equal to the overall average number of charged particles with $|\eta| < 0.8$ and $p_T > 0.5$ GeV/c or with $|\eta| < 0.8$ and $p_T > 1.0$ GeV/c for events with at least one charged particle with $|\eta| < 0.8$ and $p_T > 0.5$ GeV/c or $p_T > 1.0$ GeV/c, respectively, as follows:

$$N_{chg} = \int_{-0.8}^{0.8} \frac{dN}{d\eta} d\eta \qquad (1)$$

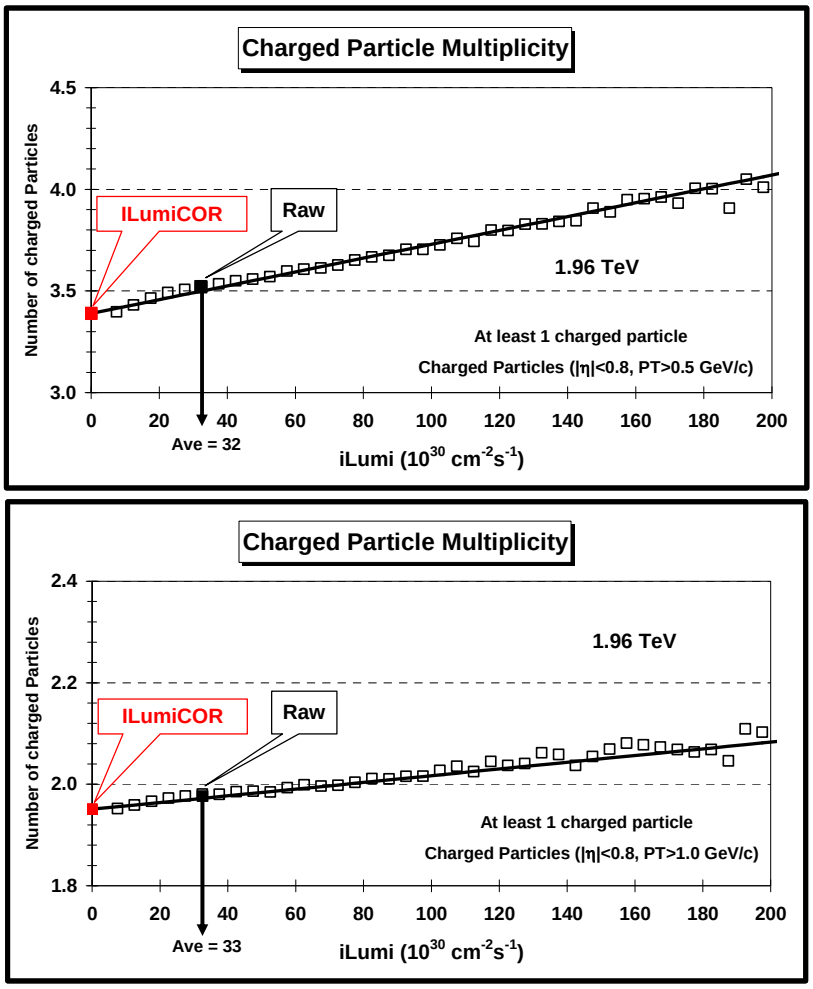

Fig. 30. Shows the raw data at 1.96 TeV (TC1_V01) on the average number of charged particles with $|\eta| < 0.8$ and $p_T > 0.5$ GeV/c (*top*) and $p_T > 1.0$ GeV/c (*bottom*) for events with at least one charged particle with $|\eta| < 0.8$ and $p_T > 0.5$ GeV/c or $p_T > 1.0$ GeV/c, respectively, plotted versus the instantaneous luminosity. The overall raw data point (solid black square) is plotted at the average instantaneous luminosity and the pile-up corrected iLumiCOR point (solid red square) is plotted at zero instantaneous luminosity.

Figure 30 shows the raw data at 1.96 TeV (TC1_V01) on the overall average number of charged particles with $|\eta| < 0.8$ and $p_T > 0.5$ GeV/c and $p_T > 1.0$ GeV/c for events with at least one charged particle with $|\eta| < 0.8$ and $p_T > 0.5$ GeV/c or $p_T > 1.0$ GeV/c, respectively, plotted versus the instantaneous luminosity. The overall raw data point (solid black square) is plotted at the average instantaneous luminosity value and the pile-up corrected iLumiCOR point (solid red square) is plotted at zero instantaneous luminosity. For $|\eta| < 0.8$ and $p_T > 0.5$ GeV/c the overall average number of charged particles is multiplied by a factor 0.963 to account for pile-up. For $|\eta| < 0.8$ and $p_T > 1.0$ GeV/c pile-up the affect of pile-up is smaller and the overall average number of charged particles is multiplied by a factor 0.987 to account for pile-up.

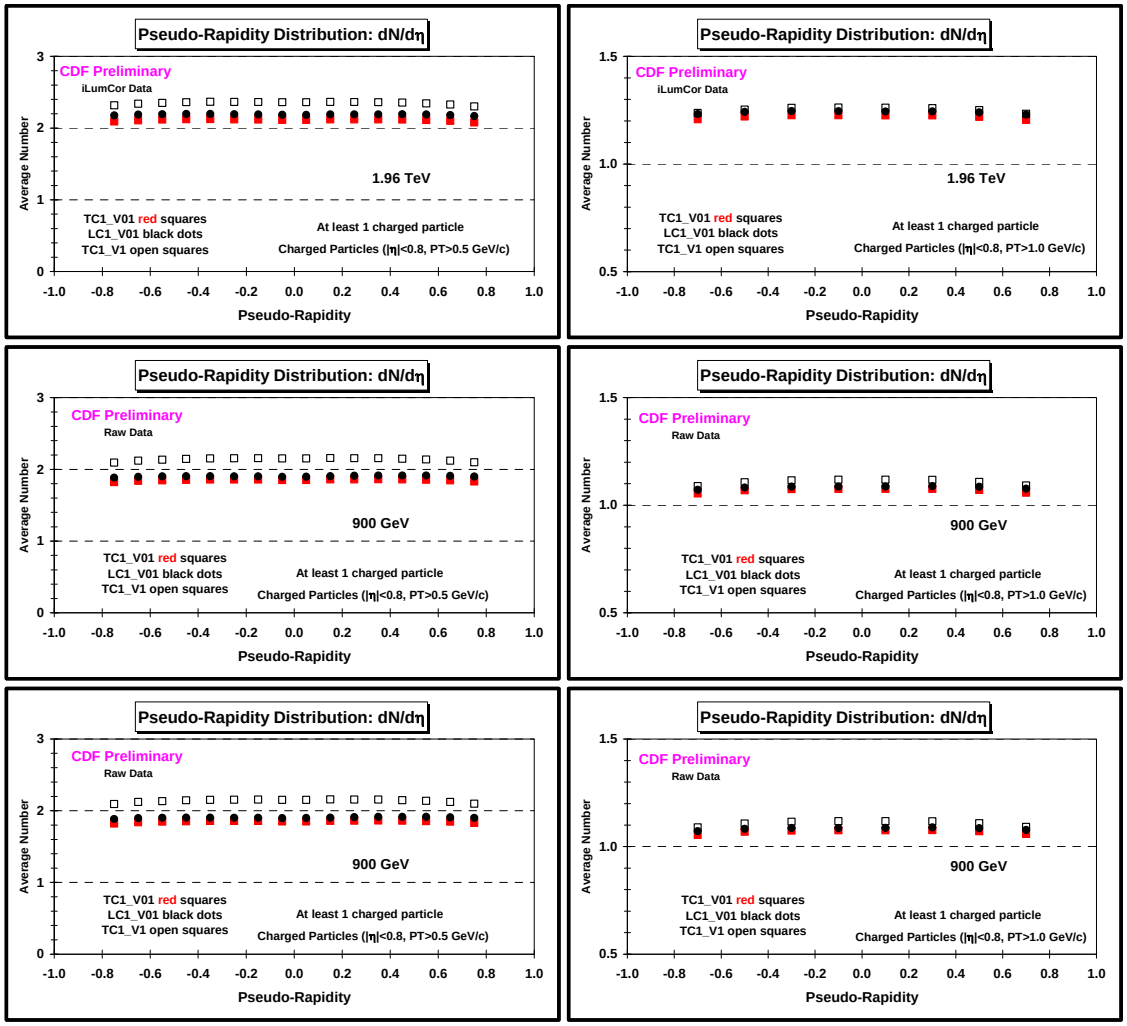

Fig. 31. Pseudo-rapidity distribution, dN/dη, for charged particles with $|\eta| < 0.8$ and $p_T > 0.5$ GeV/c (*left column*) and $p_T > 1.0$ GeV/c (*left column*) for events with at least one charged particle with $|\eta| < 0.8$ and $p_T > 0.5$ GeV/c or $p_T > 1.0$ GeV/c, respectively. Shows the pile-up corrected data (TC1_V01, LC1_V01, TC1_V1) at 1.96 (*top row*), the raw data (TC1_V01, LC1_V01, TC1_V1) at 900 GeV (*middle row*), and the raw data (TC1_V01, LC1_V01, TC1_V1) at 300 GeV (*bottom row*).

Figure 31 shows the pile-up corrected data on the pseudo-rapidity distributions at 1.96 TeV for the three datasets: TC1_V01, LC1_V01, TC1_V1 together with the raw data at 300 GeV and 900 GeV for the three data sets. The results after correcting these three datasets to the

particle level using their corresponding "correction factors" are shown in Fig. 32. Fig. 33 shows the fractional statistical and systematic errors on the pseudo-rapidity distributions at the three energies which are constructed using the same method that was used for the "transverse" charged particle density (see Table 6). Figure 34 shows the resulting corrected data at 1.96 TeV, 900 GeV, and 300 GeV on the pseudo-rapidity distributions with errors that include both the statistical error and the systematic uncertainty.

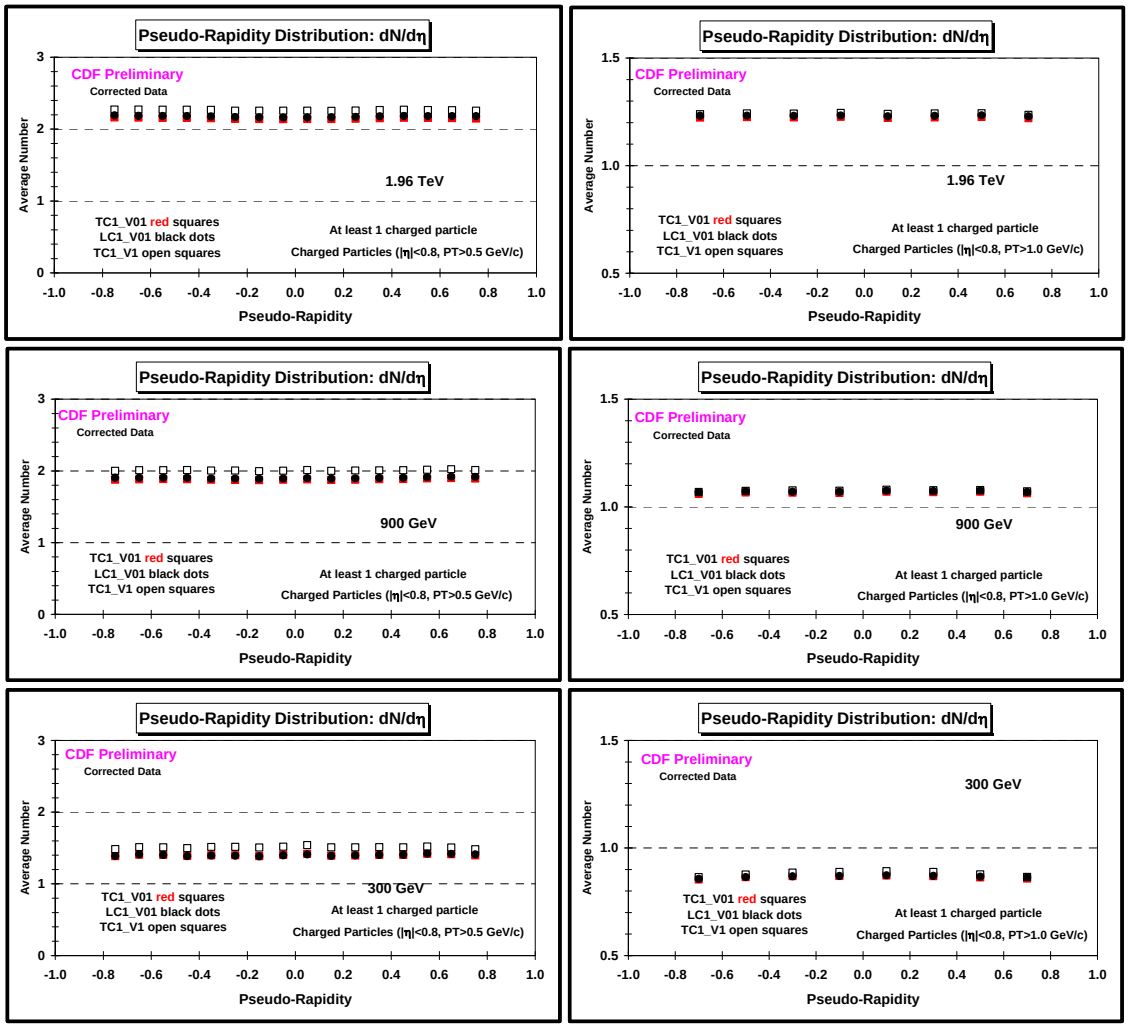

Fig. 32. Pseudo-rapidity distribution, dN/dη, for charged particles with $|\eta| < 0.8$ and $p_T > 0.5$ GeV/c (*left column*) and $p_T > 1.0$ GeV/c (*left column*) for events with at least one charged particle with $|\eta| < 0.8$ and $p_T > 0.5$ GeV/c or $p_T > 1.0$ GeV/c, respectively. Shows the corrected data (TC1_V01, LC1_V01, TC1_V1) at 1.96 (*top row*), 900 GeV (*middle row*), and 300 GeV (*bottom row*).

The dominate systematic error for dN/dη with $|\eta| < 0.8$ and $p_T > 0.5$ GeV/c is Sys-Err2 which becomes large for small p_T. This can be seen by looking at the first bin ($0.5 <$ PTmax $<$ 1.0 GeV/c) in Figure 7. The dominate systematic error for dN/dη with $|\eta| < 0.8$ and $p_T > 1.0$ GeV/c is also Sys-Err2, but here it is much smaller since p_T is larger. For dN/dη with $|\eta| < 0.8$ and $p_T > 0.5$ GeV/c the overall errors are around 7% and hence we set Sys-Err3 = 0%. The errors are large enough to incorporate all other possible systematic errors. For dN/dη with $|\eta| <$ 0.8 and $p_T > 1.0$ GeV/c the overall errors are much smaller and we set Sys-Err3 = 1%.

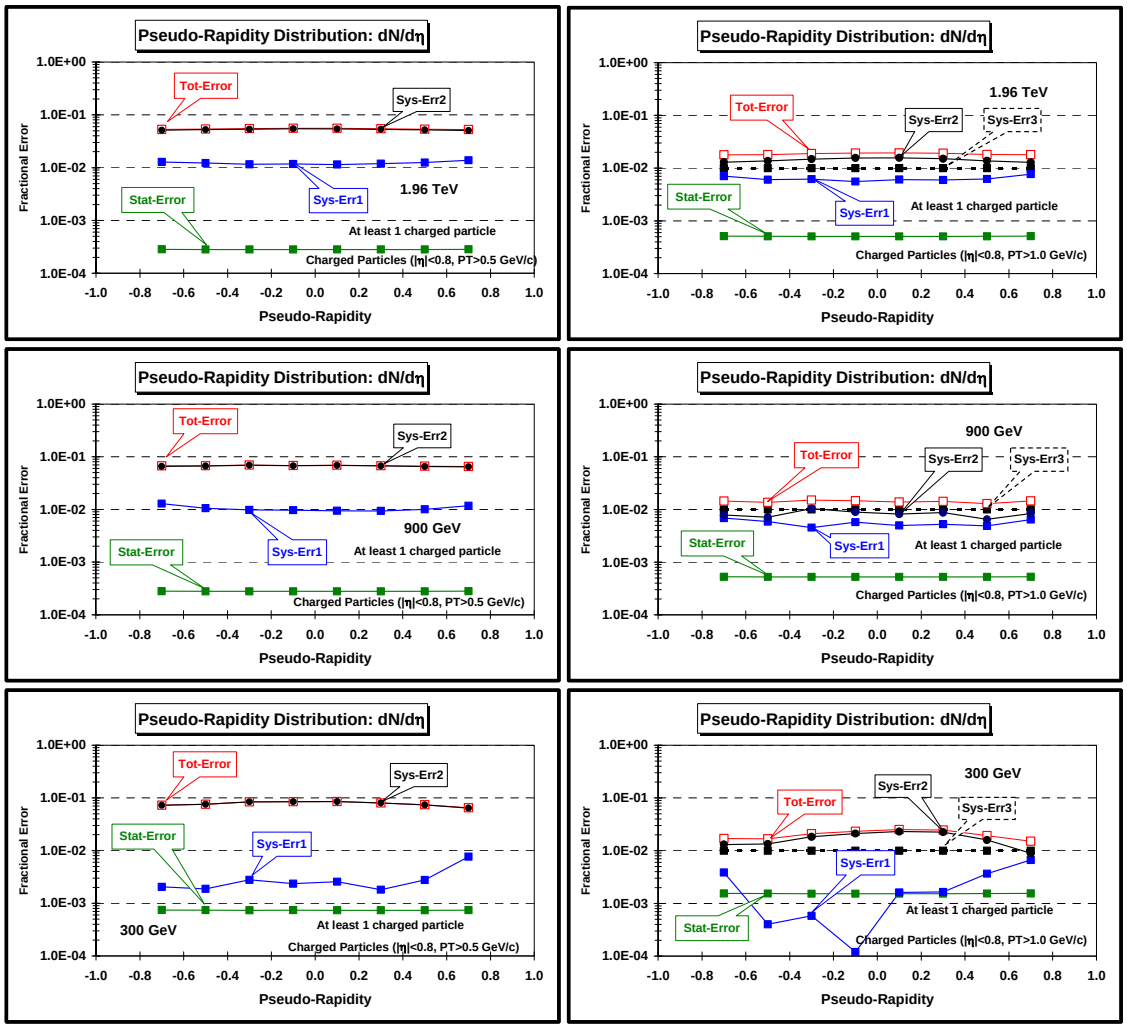

Fig. 33. Fractional statistical and systematic errors on the pseudo-rapidity distribution, dN/dη, for charged particles with $|\eta| < 0.8$ and $p_T > 0.5$ GeV/c (*left column*) and $p_T > 1.0$ GeV/c (*left column*) for events with at least one charged particle with $|\eta| < 0.8$ and $p_T > 0.5$ GeV/c or $p_T > 1.0$ GeV/c, respectively. at 1.96 TeV (*top row*), 900 GeV (*middle row*), and 300 GeV (*bottom row*). Stat-Error is the statistical error, Sys-Err1 = |LC1_V01 – TC1_V01|/TC1_V01, Sys-Err2 = |TC1_V01 – TC1_V1|/TC1_V01, and Sys-Err3 = 0% ($p_T > 0.5$ GeV/c) and Sys-Err3 = 1% ($p_T > 1.0$ GeV/c). The overall total error (Tot-Error) results from adding statistical error in quadrature with the three systematic errors.

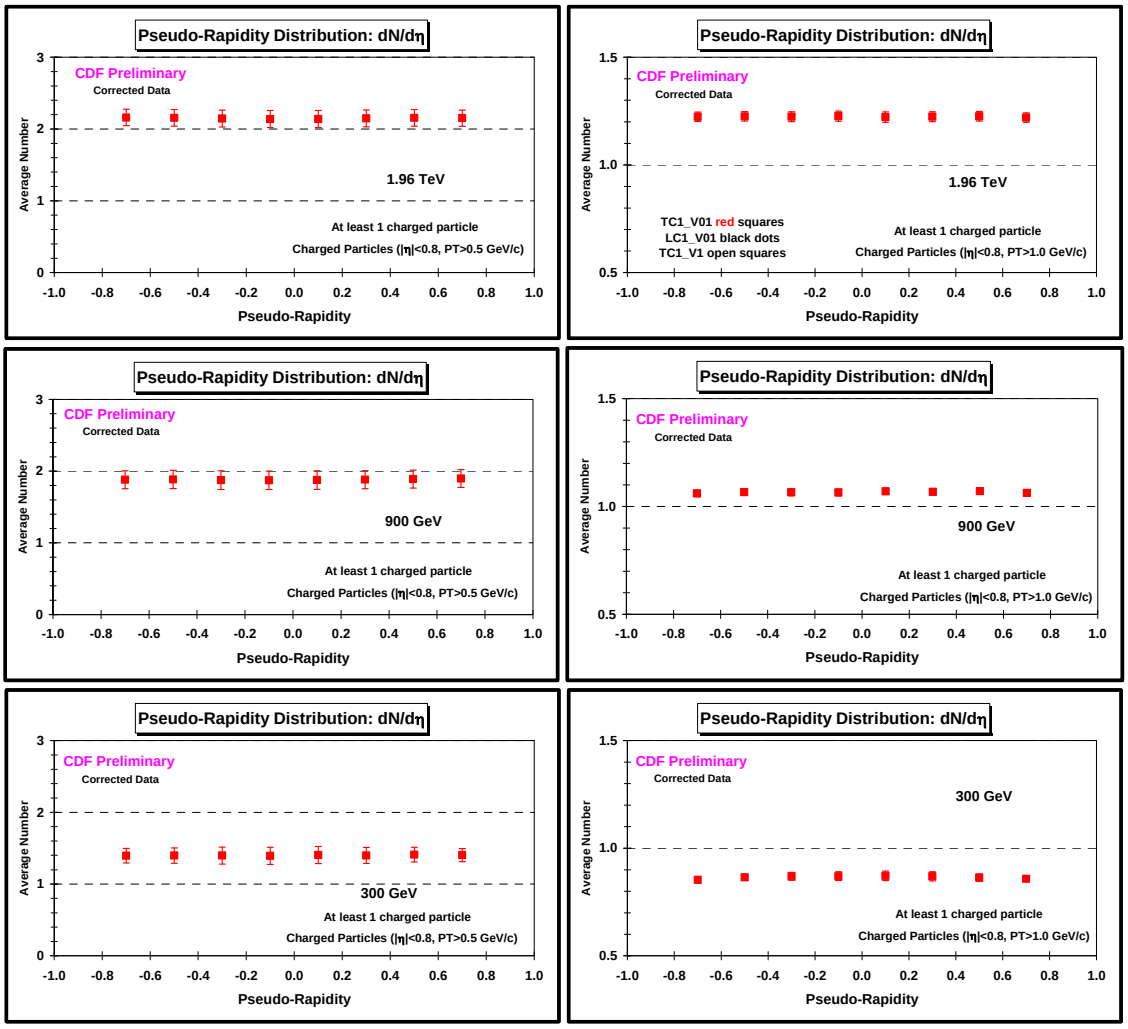

Fig. 34. Data on the pseudo-rapidity distribution, dN/dη, for charged particles with $|\eta| < 0.8$ and $p_T > 0.5$ GeV/c (*left column*) and $p_T > 1.0$ GeV/c (*left column*) for events with at least one charged particle with $|\eta| < 0.8$ and $p_T > 0.5$ GeV/c or $p_T > 1.0$ GeV/c, respectively, at 1.96 (*top row*), 900 GeV (*middle row*), and 300 GeV (*bottom row*). The data are corrected to the particle level with errors that include both the statistical error and the systematic uncertainty.

Figure 35 the CDF data at 1.96 TeV, 900 GeV, and 300 GeV on the pseudo-rapidity distribution, dN/dη, for charged particles with $|\eta| < 0.8$ and $p_T > 0.5$ GeV/c and $p_T > 1.0$ GeV/c for events with at least one charged particle with $|\eta| < 0.8$ and $p_T > 0.5$ GeV/c or $p_T > 1.0$ GeV/c, respectively. The data are corrected to the particle level with errors that include both the statistical error and the systematic uncertainty. Figure 36 compares the 900 GeV CDF data with the 900 GeV CMS data. The agreement is excellent! It is interesting that for $p_T > 0.5$ GeV the CDF systematic errors are bigger than the CMS systematic errors, but for $p_T > 1.0$ GeV the CMS systematic errors are slightly bigger than the CDF systematic errors. We know from Figure 17 that the systematic errors decrease rapidly as p_T increases.

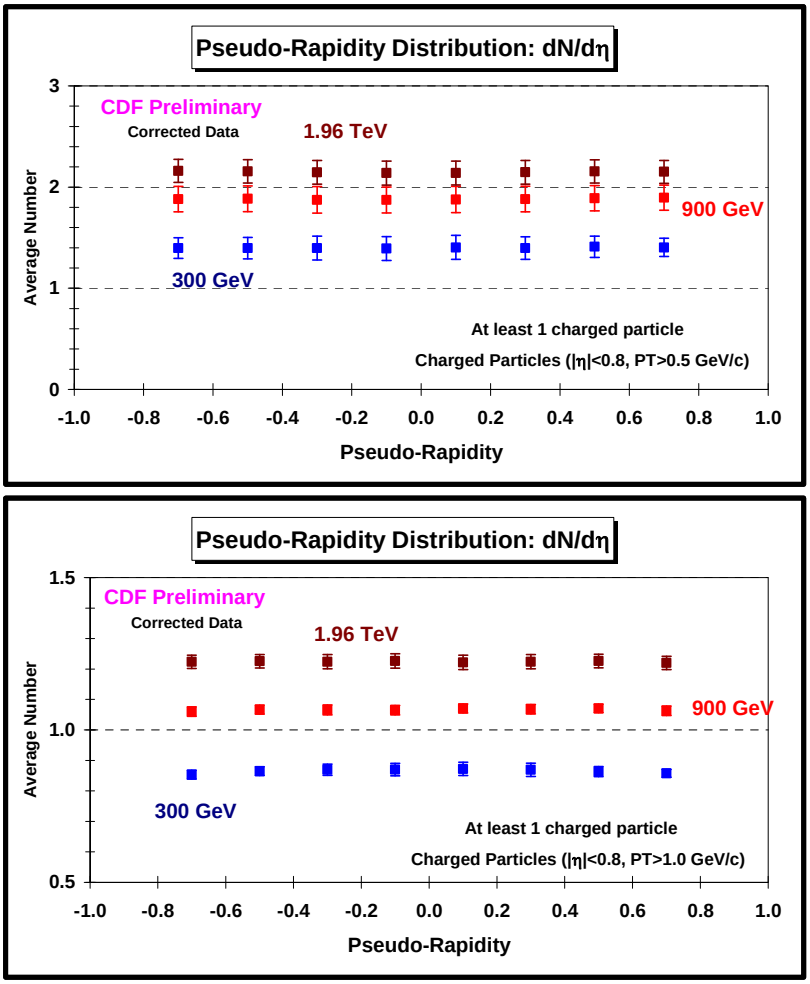

Fig. 35. Data at 1.96 TeV, 900 GeV, and 300 GeV on the pseudo-rapidity distribution, dN/dη, for charged particles with $|\eta| < 0.8$ and $p_T > 0.5$ GeV/c (*top*) and $p_T > 1.0$ GeV/c (*bottom*) for events with at least one charged particle with $|\eta| < 0.8$ and $p_T > 0.5$ GeV/c or $p_T > 1.0$ GeV/c, respectively. The data are corrected to the particle level with errors that include both the statistical error and the systematic uncertainty.

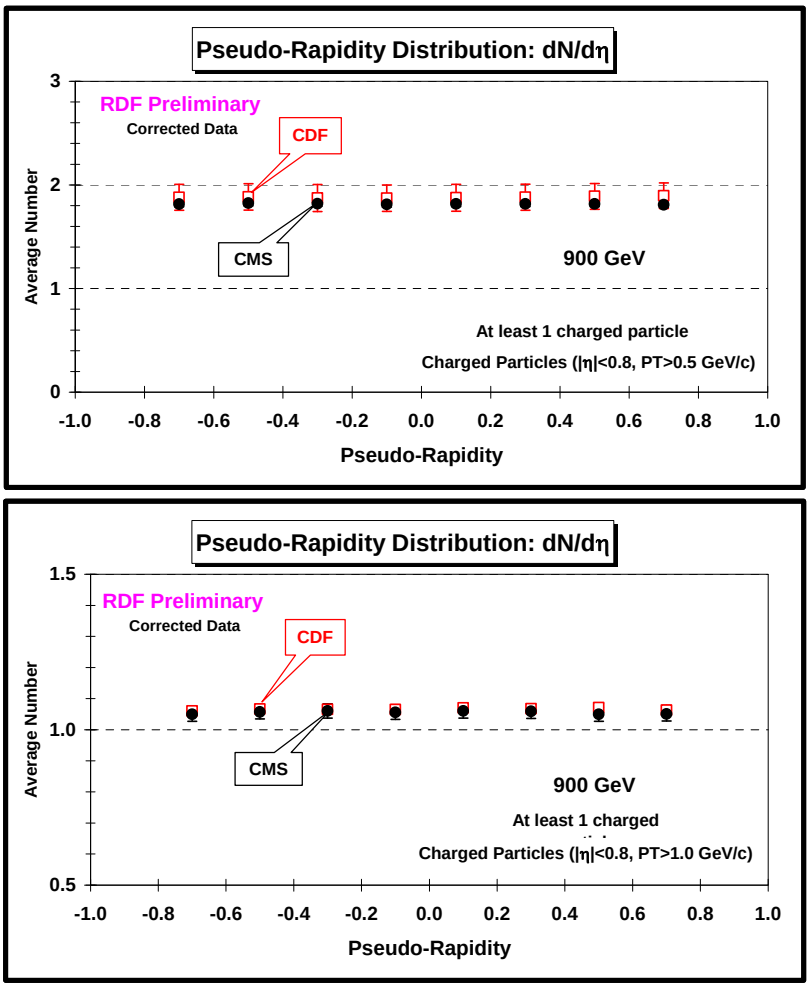

Fig. 36. CDF and CMS data at 900 GeV on the pseudo-rapidity distribution, dN/dη, for charged particles with $|\eta| < 0.8$ and $p_T > 0.5$ GeV/c (*top*) and $p_T > 1.0$ GeV/c (*bottom*) for events with at least one charged particle with $|\eta| < 0.8$ and $p_T > 0.5$ GeV/c or $p_T > 1.0$ GeV/c, respectively. The data are corrected to the particle level with errors that include both the statistical error and the systematic uncertainty.

Figure 37 shows CDF data on the pseudo-rapidity distribution, dN/dη, at $\eta = 0$ for charged particles with $|\eta| < 0.8$ and $p_T > 0.5$ GeV/c and $p_T > 1.0$ GeV/c for events with at least one charged particle with $|\eta| < 0.8$ and $p_T > 0.5$ GeV/c or $p_T > 1.0$ GeV/c, respectively, plotted versus the center-of-mass energy (on a log scale).

Table 7 shows The CDF data on the average overall number of charged particles and the average overall density of charged particle with $|\eta| < 0.8$ and $p_T > 0.5$ GeV/c for events with at least one charged particle with $|\eta| < 0.8$ and $p_T > 0.5$ GeV/c. The data are corrected to the particle level with errors that include both the statistical error and the systematic uncertainty. The overall number of charged particles is the integral of the pseudo-rapidity distribution in Fig. 35 (see Eq. 1). The overall density is computed by dividing by $1.6 \times 2\pi$.

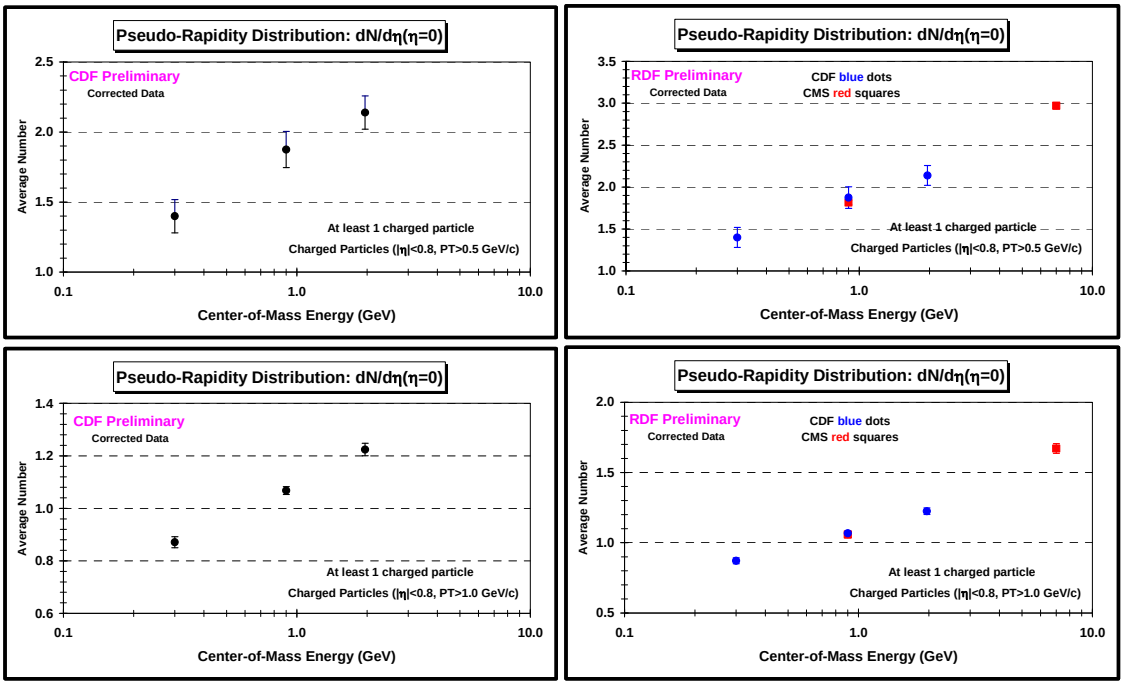

Fig. 37. CDF data (*left column*) and CDF and CMS data (*right column*) on the pseudo-rapidity distribution, dN/dη, at η = 0 for charged particles with $|\eta| < 0.8$ and $p_T > 0.5$ GeV/c (*top row*) and $p_T > 1.0$ GeV/c (*bottom row*) for events with at least one charged particle with $|\eta| < 0.8$ and $p_T > 0.5$ GeV/c or $p_T > 1.0$ GeV/c, respectively, plotted versus the center-of-mass energy (on a log scale). The data are corrected to the particle level with errors that include both the statistical error and the systematic uncertainty.

Table 7. CDF data at 1.96 TeV, 900 GeV, and 300 GeV on the average overall number of charged particles and the average overall density of charged particle with $|\eta| < 0.8$ and $p_T > 0.5$ GeV/c for events with at least one charged particle with $|\eta| < 0.8$ and $p_T > 0.5$ GeV/c. The data are corrected to the particle level with errors that include both the statistical error and the systematic uncertainty.

Ecm	Nchg	error	NchgDen	error
300 GeV	2.241	0.175	0.223	0.017
900 GeV	3.012	0.203	0.300	0.020
1.96 TeV	3.439	0.186	0.342	0.019

Figure 37 shows the CMS data at 7 TeV and 900 GeV and CDF data at 1.96 TeV, 900 GeV, and 300 GeV on the average overall number of charged particles and the average overall density of charged particle with $|\eta| < 0.8$ and $p_T > 0.5$ GeV/c for events with at least one charged particle with $|\eta| < 0.8$ and $p_T > 0.5$ GeV/c plotted versus the center-of-mass energy (on a log scale).

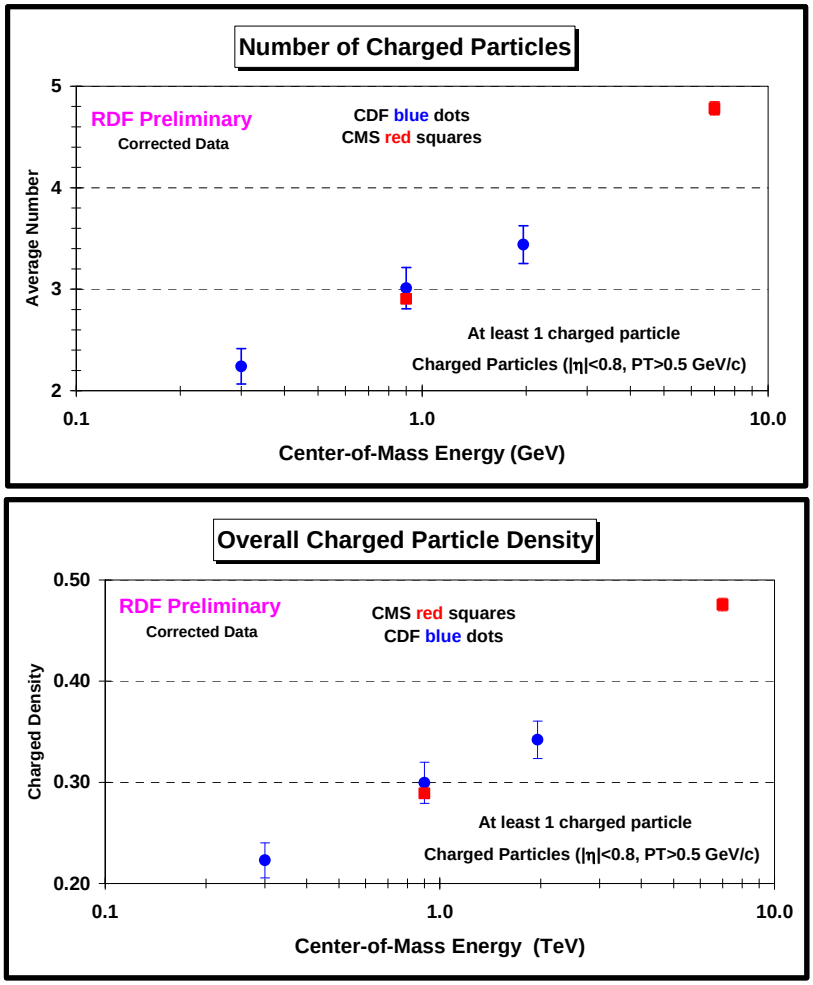

Fig. 37. CMS data at 7 TeV and 900 GeV and CDF data at 1.96 TeV, 900 GeV, and 300 GeV on the average overall number of charged particles (*top*) and the average overall density of charged particle (*bottom*) with $|\eta| < 0.8$ and $p_T > 0.5$ GeV/c for events with at least one charged particle with $|\eta| < 0.8$ and $p_T > 0.5$ GeV/c plotted versus the center-of-mass energy (on a log scale). The data are corrected to the particle level with errors that include both the statistical error and the systematic uncertainty.

(7) Comparing MB and UE

MB and UE are not the same object. The majority of MB collisions are "soft" while the UE is studied in events in which a hard-scattering has occurred. Nevertheless, it is interesting to compare MB and UE. This is done by comparing the density of charged particles in the "transverse" region as defined by the leading charged particle, PTmax, with the overall charged particle density from Table 7. Figure 38 shows CDF data at 1.96 TeV, 900 GeV, and 300 GeV on the "transverse" charged particle density as defined by the leading charged particle, PTmax, as a function of PTmax for charged particles with $p_T > 0.5$ GeV $|\eta| < 0.8$ compared with the overall charged particle density (*straight lines*) for events with at least one charged particle with $|\eta| < 0.8$ and $p_T > 0.5$ GeV/c. The density of charged particles in the "plateau" region of the UE is considerably larger than the overall density of charged particles!

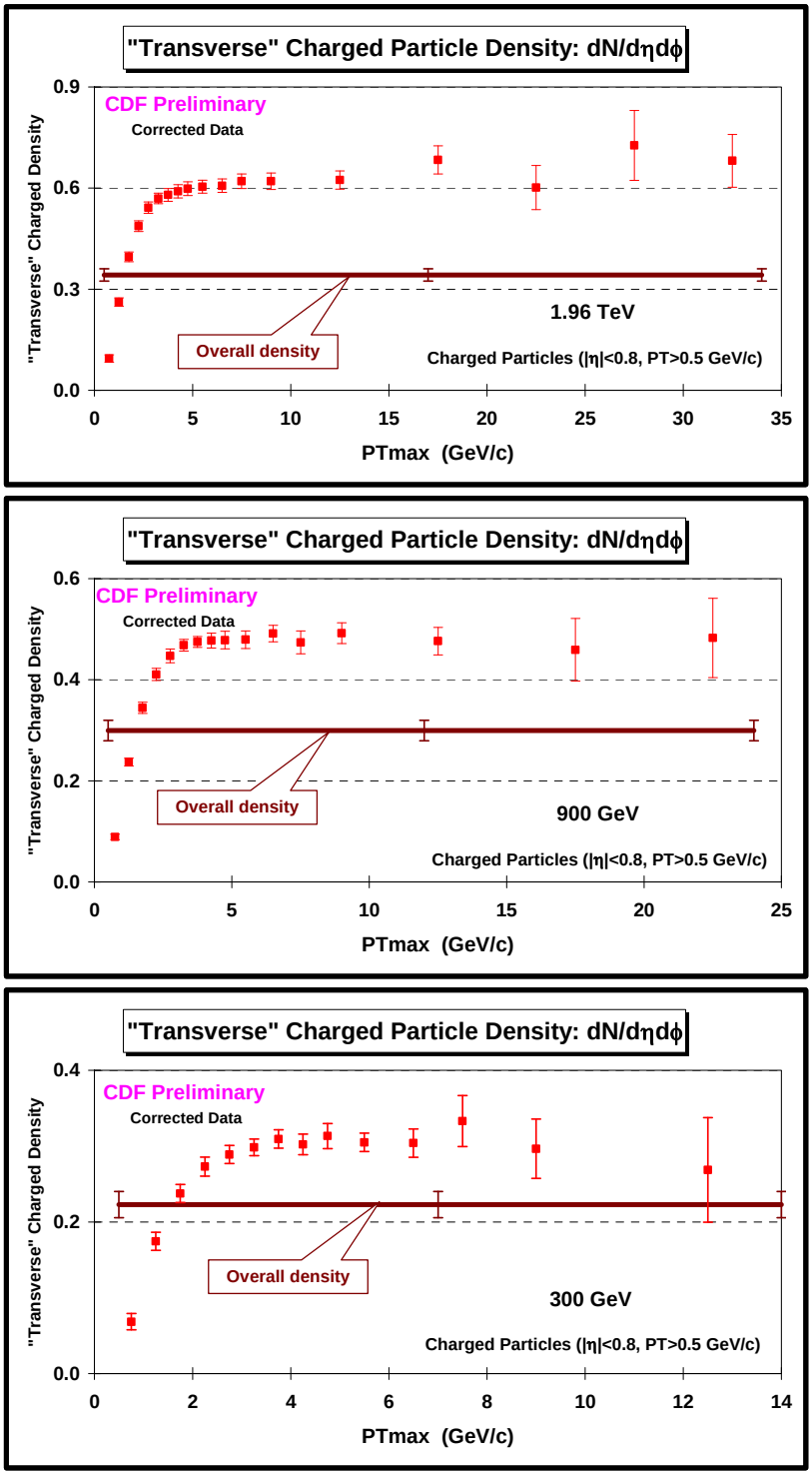

Fig. 38. Data at 1.96 TeV (*top*), 900 GeV (*middle*), and 300 GeV (*bottom*) on the "transverse" charged particle density as defined by the leading charged particle, PTmax, as a function of PTmax for charged particles with $p_T >$ 0.5 GeV $|\eta| < 0.8$ The data are corrected to the particle level with errors that include both the statistical error and the systematic uncertainty. At each energy the "transverse" charged particle density is compared with the overall charged particle density (*straight lines*) for events with at least one charged particle with $|\eta| < 0.8$ and $p_T > 0.5$ GeV/c.

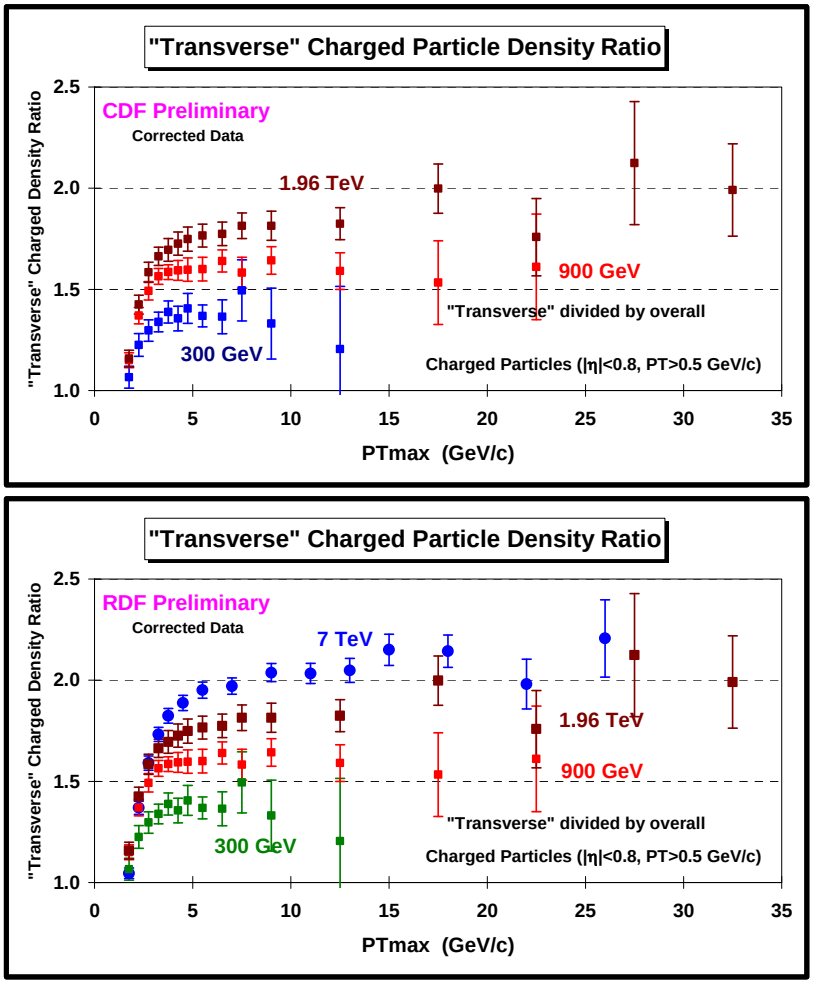

Fig. 39. (*top & bottom*) CDF data at 1.96 TeV, 900 GeV, and 300 GeV and (*bottom*) CMS data at 7 TeV on the "transverse" charged particle density ratio as defined by the leading charged particle, PTmax, as a function of PTmax for charged particles with $p_T > 0.5$ GeV $|\eta| < 0.8$. At each energy the ratio corresponds to the "transverse" charged particle density divided by the overall charged particle density for events with at least one charged particle with $|\eta| < 0.8$ and $p_T > 0.5$ GeV/c.

Figure 39 shows data on the "transverse" charged particle density ratio as defined by the leading charged particle, PTmax, as a function of PTmax for charged particles with $p_T > 0.5$ GeV $|\eta| < 0.8$. At each energy the ratio corresponds to the "transverse" charged particle density divided by the overall charged particle density for events with at least one charged particle with $|\eta| < 0.8$ and $p_T > 0.5$ GeV/c. The data show that this ratio increases with increasing center-of-mass energy. At 300 GeV it is around 1.4 and increases to around 2.0 at 7 TeV. Figure 40 shows this ratio for $5.0 < \text{PTmax} < 6.0$ GeV/c plotted versus the center-of-mass energy (on a log scale). This is the first study of the energy dependence of this ratio. The density of charged particles in the "plateau" region of the UE rises more rapidly with center-of-mass energy than does the overall density of charged particles!

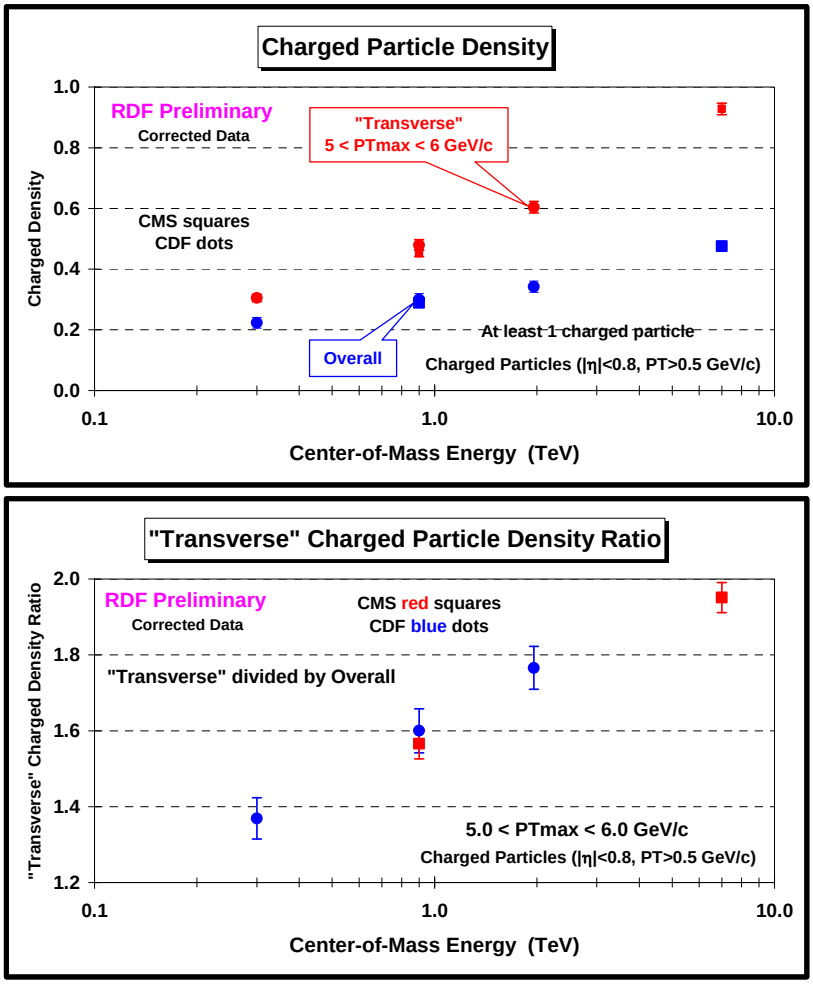

Fig. 40. (*top*) CDF data at 1.96 TeV, 900 GeV, and 300 GeV and CMS data at 900 GeV and 7 TeV on the "transverse" charged particle density as defined by the leading charged particle, PTmax, for 5.0 < PTmax < 6.0 GeV/c plotted versus the center-of-mass energy (on a log scale) for charged particles with $p_T > 0.5$ GeV/c and $|\eta| < 0.8$ compared with the overall charged particle density for events with at least one charged particle with $|\eta| < 0.8$ and $p_T > 0.5$ GeV/c. (*bottom*) CDF and CMS data at 7 TeV on the "transverse" charged particle density ratio as defined by the leading charged particle, PTmax, for 5.0 < PTmax < 6.0 GeV/c plotted versus the center-of-mass energy (on a log scale) for charged particles with $p_T > 0.5$ GeV/c and $|\eta| < 0.8$. At each energy the ratio corresponds "transverse" charged particle density divided by the overall charged particle density for events with at least one charged particle with $|\eta| < 0.8$ and $p_T > 0.5$ GeV/c.

IV. QCD Monte-Carlo Comparisons

Figures 41, 42, and 43 compare the data on the "transverse" charged particle density with the PYTHIA 6.2 Tune A and Tune DW and the PYTHIA 6.4 Tune Z1. Tune A does a nice job on the energy dependence but is low by about 14% at each energy. Tune DW does a very poor job in describing the 300 GeV data and hence does not fit the energy dependence. Figures 44, 45, and 46 compare the data on the "transverse" charged PTsum density and "transverse" charged particle average p_T with the PYTHIA 6.4 Tune Z1. The "transverse" average p_T predicted by Tune Z1 is slightly smaller than the data. However, Tune Z1 fits very well the energy dependence of the "transverse" average p_T.

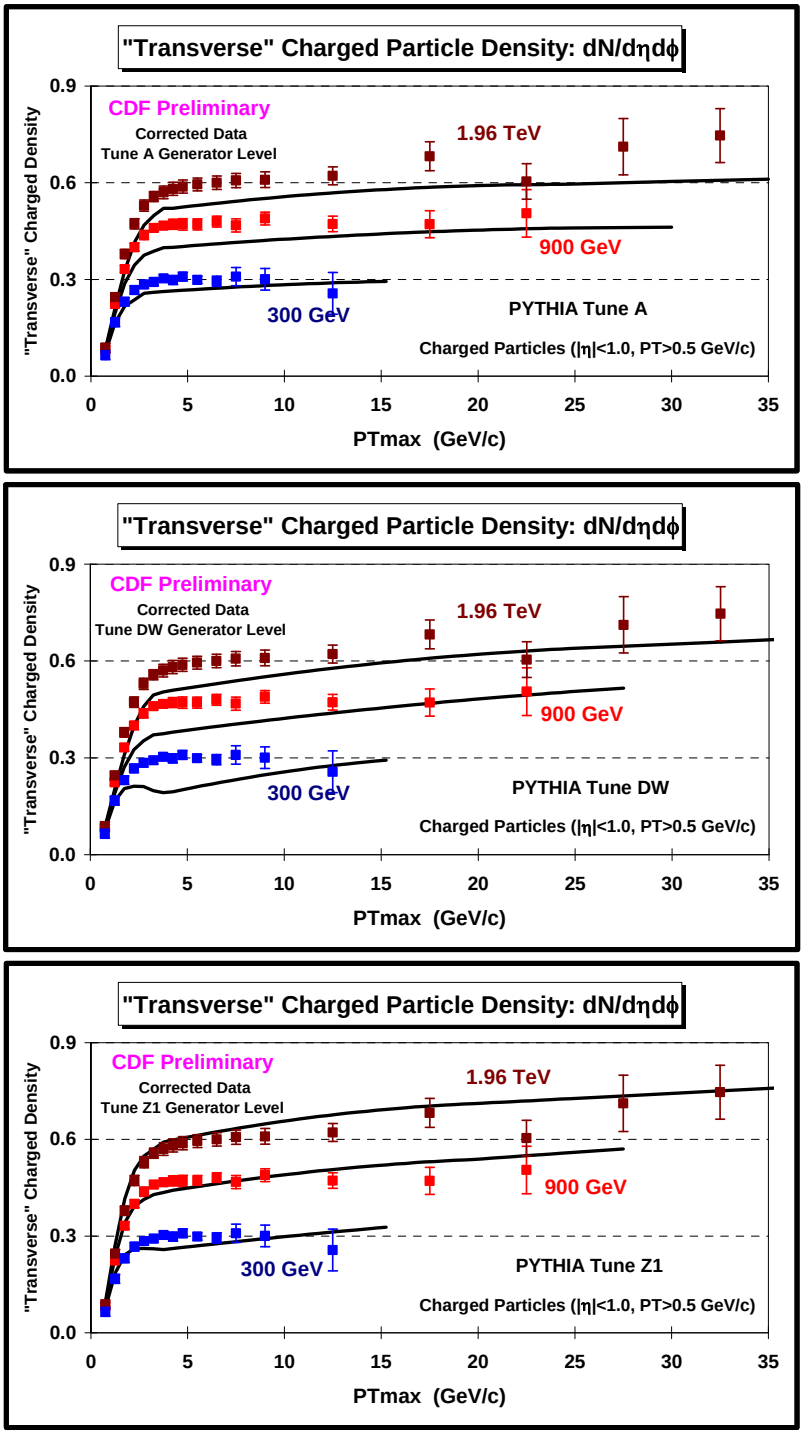

Fig. 41. Data at 1.96 TeV, 900 GeV, and 300 GeV on the "transverse" charged particle density as defined by the leading charged particle, PTmax, as a function of PTmax. The data are corrected to the particle level (with errors that include both the statistical error and the systematic uncertainty) and are compared with PHTYIA 6.2 Tune A (*top*), PYTHIA 6.2 Tune DW (*middle*), and PYTHIA 6.4 Tune Z1 (*bottom*) at the particle level (*i.e.* generator level).

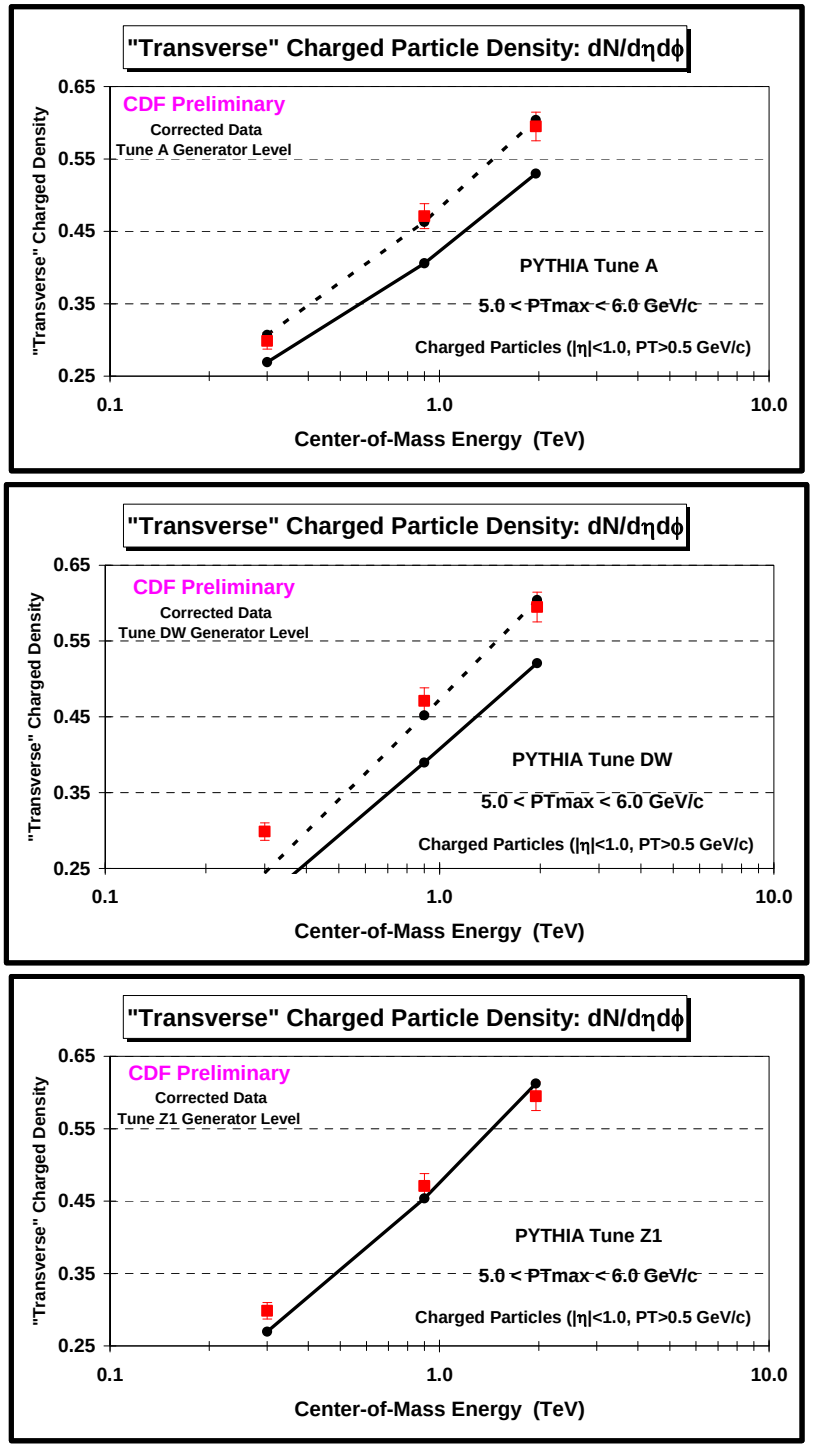

Fig. 42. Data at 1.96 TeV, 900 GeV, and 300 GeV on the "transverse" charged particle density as defined by the leading charged particle, PTmax, for 5.0 < PTmax < 6.0 GeV/c plotted versus the center-of-mass energy (on a log scale). The data are corrected to the particle level (with errors that include both the statistical error and the systematic uncertainty) and are compared with (*top*) PHTYIA 6.2 Tune A (solid curve) and Tune A scaled be a factor of 1.14 (dashed curve), (*middle*) PYTHIA 6.2 Tune DW (solid curve) and Tune DW scaled be a factor of 1.16 (dashed curve), and (*bottom*) PYTHIA 6.4 Tune Z1 (solid curve).

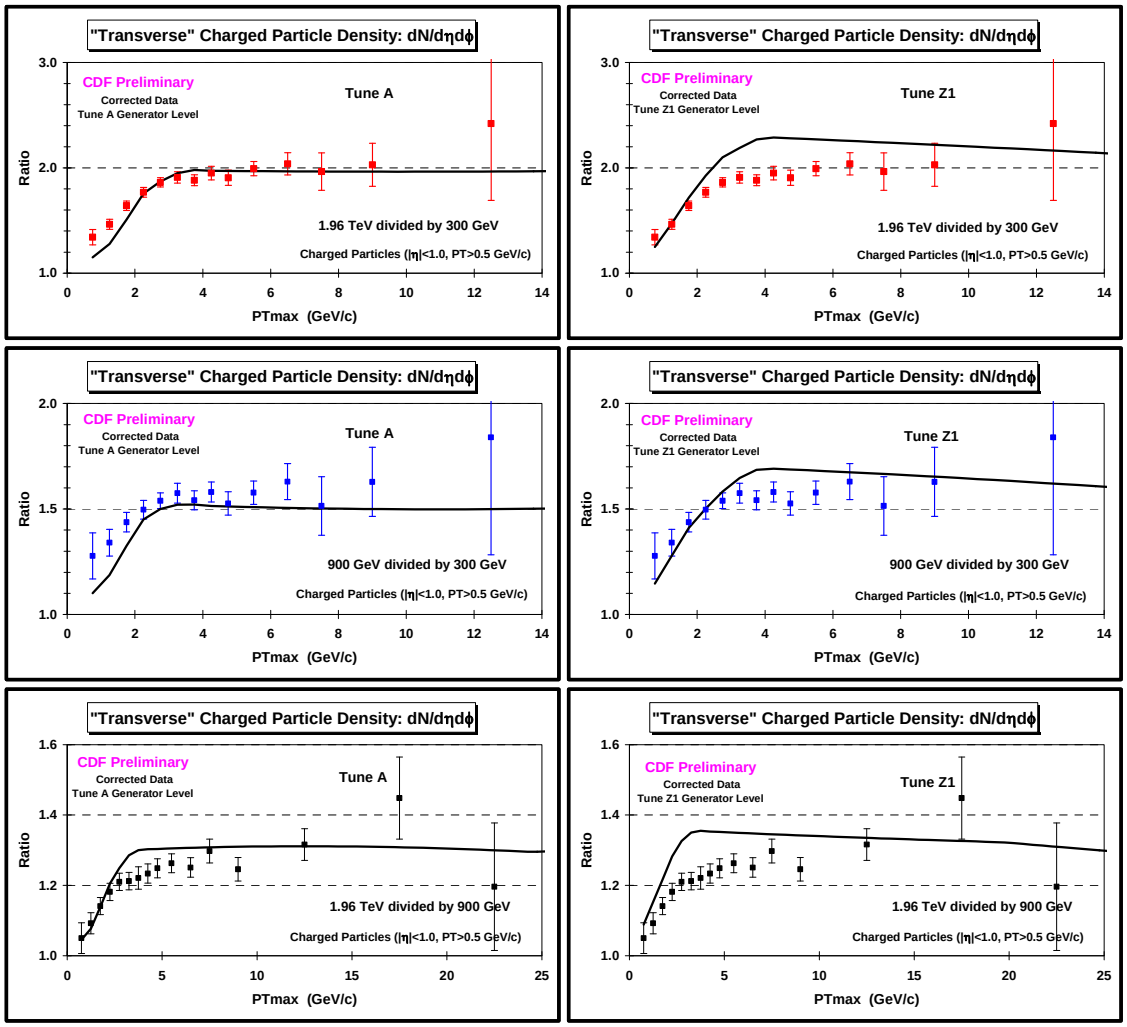

Fig. 43. (*top*) Ratio of the data at 1.96 TeV and 300 GeV on the "transverse" charged particle density as defined by the leading charged particle, PTmax, as a function of PTmax compared with PYTHIA 6.2 Tune A (*left*) and with PYTHIA 6.4 Tune Z1 (*right*). (*middle*) Ratio of the data at 900 GeV and 300 GeV on the "transverse" charged particle density as defined by the leading charged particle, PTmax, as a function of PTmax compared with PYTHIA 6.2 Tune A (*left*) and with PYTHIA 6.4 Tune Z1 (*right*). (*bottom*) Ratio of the data at 1.96 TeV and 900 GeV on the "transverse" charged particle density as defined by the leading charged particle, PTmax, as a function of PTmax compared with PYTHIA 6.2 Tune A (*left*) and with PYTHIA 6.4 Tune Z1 (*right*).

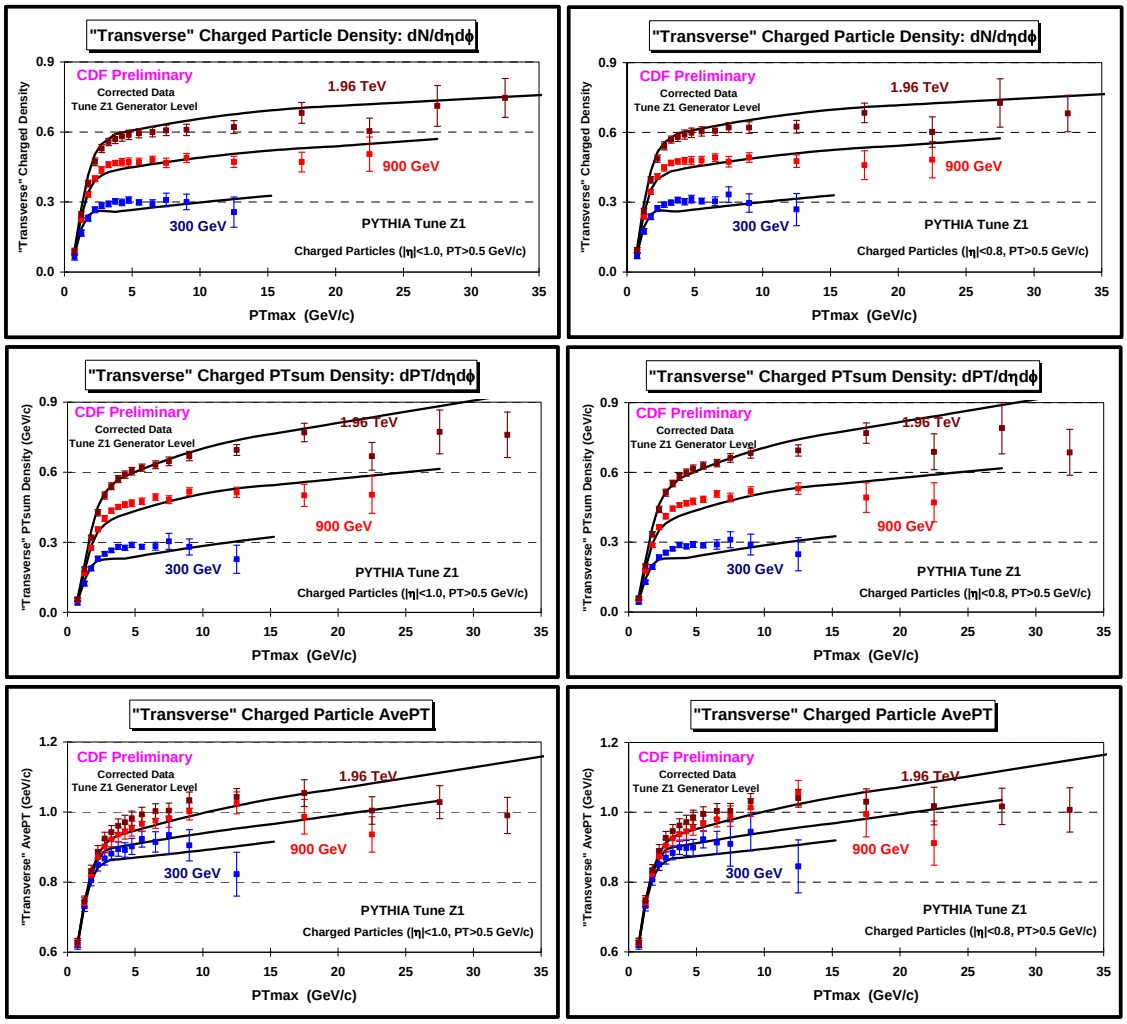

Fig. 44. Data at 1.96 TeV, 900 GeV, and 300 GeV on the "transverse" charged particle density (*top row*), the "transverse" charged PTsum density (*middle row*), and the "transverse" charged particle average p_T (*bottom row*) as defined by the leading charged particle, PTmax, as a function of PTmax. The data are corrected to the particle level with errors that include both the statistical error and the systematic uncertainty and are compared with PYTHIA 6.4 Tune Z1 at the particle level (*i.e.* generator level). The charged particles have $p_T > 0.5$ GeV and $|\eta| < 1.0$ (*left column*) and $|\eta| < 0.8$ (*right column*).

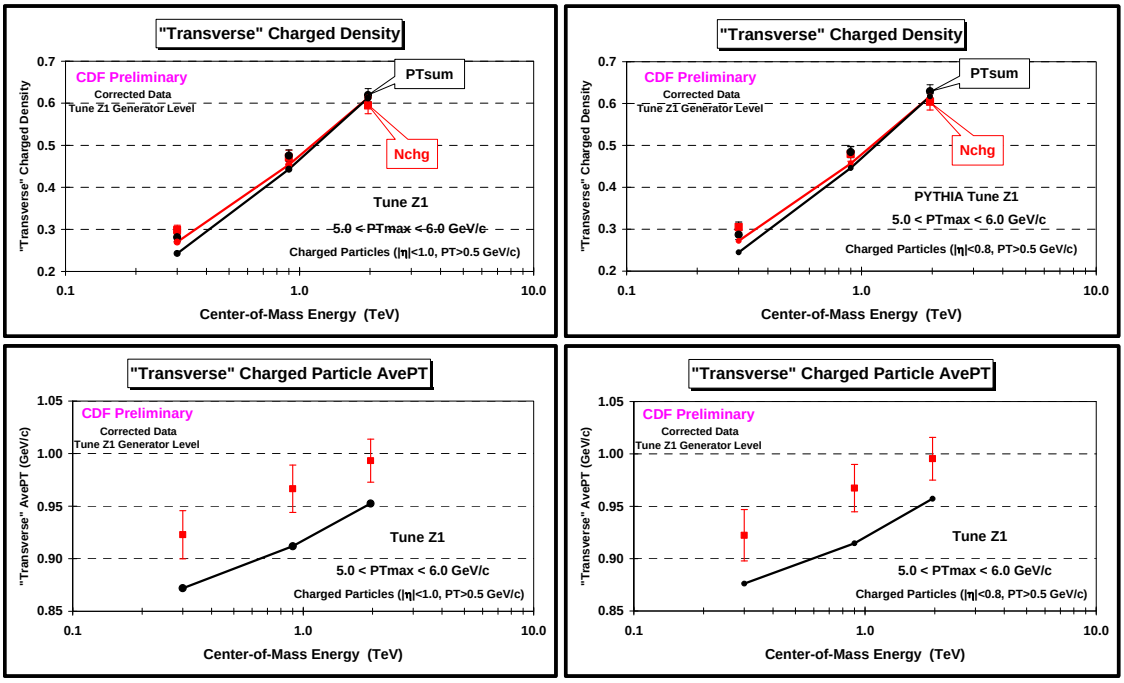

Fig. 45. (*top row*) Data at 1.96 TeV, 900 GeV, and 300 GeV on the "transverse" charged particle density and the "transverse" charged PTsum density and (*bottom row*) on the "transverse" charged particle average p_T as defined by the leading charged particle, PTmax, for 5.0 < PTmax < 6.0 GeV/c plotted versus the center-of-mass energy (on a log scale). The data are corrected to the particle level with errors that include both the statistical error and the systematic uncertainty and are compared with PYTHIA 6.4 Tune Z1 at the particle level (*i.e.* generator level). The charged particles have $p_T > 0.5$ GeV and $|\eta| < 1.0$ (*left column*) and $|\eta| < 0.8$ (*right column*).

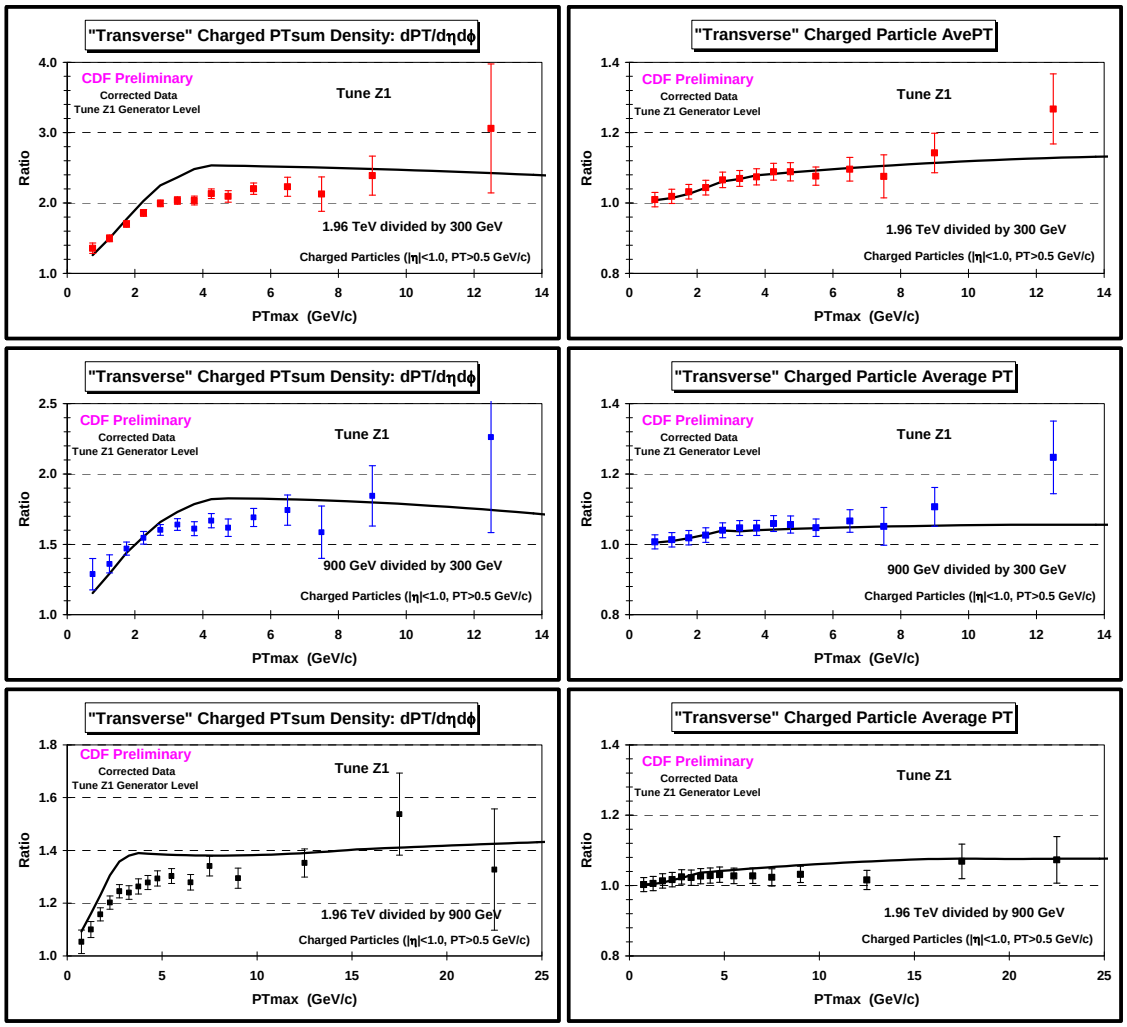

Fig. 46. Ratio of the data at 1.96 TeV and 300 GeV on the "transverse" charged PTsum density (*top-left*) and the "transverse" charged particle average p_T (*top-right*) as defined by the leading charged particle, PTmax, as a function of PTmax compared with PYTHIA 6.4 Tune Z1. Ratio of the data at 900 GeV and 300 GeV on the "transverse" charged PTsum density (*middle-left*) and the "transverse" charged particle average p_T (*middle-right*) as defined by the leading charged particle, PTmax, as a function of PTmax compared with PYTHIA 6.4 Tune Z1. Ratio of the data at 1.96 TeV and 900 GeV on the "transverse" charged PTsum density (*bottom-left*) and the "transverse" charged particle average p_T (*bottom-right*) as defined by the leading charged particle, PTmax, as a function of PTmax compared with PYTHIA 6.4 Tune Z1.

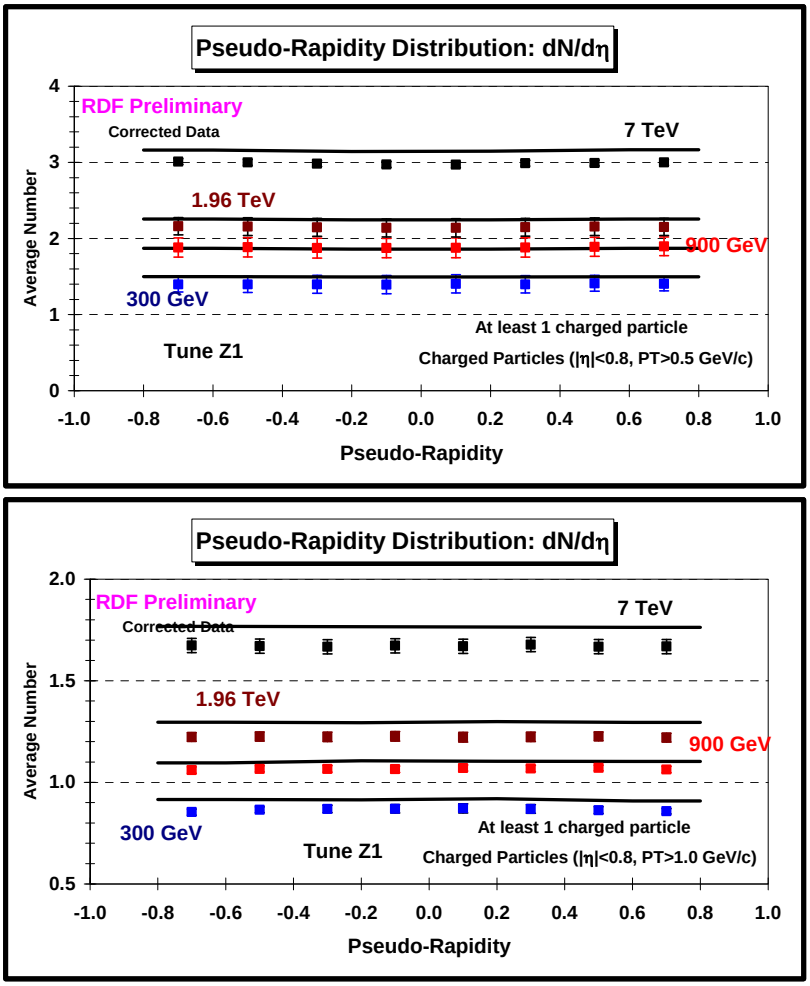

Fig. 47. CDF data at 1.96 TeV, 900 GeV, and 300 GeV and CMS data at 7 TeV on the pseudo-rapidity distribution, dN/dη, for charged particles with $|\eta| < 0.8$ and $p_T > 0.5$ GeV/c (*top*) and $p_T > 1.0$ GeV/c (*bottom*) for events with at least one charged particle with $|\eta| < 0.8$ and $p_T > 0.5$ GeV/c or $p_T > 1.0$ GeV/c, respectively. The data are corrected to the particle level with errors that include both the statistical error and the systematic uncertainty and are compared with PYTHIA 6.4 Tune Z1.

Figure 47 shows CDF data at 1.96 TeV, 900 GeV, and 300 GeV and CMS data at 7 TeV on the pseudo-rapidity distribution, dN/dη, for charged particles with $|\eta| < 0.8$ and $p_T > 0.5$ GeV/c and $p_T > 1.0$ GeV/c for events with at least one charged particle with $|\eta| < 0.8$ and $p_T > 0.5$ GeV/c or $p_T > 1.0$ GeV/c, respectively, compared with PYTHIA 6.4 Tune Z1. Figure 48 shows CDF and CMS data on the pseudo-rapidity distribution, dN/dη, at $\eta = 0$ for charged particles with $|\eta| < 0.8$ and $p_T > 0.5$ GeV/c and $p_T > 1.0$ GeV/c for events with at least one charged particle with $|\eta| < 0.8$ and $p_T > 0.5$ GeV/c or $p_T > 1.0$ GeV/c, respectively, compared with PYTHIA 6.4 Tune Z1.

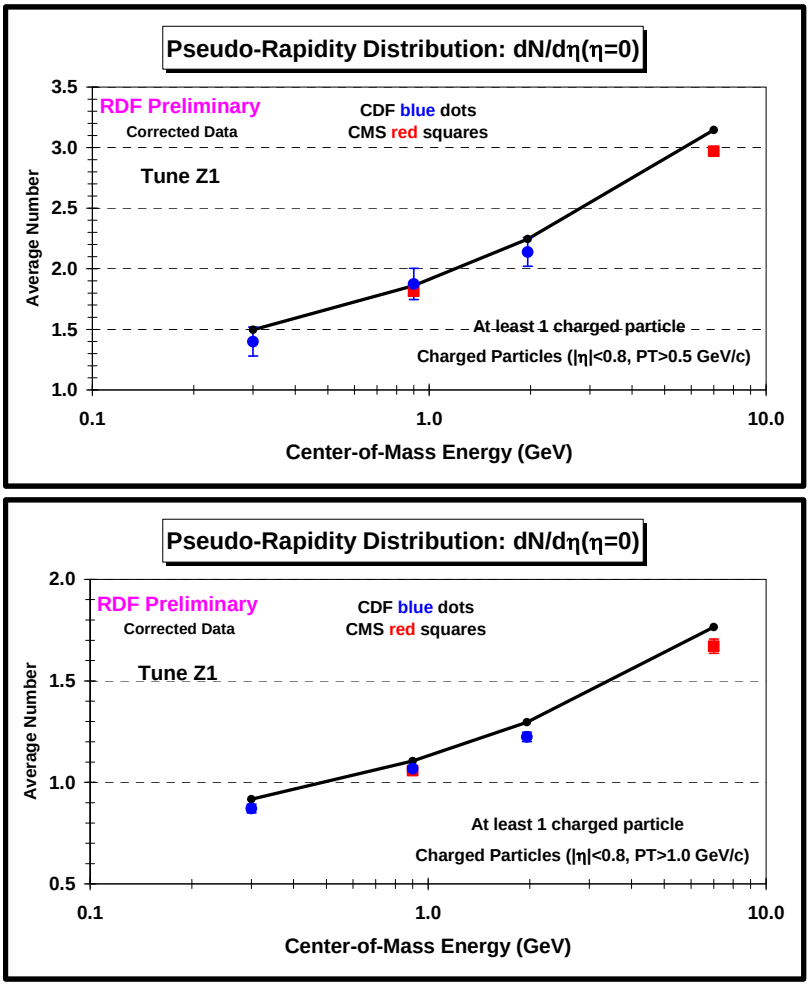

Fig. 48. CDF and CMS data on the pseudo-rapidity distribution, dN/dη, at η = 0 for charged particles with $|\eta| < 0.8$ and $p_T > 0.5$ GeV/c (*top*) and $p_T > 1.0$ GeV/c (*bottom*) for events with at least one charged particle with $|\eta| < 0.8$ and $p_T > 0.5$ GeV/c or $p_T > 1.0$ GeV/c, respectively, plotted versus the center-of-mass energy (on a log scale). The data are corrected to the particle level with errors that include both the statistical error and the systematic uncertainty and are compared with PYTHIA 6.4 Tune Z1.

Figure 49 shows data on the "transverse" charged particle density ratio as defined by the leading charged particle, PTmax, as a function of PTmax for charged particles with $p_T > 0.5$ GeV $|\eta| < 0.8$ compared with PYTHIA 6.4 Tune Z1. At each energy the ratio corresponds to the "transverse" charged particle density divided by the overall charged particle density for events with at least one charged particle with $|\eta| < 0.8$ and $p_T > 0.5$ GeV/c. PYTHIA predicts that this ratio increases with increasing center-of-mass energy. In PYTHIA as in the data the density of charged particles in the "plateau" region of the UE rises more rapidly with center-of-mass energy than does than the overall density of charged particles!

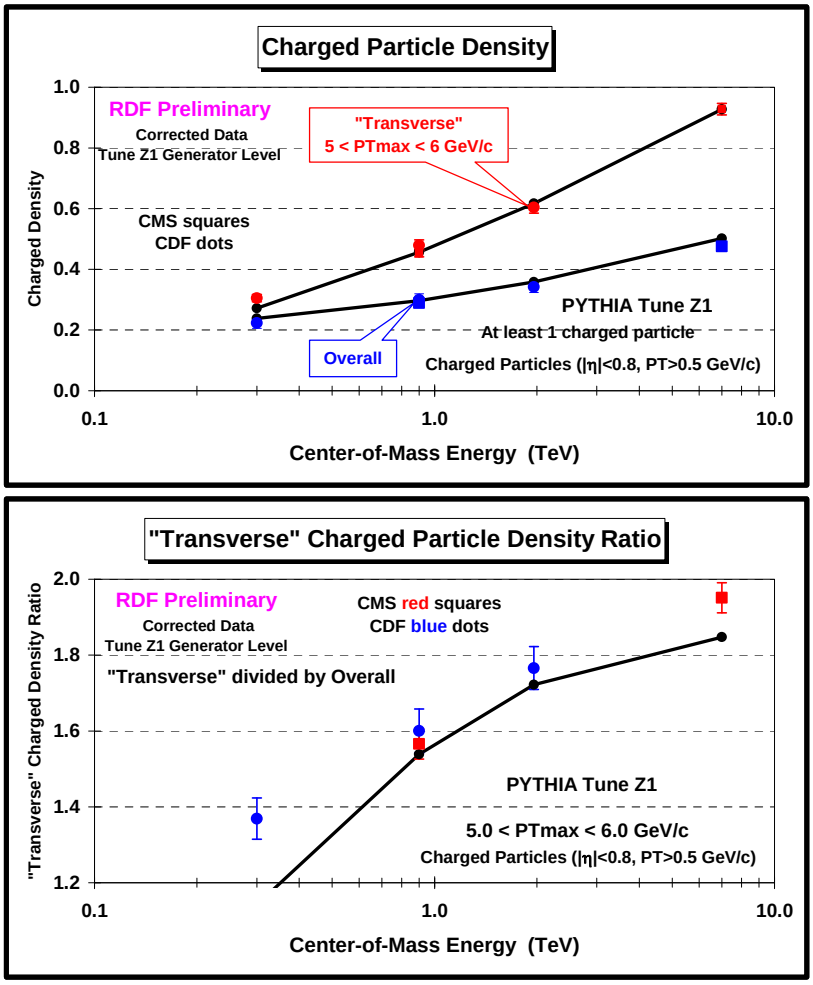

Fig. 49. (*top*) CDF data at 1.96 TeV, 900 GeV, and 300 GeV and CMS data at 900 GeV and 7 TeV on the "transverse" charged particle density as defined by the leading charged particle, PTmax, for 5.0 < PTmax < 6.0 GeV/c plotted versus the center-of-mass energy (on a log scale) for charged particles with $p_T > 0.5$ GeV/c and $|\eta| < 0.8$ compared with the overall charged particle density for events with at least one charged particle with $|\eta| < 0.8$ and $p_T > 0.5$ GeV/c. (*bottom*) CDF and CMS data at 7 TeV on the "transverse" charged particle density ratio as defined by the leading charged particle, PTmax, for 5.0 < PTmax < 6.0 GeV/c plotted versus the center-of-mass energy (on a log scale) for charged particles with $p_T > 0.5$ GeV/c and $|\eta| < 0.8$. At each energy the ratio corresponds "transverse" charged particle density divided by the overall charged particle density for events with at least one charged particle with $|\eta| < 0.8$ and $p_T > 0.5$ GeV/c. The data are corrected to the particle level with errors that include both the statistical error and the systematic uncertainty and are compared with PYTHIA 6.4 Tune Z1.

V. Summary & Conclusions

The data presented here together with the LHC data allows for a precise study of the energy dependence of the MB and UE. Tune Z1 fits very well the LHC data [6,7] and also does a fairly good job (although not perfect) with the CDF data presented here. None of the QCD Monte-Carlo models fit all the data perfectly yet, however, the data presented here will result in new and improved tunes. There is much remaining to do. Later we will update this note to include other MB and UE observables.

ACKNOWLEDGMENTS

We want to thank Mary Convery, Ray Culbertson, and Jonathan Lewis for their help with the datasets.

References

[1] *Charged Jet Evolution and the Underlying Event in Proton-Antiproton Collisions at 1.8 TeV*, The CDF Collaboration, Phys. Rev. **D65**, 092002, (2002).

[2] *Studying the Underlying Event in Drell-Yan and High Transverse Momentum Jet Production at the Tevatron*, The CDF Collaboration, Phys. Rev. **D82**, 034001 (2010), arXiv:1003.3146.

[3] T. Sjöstrand, Phys. Lett. **157B**, 321 (1985); M. Bengtsson, T. Sjöstrand, and M. van Zijl, Z. Phys. **C32**, 67 (1986); T. Sjöstrand and M. van Zijl, Phys. Rev. **D36**, 2019 (1987). T. Sjöstrand, P. Eden, C. Friberg, L. Lonnblad, G. Miu, S. Mrenna and E. Norrbin, Computer Physics Commun. **135**, 238 (2001).

[4] *CDF Run 2 Monte-Carlo Tunes*, R. Field, Tevatron-for-LHC: Report of the QCD Working Group, arXiv:hep-ph/0610012, FERMILAB-Conf-06-359, October 1, 2006.

[5] P. Skands, *The Perugia Tunes*, 2009. arXiv:0905.3418.

[6] *Min-Bias and the Underlying Event at the LHC*, R. Field, arXiv:1110.5530, proceedings of the 51st Cracow School of Theoretical Physics: *The Soft Side of the LHC*, Zakopane, June 11 - 19, 2011, Acta Physica Polonica **B42**, 2631 (2011).

[7] *Early LHC Underlying Event Data - Findings and Surprises*, R. Field, arXiv:1010.3558, proceedings of the Hadron Collider Physics Symposium (HCP2010), August 23-27, 2010.

[8] For example see, *Underlying Event Measurements in pp Collisions at 0.9 and 7 TeV with the ALICE experiment at the LHC*, The ALICE Collaboration, arXiv:1112.2082v2, December 2011.

[9] *Using MAX/MIN Transverse Regions to Study the Underlying Event in Run 2 at the Tevatron*, Alberto Cruz, Rick Field, and Craig Group, CDF/ANAL/CDF/CDFR/7703.

[10] *CDF-QCD Data for Theorists Part 1 Leading Jet Events*, Rick Field and Craig Group, CDF/ANAL//CDFR/9087.

[11] *Using Drell-Yan to Probe the Underlying Event in Run 2 at CDF*, Deepak Kar and Rick Field, CDF/ANAL/CDF/CDFR/9242.